2013

Study of pH(Low) Insertion Peptides (pHLIPS) Interaction with Lipid Bilayer of Membrane

Dhammika Anuradha Weerakkody
University of Rhode Island, anuradha@my.uri.edu

STUDY OF PH (LOW) INSERTION PEPTIDES (PHLIPS) INTERACTION WITH LIPID BILAYER OF MEMBRANE

BY

DHAMMIKA WEERAKKODY

A DISSERTATION SUBMITTED IN PARTIAL FULFILLMENT OF THE REQUIREMENTS FOR THE DEGREE OF

DOCTOR OF PHILOSOPHY

IN

PHYSICS

UNIVERSITY OF RHODE ISLAND

2013

DOCTOR OF PHILOSOPHY DISSERTATION

OF

DHAMMIKA WEERAKKODY

APPROVED:

Thesis Committee:

Major Professor: Yana Reshetnyak

Mindy Levine

Leonard Kahn

Nasser H. Zawia

DEAN OF THE GRADUATE SCHOOL

UNIVERSITY OF RHODE ISLAND

2013

ABSTRACT

The pH-dependent interactions of pHLIPs® (pH (Low) Insertion Peptides) with lipid bilayer of membrane provides an opportunity to study and address fundamental questions of protein folding/insertion into membrane and unfolding/exit, as well as develop novel approach to target acidic diseased tissue such as cancer, ischemic myocardium, infection and others.

The main goal of the work presented here is to answer the following questions:

- What is the molecular mechanism of spontaneous insertion and folding of a peptide in a lipid bilayer of membrane;
- What is the molecular mechanism of unfolding and exit of a peptide from a lipid bilayer of membrane;
- How polar cargo attached to a peptide's inserting end might affect the process of insertion into a lipid bilayer of membrane;

  How sequence variation will affect a peptide's interactions with a lipid bilayer of membrane (partitioning into bilayer at neutral and low pH; apparent pK of insertion) with the main goal to identify the best pHLIP variants for imaging and therapy of pathological states such as cancer and others.

It has been demonstrated that pHLIP insertion into a membrane is associated with the protonation of Asp/Glu residues, which leads to an increase of hydrophobicity that triggers the folding and insertion of the peptide across a lipid bilayer. The insertion of the pHLIP is unidirectional and it is accompanied by the release of energy.. Therefore, the energy of membrane associated-folding can be used to favor the movement of cell-

impermeable polar cargo molecules across the hydrophobic membrane bilayer when they are attached to the inserting end of pHLIP. Both pH-targeting behavior and molecular translocation have been demonstrated in cultured cells and *in vivo*. Thus, there is an opportunity to develop a novel concept in drug delivery, which is based on the use of a monomeric, pH-sensitive peptide molecular transporter, to deliver agents that are significantly more polar than conventional drugs. Understanding the molecular events that occur when a peptide inserts across a membrane, folds, or exits from it and unfolds provides crucial information for the development of new drug delivery agents, as well as improving our understanding of the first step of membrane-associate protein folding.

The promise of exploiting tumor acidosis as a cancer biomarker has not been fully realized in clinical practice, even though the acidity has been a known property since the work of Otto Warburg nearly a century ago. The problem has been to find a practical way to target acidity. pHLIP reversibly folds and inserts across membranes in response to pH changes, and this discovery has led to a novel way to target acidic tissue. Steady state biophysical studies have revealed the molecular mechanism of pHLIP action, which is based on the increase of hydrophobicity of carboxyl groups when they become protonated under mildly acidic conditions, leading to peptide insertion into a membrane. It has been shown that pHLIP can target acidic tissue and selectively translocate polar, cell-impermeable molecules across membranes in response to low extracellular pH. As noted in the Molecular Imaging and Contrast

Agent Database (MICAD) at NCBI, a pHLIP labeled with a fluorescent dye, or a PET- and SPECT- agents (^{64}Cu-DOTA, ^{18}F, ^{99}Tc) is a marker for *in vivo* acidity,.

All prior studies *in vivo* were carried out with the WT-pHLIP sequence and showed that a good contrast and tumor to blood ratio can be achieved only more than 24 hours after pHLIP injection, when it has accumulated in the tumor and largely cleared from the blood. However, for the use of pHLIP-based radioactive imaging agents in the clinic, a more rapid background signal reduction is absolutely essential. We have conducted research in order to address this important need, to tune tumor targeting properties, and to broaden our understanding of the molecular mechanism of pHLIP action. A family of 16 pHLIP variants has been designed based on chemical and physical principles and comprehensive biophysical studies were performed with non-labeled peptides. We have successfully established a set of design criteria and identified the pHLIP candidates for imaging and therapeutic applications, including lead compounds for PET/SPECT and fluorescence/MR imaging.

ACKNOWLEDGMENTS

First I would like to thank my advisor Dr Yana Reshetnyak for her support for making this thesis a reality. If it hadn't been for her immense support, patient and guidance this thesis would have remained impossible. There is no doubt that one could not possibly have a better advisor and I feel privileged have Dr Reshetnyak as my mentor. I convey my heartfelt gratitude for going beyond the duties of a graduate adviser to help and guide me whenever it was necessary. I have always recognized her insight into the subject and ability guide through challenging research projects as a mark of a great teacher as well as a brilliant scientist.

I would also like to thank Dr Oleg Andreev for this guidance and support with research and other difficulties as a graduate student. I continue to be amazed by his knowledge and level of understanding of difficult research problems.

I am grateful for both Dr Reshetnyak and Dr Andreev for believing in me when all hope seemed to have lost and always willing to lend a helping hand when things seemed too difficult.

I would like to thank my graduate program committee members Dr Mindy Levine , Dr Leonard Kahn, Dr Gerhard Müller and Dr Arijit Bose for giving their precious time even when it is not convenient for them. I feel lucky to have such a collection of wonderful professors as my graduate committee.

I greatly appreciate the support and patient from my dear professors from URI Physics department during coursework and many other instances when I needed help. Also I would like to thank all the staff members of the Physics department for their support

and kindness. I am thankful to Steve Pellegrino for not only because of always finding the time to help with the technical matters but also for being a kind friend.

I am thankful to the staff members of URI graduate school and appreciate their interest for helping and always willing welcome questions with a smile.

I am grateful to my undergraduate Physics teachers Dr Upali Karunasiri and Dr Nimal Hettiarachchi whom I consider my inspiration for pursuing higher studies in Physics.

I thank my colleagues and friends from our lab for their valuable discussions and help with experiments. I appreciate their many contributions to the work presented in this thesis.

I thank my parents and my brother for always being supportive and understanding for being so far away from the family. For always making me smile and giving me the courage to get pass difficult obstacles, I thank my two beautiful children Dewni and Maneka.

I am forever grateful to Dayanjali Wijesinghe for her constant encouragement during my graduate studies. If it hadn't been for her constant support not only as a wife but also as a bright college, my journey as a graduate student could have been a much less pleasant experience. I am beyond grateful to her for sharing my many sleepless nights and stying up with me so I could keep working.

I owe my deepest gratitude to every person I met along my way because each one of them led me to where I am now.

PREFACE

This dissertation is written in the 'Manuscript Format' using the Thesis/ Dissertation template of University of Rhode Island. There are four manuscripts, each organized into a chapter. Tables and figures of each manuscript are listed under the corresponding chapter in the list of tables and figures.

The results of our studies presented here were published in four papers:

1. **D. Weerakkody**, A. Moshnikova, M. S. Thakur, V. Moshnikova, J. Danniels, D. M. Engelman, O. A. Andreev, Y. K. Reshetnyak, A Family of pH (Low) Insertion Peptides for Tumor Targeting, *Proced. Natl. Acad. Sci U.S.A.*, *Proced. Natl. Acad. Sci U.S.A.*, 110, 15, 5834-5839 (2013).
2. A.G. Karabadzhak, **D. Weerakkody**, D. Wijesinghe, M.S. Thakur, D.M. Engelman, O.A. Andreev, V.S. Markin, Y.K. Reshetnyak , Modulation of the pHLIP Transmembrane Helix Insertion Pathway, *Biophysical Journal*, 102, 1846-1855 (2012).
3. Barrera, F. N., **Weerakkody, D.,** Anderson, M., Andreev, O. A., Reshetnyak, Y. K. and Engelman, D. M. Roles of Carboxyl Groups in the Transmembrane Insertion of Peptides, *J. Mol. Biol*. 413, 359-371 (2001).
4. Andreev O.A., A. G. Karabadzhak**, D. Weerakkody**, G. O. Andreev, D. M. Engelman, Y. K. Reshetnyak The pHLIP peptide inserts across a lipid bilayer as a helix, and exits by a different path, *Proced. Natl. Acad. Sci U.S.A.*, 107, 4081-4086 (2010).

Work was presented on the following 13 Meetings/Conferences:

2013

D. Weerakkody, A. Moshnikova, M. S. Thakur, V. Moshnikova, J. Danniels, D. M. Engelman, O. A. Andreev, Y. K. Reshetnyak, A Family of pH (Low) Insertion Peptides for Tumor Targeting, ***Biophysical Society 57 Annual Meeting,*** Philadelphia, PA.

A.G. Karabadzhak, D. Weerakkody, D. Wijesinghe, M.S. Thakur, D.M. Engelman, O.A. Andreev, V.S. Markin, Y.K. Reshetnyak, Modulation of the pHLIP Transmembrane Helix Insertion Pathway, ***Biophysical Society 57 Annual Meeting,*** Philadelphia, PA.

2012

D. Weerakkody, A. Moshnikova, M. Anderson, M. S. Thakur, V. Moshnikova, D. M. Engelman, O. A. Andreev, Y. K. Reshetnyak. A Family of pH (Low) Insertion Peptides for Tumor Targeting, ***Gordon Research Conference "Drug Carriers in Biology and Medicine"***, Waterville Valley, NH

D. Weerakkody, A. Moshnikova, M, Thakur, B. Healy-Rossi, D. M. Engelman, O. A. Andreev, Y.K. Reshetnyak. Family of pH-Low-Insertion-Peptides (pHLIPs), ***March Meeting of American Physics Society***, Boston, Massachusetts.

A. G. Karabadzhak, D. Weerakkody M. Thakur, D. M. Engelman, O. A. Andreev, V. Markin, Y.K. Reshetnyak. Membrane-associated peptide folding: pH triggered insertion and helical structure formation, ***March Meeting of American Physics Society***, Boston, Massachusetts.

2011

D. Wijesinghe, M. An, D. Weerakkody, A. G. Karabadzhak, D. M. Engelman, O. A. Andreev, Y. K. Reshetnyak, pH-dependent translocation of cell-impermeable cargo molecules across membrane by pHLIP^{TM}, ***Innovative Minds in Prostate Cancer Today (IMPaCT),*** Orlando, Florida

A. G. Karabadzhak, D. Weerakkody, M. S. Thakur, M. D. Anderson, D. M. Engelman, O. A. Andreev, V. S. Markin, Y. K. Reshetnyak, First step in folding of nonconstitutive membrane proteins: spontaneous insertion of a polypeptide into a lipid bilayer and formation of helical structure, ***Biophysical Society 55 Annual Meeting,*** Baltimore, Maryland.

D. Weerakkody, A. G. Karabadzhak, M. S. Thakur, B. Healy-Rossi**,** D. M. Engelman, O. A. Andreev, Y. K. Reshetnyak, Correlation between properties of pHLIP peptide-lipid interaction and tumor targeting in vivo. ***Biophysical Society 55 Annual Meeting,*** Baltimore, Maryland.

Y. K. Reshetnyak, A. G. Karabadzhak, D. Weerakkody, D. M. Engelman, V.S. Markin, O. A. Andreev, First step in folding of nonconstitutive membrane proteins: Spontaneous insertion of a polypeptide into a lipid bilayer and formation of helical structure, ***March Meeting of American Physics Society***, Dallas, Texas

F. N. Barrera, M. An, D. Wijesinghe, D. Weerakkody, M. Anderson, O. A. Andreev, Y. K. Reshetnyak, D. M. Engelman, Aspartic acid residues drive the membrane translocation of pHLIP, a therapeutic and imaging agent for solid tumors, ***Special Meeting of American Association of Cancer Research,*** San Francisco, CA

2010

D. Wijesinghe, M. An, D. Weerakkody, A. G. Karabadzhak, D. M. Engelman, O. A. Andreev, Y. K. Reshetnyak, pH-dependent translocation of cell-impermeable cargo molecules across membrane by pHLIP^{TM}, ***Gordon Research Conference,*** Waterville Valley, NH

Y. K. Reshetnyak, A. G. Karabadzhak, D. Weerakkody, M. S. Thakur, G. O. Andreev, D. M. Engelman, O. A. Andreev, Membrane-associated folding and unfolding, ***March Meeting of American Physics Society***, Portland, Oregon

A. G. Karabadzhak, D. Weerakkody, M. S. Thakur, G. O. Andreev, D. M. Engelman, O. A. Andreev, Y. K. Reshetnyak, Membrane-associated folding and unfolding, ***Biophysical Society 54 Annual Meeting,*** San Francisco, California

A. G. Karabadzhak, D. Weerakkody, M. S. Thakur, M. D. Anderson, D. Wijesinghe, L. Yao, J. Daniels, S. Zheng, O. A. Andreev, Y. K. Reshetnyak, Energy of membrane-associated folding of pHLIP peptide could be used for selective delivery of molecules across membrane of cancer cells and targeting tumors in vivo, ***Meeting of the New England Section of American Physics Society,*** Providence, RI

2009

O. A. Andreev, A. Karabadzhak, D. Weerakkody, V. S. Markin, D. M. Engelman, Y. K. Reshetnyak, Kinetics and Thermodynamics of Peptide (pHLIP) insertion and folding in a lipid bilayer membrane, ***March Meeting of American Physics Society***, Pittsburgh, Pennsylvania

A. Karabadzhak, D. Weerakkody, D. M. Engelman, O. A. Andreev, Y. K. Reshetnyak, Kinetics of Peptide (pHLIP) insertion and folding in a lipid bilayer membrane. ***Biophysical Society 53 Annual Meeting,*** Boston, Massachusetts.

TABLE OF CONTENTS

LIST OF TABLES

LIST OF FIGURES

CHAPTER 1 PAGE

CHAPTER 2

CHAPTER 3

CHAPTER 4

CHAPTER 1

Published in Proceedings of National Academy of Sciences (PNAS) on

22nd of December, 2010

BIOLOGICAL SCIENCES: Biophysics and Computational Biology

The pHLIP peptide inserts across a lipid bilayer as a helix, and exits by a different path

Oleg A. Andreev[1], Alexander G. Karabadzhak[1*], Dhammika Weerakkody[1]*, Gregory O. Andreev[2], Donald M. Engelman[3], Yana K. Reshetnyak[1]

[1]Physics Department, University of Rhode Island, 2 Lippitt Rd., Kingston, RI, 02881, USA

[2]Physics Department, University of California San Diego, 9500 Gilman Dr. #0319 La Jolla, CA 92093

[3]Department of Molecular Biophysics and Biochemistry, Yale University, P.O. Box 208114, New Haven, CT 06520, USA

* Authors equally contributed to the work

Corresponding authors:

Oleg Andreev, Physics Department, University of Rhode Island, 2 Lippitt Rd., Kingston, RI, 02881, USA, Phone: (401)-874-2054, Fax: (401) 874-2380, E-mail: andreev@mail.uri.edu

Donald Engelman, Department of Molecular Biophysics and Biochemistry, Yale University, P.O. Box 208114, New Haven, CT 06520, USA, Phone: (203)-432-5601; Fax: (203) 432-6381, E-mail: donald.engelman@yale.edu

Yana Reshetnyak, Physics Department, University of Rhode Island, 2 Lippitt Rd., Kingston, RI, 02881, USA, Phone: (401)-874-2060, Fax: (401) 874-2380, E-mail: reshetnyak@mail.uri.edu

Authors Contribution

O.A.A. and Y.K.R. designed research; A.G.K. and D.W. performed experimental work; G.O.A., O.A.A. and Y.K.R. analyzed data; O.A.A., D.M.E. and Y.K.R. conceptualized the model and wrote the paper.

Abstract

What are the molecular events that occur when a peptide inserts across a membrane or exits from it? Using the pH-triggered insertion of the pHLIP (pH Low Insertion Peptide) peptide to enable kinetic analysis, we show that insertion occurs in several steps, with rapid (0.1 s) interfacial helix formation followed by a much slower (45 s) insertion pathway to give a transmembrane helix. The reverse process of unfolding and peptide exit from the bilayer core, which can be induced by a rapid rise of the pH from acidic to basic, proceeds ~800 times faster than folding/insertion and through different intermediate states. In the exit pathway, the helix-coil transition is initiated inside the membrane, and the polypeptide starts to exit when about 30% of the helix is unfolded (17 ms). These insights may guide understanding of membrane protein folding and the design of medically useful peptides for imaging and drug delivery.

Introduction

The stability and folding of membrane proteins are strongly constrained by the formation of secondary structures in the lipid bilayer environment, driven by the hydrophobic effect and hydrogen bonding. Consideration of these factors has led to versions of a thermodynamic framework model for the folding and unfolding of helical membrane proteins (*1*-*5*). One concept is that spontaneous insertion and folding includes the formation of helical intermediates at the bilayer surface, followed by insertion, and that unfolding includes the same steps, but in reverse order. Because folding to form a helix is coupled to insertion, a significant experimental challenge in testing the concepts is to separate the process of peptide partitioning into a membrane from the folding events leading to secondary structure. We have studied a water-

soluble membrane peptide, pHLIP (pH Low Insertion Peptide), that binds to the surface of a lipid bilayer in an unstructured monomeric state at neutral pH (*6-12*). Lowering the pH triggers the spontaneous insertion of the peptide across the bilayer and the formation of a transmembrane helix. Because the pH drop can be accomplished by rapid mixing, kinetic analysis can be used to examine steps in the process, and the predictions of the thermodynamic models can be tested.

Results

pHLIP is a remarkable 35-residue peptide found as a transmembrane helix in bacteriorhodopsin, yet soluble when isolated in aqueous solution. At neutral and high pHs pHLIP is monomeric at concentrations less than 8-10 μM, and equilibrates between unstructured forms in aqueous solution (state I) and bound to the surface of a lipid bilayer if one is available (state II) (*6, 9*) (Figure 1a supplementary information). In an acidic environment the equilibrium is shifted toward a monomeric transmembrane helical form (state III) (*6, 9*), and the process of insertion is accompanied by an energy release of about 1.8 kcal/mol in addition to the binding energy (6-7 kcal/mol) locating the peptide at the surface (*11*). The pKa of the transition from state II to state III is 6.0 (*6, 11*). The transmembrane orientation of the peptide at low pH was previously established by FTIR spectroscopy (*6*); here, we additionally confirmed a transmembrane orientation by oriented circular dichroism (OCD) spectroscopy (Figure 1b supplementary information). A characteristic OCD spectrum for transmembrane helix orientation was obtained using direct insertion of pHLIP peptides into supported bilayers (in contrast to earlier experiments, where bilayers were assembled with membrane peptides (*13, 14*). The protonation of two

Asp residues in the transmembrane region leads to an increase of hydrophobicity that result in the folding and insertion of the peptide across a membrane (*8*). Increasing the pH promotes the unfolding and exit of the peptide from the core of the lipid bilayer. The insertion of pHLIP across a membrane is unidirectional: the C-terminus goes inside a cell or vesicle, and the N-terminus stays outside (*7, 9*). Neither partitioning of an unstructured peptide onto the bilayer surface at neutral pH nor insertion as a transmembrane helix at low pH promotes membrane fusion or leakage of vesicles, red blood cells, or cancer cells (*7, 8, 10*). Fluorescence and CD spectroscopy have been used to monitor transitions between the states (*6, 8, 9*). (Figure 1c, d supplementary information): transmembrane helix is accompanied by the appearance of a characteristic helical CD signal, and a shift of the fluorescence spectrum maximum and increase of fluorescence intensity. These signals are the basis of our kinetic studies.

The pHLIP peptide gives an opportunity to observe membrane-associated transitions between surface coil and transmembrane helix and vice versa. An enabling advantage of our system is that an initial state is defined, with the peptide bound to the surface of a membrane as an unstructured monomer. Transitions were induced by rapid changes of pH by fast mixing of the aqueous solution of pHLIP pre-incubated with POPC at pH8.0 or pH4.0 with equal volumes of appropriately diluted solutions of HCl or NaOH, respectively. Membrane-associated peptide folding/insertion and unfolding/exit were monitored by the changes of CD and fluorescence signals we previously used to study equilibrium states (Figure 1a-b, d-e). Such parameters (mostly fluorescence) are widely used for the observation of conformational changes

that occur in polypeptides interacting with a membrane or detergent (*15-18*). For fast fluorescence measurements, a filter was used to capture the emission above 320 nm, but changes of the entire fluorescence spectrum were also recorded in a global mode with use of emission monochromator (Figure 1c, f). The obtained in stopped-flow mode fluorescence spectra clearly show that the increase of fluorescence is accompanied with shift of position of maximum, which indicative to the peptide insertion into hydrophobic core of membrane.

Since the pHLIP peptide contains a Pro residue in the transmembrane part, we speculated that proline might act as a helix breaker and/or exhibit isomerization during folding. To examine these possibilities, a pHLIP variant was synthesized with Pro replaced by Ala. We observed that the variant shows some helical structure in solution at neutral pH (Figure 2 supplemental information), and that vesicle binding of the variant further promotes the coil-helix transition. Since replacement of Pro led to changes in solution and in the peptide-membrane interactions, we asked whether the presence of prolyl isomerase (cyclophilin A), which promotes Pro isomerization (*19*), would affect folding and insertion of the non-mutated peptide. Experiments were carried out at various temperatures. No differences were observed in membrane-associated folding in absence and presence of prolyl isomerase (data not shown), so we conclude that the proline is simply acting as a helix breaker in solution and on the bilayer surface. A detailed description of the experimental protocol is presented in the supplementary section.

To avoid crowding of the peptide on the surface of vesicles (parking problem) we set the peptide:POPC molar ratio at ~ 1:140 (*11*). Given the surface binding energy of 6-7

kcal/mol (from our earlier measurements), the bound to free ratio is ~ 10^4 to 10^5, so the initial state in the insertion experiments is predominantly an unstructured surface bound state of the peptide (state II, Figure 1 supplementary information). In the unfolding experiments, the initial state, at low pH, is predominantly a transmembrane helical configuration of the peptide (>95% state III).

As seen by fluorescence, the entire process of insertion (transition form state II to state III) upon a rapid drop of pH is found to be well described by a pseudo-first order kinetics model with 4 consecutive steps involving State II, three intermediates, and State III:

$$I_1 \xrightarrow{k_1} I_2 \xrightarrow{k_2} I_3 \xrightarrow{k_3} I_4 \xrightarrow{k_4} I_5$$

The rate equations for the time dependence can be written as differential equations:

$$\begin{aligned}
-\frac{d[I_1]}{dt} &= k_1[I_1] \\
-\frac{d[I_2]}{dt} &= k_2[I_2] - k_1[I_1] \\
-\frac{d[I_3]}{dt} &= k_3[I_3] - k_2[I_2] \\
-\frac{d[I_4]}{dt} &= k_4[I_4] - k_3[I_3] \\
-\frac{d[I_5]}{dt} &= k_4[I_4]
\end{aligned} \qquad (1)$$

These differential equations can be solved analytically and the rate equations integrated, assuming that the initial concentrations of every intermediate except I_1 are zero. The function used for fitting of the experimental data can be written in general form as:

$$g(t) = \sum_{i=1}^{n+2} f_i [I_i] \tag{2}$$

where f_i are the changes of fluorescence or CD signals associated with the i-th transition from one intermediate to another, and n is the number of intermediates used in the model. For the kinetic model with three intermediates the function used to fit the experimental data is

$$\begin{aligned}
g(t) = {} & f_1 e^{-k_1 t} + f_2 e^{-k_1 t} \frac{k_1 \left(e^{(k_1 - k_2)t} - 1\right)}{k_1 - k_2} + \\
& f_3 e^{-k_1 t} \frac{k_1 k_2 \left(e^{(k_1 - k_3)t}(k_1 - k_2) + e^{(k_1 - k_2)t}(k_3 - k_1) + (k_2 - k_3)\right)}{(k_1 - k_2)(k_1 - k_3)(k_2 - k_3)} + \\
& f_4 e^{-k_1 t} \frac{k_1 k_2 k_3}{(k_2 - k_1)(k_2 - k_3)(k_3 - k_1)(k_2 - k_4)(k_3 - k_4)(k_4 - k_1)} \times \\
& \left(\begin{array}{l} e^{(k_1 - k_3)t}(k_1 - k_2)(k_1 - k_4)(k_2 - k_4) - e^{(k_1 - k_4)t}(k_1 - k_2)(k_1 - k_3)(k_2 - k_3) - \\ e^{(k_1 - k_2)t}(k_1 - k_3)(k_1 - k_4)(k_3 - k_4) + (k_2 - k_3)(k_2 - k_4)(k_3 - k_4) \end{array} \right) + \\
& f_5 e^{-k_1 t} \frac{1}{(k_2 - k_1)(k_2 - k_3)(k_3 - k_1)(k_2 - k_4)(k_3 - k_4)(k_4 - k_1)} \times \\
& \left(\begin{array}{l} e^{(k_1 - k_4)t} k_1 k_2 k_3 (k_1 - k_2)(k_1 - k_3)(k_2 - k_3) - \\ e^{k_1 t}(k_1 - k_2)(k_1 - k_3)(k_2 - k_3)(k_1 - k_4)(k_2 - k_4)(k_3 - k_4) - \\ e^{(k_1 - k_3)t} k_1 k_2 k_4 (k_1 - k_2)(k_1 - k_4)(k_2 - k_4) + \\ e^{(k_1 - k_2)t} k_1 k_3 k_4 (k_1 - k_3)(k_1 - k_4)(k_3 - k_4) - k_2 k_3 k_4 (k_2 - k_3)(k_2 - k_4)(k_3 - k_4) \end{array} \right)
\end{aligned} \tag{3}$$

All fluorescence kinetic data were normalized to the initial values, so that f_1 was about 1. From steady-state experiments performed at various temperatures we established that the absolute increase of fluorescence signal induced by the drop of pH was the same at all temperatures. Therefore, asymptotic values (f_5) were chosen to be the same

for kinetics runs performed at different temperatures, and the values varied from 1.55 to 1.6.

CD folding and unfolding curves (Figure 1a, d) were fitted well using a simpler kinetic model with one intermediate state:

$$g(t) = f_1[I_1] + f_2[I_2] + f_3[I_3] \qquad (4)$$

For each step, the characteristic times t_i $\left(t_i = 1/k_i\right)$ and contributions (F_i in %) to the spectral signal (with the total change of the CD or fluorescence signal taken as 100%) are presented on Figure 1. The % contributions to the total signal, F_i, were calculated according to the formula:

$$F_i = 100\frac{f_{i+1} - f_i}{f_{n+2} - f_1}, \qquad \text{where } i = 1,\ldots, n+1 \qquad (6)$$

The fluorescence kinetic curves measured at various temperatures (Figure 2a) were fitted using models with one, two or three intermediate states. A model with three intermediate states (eq. 3) was required for an adequate fit of the experimental data after taking into consideration some increase of fluorescence signal within the first few seconds (insert in Figure 2a). Starting with the inserted helix, an increase of pH led to a short delay (about 12 ms) followed by a decrease of the fluorescence signal. The fluorescence decay reporting the helix-coil exit pathway was well fitted by a kinetic model with one intermediate (eq. 4). Kinetic parameters obtained from the fitting of fluorescence kinetic data recorded at various temperatures are presented in Table 1. Increasing the temperature speeds up the process of insertion, presumably as a result of increased thermal fluctuations.

Using kinetic measurements at various temperatures, the activation energies E_i^a for each transition were calculated from Arrhenius plots (Figure 2b) according to the Arrhenius equation:

$$\ln k_i = -\frac{E_i^a}{RT} \tag{6}$$

where k_i are the rates presented in Table 2; R is the gas constant; T is the absolute temperature. Assuming that the transition from one intermediate to another occurs through a single transition state, the Eyring equation can be applied for the calculation of the activation enthalpy $\Delta H_i^{\#}$ and the activation entropy $\Delta S_i^{\#}$ associated with the transitions from one intermediate to another:.

$$\ln\left(\frac{hk_i}{k_b T}\right) = -\frac{\Delta H_i^{\#}}{RT} + \frac{\Delta S_i^{\#}}{R} \tag{7}$$

The activation Gibbs free energy, $\Delta G_i^{\#}$ is then:

$$\Delta G_i^{\#} = \Delta H_i^{\#} - T\Delta S_i^{\#} \tag{8}$$

where h is Planck's constant and k_b is Boltzmann's constant. Thermodynamic activation parameters are summarized in Table 2 and their changes during the transition from one state to another are presented in Figure 2c.

Discussion

To interpret the results, we have constructed a model that is based on and consistent with the data, but which is incompletely constrained by it. Thus, some features are viewed with confidence while others are less certain. The model assumes single pathways of insertion and exit, and is shown in figure 3. Starting with the surface bound peptide of State II, and following the drop in pH, we see a rapid formation of

helix, in two steps (Folding intermediates 1 and 2, forming at 8 ms and 112 ms), each producing about half of the total helix. The helix might be a single straight helix, or it might consist of several short helices with breaks in between (these possibilities are experimentally indistinguishable). This part of the interpretation is secure: helix formation clearly is faster than most of the fluorescence changes. It is possible that helix rotational orientation or a slight sinking of the helix at the interface could account for the fast (28ms) first fluorescence change of ~23%. Following the rapid helix formation, the rest of the insertion process is reported by fluorescence, and is about 1500 times slower, occurring in three kinetically distinct steps over the next ~45s.

While we cannot be certain of the exact nature of the kinetic intermediates during insertion, we suggest a few thoughts as working ideas. From the surface helix formation to the fully inserted transmembrane helix, two intermediate states are apparent, folding intermediates FI_3 and FI_4. Some features of the process to consider are that significant rearrangement of lipid must occur during the peptide insertion, that the polar C terminus of pHLIP must traverse the bilayer, and that the proline may provide a point of flexibility. Our previous studies showed that there is substantial lipid perturbation when the peptide is in its surface bound configuration, and that the perturbation is much reduced when pHLIP adopts its transmembrane configuration (*8, 10, 11*). It is possible that a large collective lipid reorganization is involved, but we have no data with which to assess such a possibility. We therefore invoke a bending and partial insertion of the helix as an idea, suggested by the proline, and sketch the intermediate shown as FI_3. The highest activation energy barrier (see tables) is the

transition from the third to the fourth intermediate, although all of the energy barriers are significant (hence the slow kinetics). It may be that the fourth intermediate is a transbilayer inserted form with the C terminus across the bilayer, or that the C-terminus crosses the bilayer during the last transition. We have no direct evidence to choose one of these, but we know that the C-terminus must cross the bilayer at some point. Each step from the unfolded to the folded state is associated with a decrease of entropy (decrease of disorder) that reflects the process of folding (ordering). It is possible that both the peptide and the lipids undergo a disorder – order transition.

In contrast with previously proposed theoretical models suggesting that entry and exit pathways mirror each other, our data reveal that the folding and unfolding processes can have different rates and proceed via significantly different intermediate steps. The unfolding and exit of the peptide in response to a sudden pH increase occurs within one hundred milliseconds, orders of magnitude faster than insertion. Assuming that the increase of pH leads to the deprotonation of the Asp residues (perhaps involving proton transfer from Asp86 to Arg83, known to happen in bacteriorhodopsin, from which the pHLIP peptide is derived (*20, 21*)), followed by the helix-coil transition and a rapid exit of the polypeptide from the bilayer interior. Surprisingly, about 30% of the helix-coil transition is completed within ~12 ms, while practically no change of the fluorescence signal is observed, indicating that the polypeptide remains in the membrane interior as an unfolding intermediate (UI_1). Thus, partial unfolding of the TM helix, involving about 5-6 residues out of 20-22 residues, occurs inside the membrane and the peptide subsequently moves out of the bilayer interior. Further propagation of the helix-coil transition is accompanied by a rapid exit of part of the

polypeptide within the next 5 ms (UI_2). The remaining 30% of the membrane-embedded helical structure unfolds and exits within 65 ms (including the C terminus), and equilibrium is established between pHLIP in its unfolded membrane-bound (U^m) and soluble forms. Unfolding experiments carried out at 7°C showed that the peptide exit also occurs in two steps with characteristic times of 17.6 and 152 msec (data not shown). An interesting possibility is that the two deprotonation steps happen separately, and account for steps in the exit pathway.

The existence of interfacial folded intermediates reported by several authors has been based on indirect measurements (*22*-*24*), and the results of molecular dynamics simulations of membrane-associated folding and insertion of various peptides are not definitive (*25*-*28*). Here, we present a direct observation of the formation of an interfacial helical intermediate as a step in the process of folding and insertion of a peptide into a membrane.

We conclude that an interfacial helical intermediate is a required step during the process of pHLIP folding/insertion. Helix formation reduces the free-energy penalty associated with the partition of the peptide backbone into the low dielectric environment of the bilayer, despite the fact that the coil-helix transition is associated with a loss of entropy. Helix insertion, most probably, is accompanied by a significant perturbation of lipids, although the lipid perturbation is reduced in the overall process. The insertion of pHLIP is slow, since the peptide is initially located on the outer leaflet of the bilayer, and it takes time to cross the membrane and reorganize lipids around the transmembrane helix. In contrast to the insertion, unfolding and exit occur much faster, perhaps since the peptide can be conceptualized as occupying a small

channel across the lipid, so that the peptide can quickly exit without significant lipid reorganization. Such a channel would close immediately after exit of the peptide. We have demonstrated *in vivo* that pHLIP can target diseased tissues with elevated levels of extracellular acidity, such as tumors (*8, 12, 29*) and that the energy of the insertion events can be used for the selective translocation of polar cell-impermeable cargo molecules across the membranes of liposomes and cells (*7, 12*). Our kinetic data provide insights on the mechanisms of membrane-associated polypeptide folding and unfolding, and may be useful in improving the design of peptide based transmembrane delivery agents

Acknowledgements

This work was supported in part by grant from the National Institutes of Health, National Cancer Institute RO1 133890. We are grateful to all members of Drs Andreev, Engelman and Reshetnyak laboratories for fruitful discussion.

References

1. Jacobs RE, White SH (1989) The nature of the hydrophobic binding of small peptides at the bilayer interface: implications for the insertion of transbilayer helices *Biochemistry* 28:3421-3437.
2. Engelman DM, Steitz TA (1981) The spontaneous insertion of proteins into and across membranes: the helical hairpin hypothesis *Cell* 23:411-422.
3. Popot JL, Engelman DM (1990) Membrane protein folding and oligomerization: the two-stage model *Biochemistry* 29:4031-4037.
4. White SH, Wimley WC (1999) Membrane protein folding and stability: physical principles *Annu Rev Biophys Biomol Struct* 28:319-365.
5. Engelman DM et al (2003) Membrane protein folding: beyond the two stage model *FEBS Lett* 555:122-125.
6. Hunt JF, Rath P, Rothschild KJ, Engelman DM (1997) Spontaneous pH-dependent membrane insertion of a transbilayer alpha-helix *Biochemistry* 36:15177-151792.
7. Reshetnyak YK, Andreev OA, Lehnert U, Engelman DM (2006) Translocation of molecules into cells by pH-dependent insertion of a transmembrane helix *Proced Natl Acad Sci USA* 103:6460-6465.
8. Andreev OA et al (2007) Mechanism and uses of a peptide that targets tumors and other acidic tissue *in vivo Proced Natl Acad Sci USA* 104:893-7898.
9. Reshetnyak YK, Segala M, Andreev OA, Engelman DM (2007) A monomeric membrane peptide that lives in three worlds: in solution attached to and inserted across lipid bilayers *Biophysical J* 93:2363-2672.

10. Zoonens MA, Reshetnyak YR, Engelman DM (2008) Bilayer interactions of pHLIP a peptide that can deliver drugs and target tumors *Biophys J* 95:225-235.
11. Reshetnyak YK, Andreev OA, Segala M, Markin V, Engelman DM (2008) Energetic of peptide (pHLIP) binding to and folding across a lipid bilayer membrane *Proced Natl Acad Sci USA* 105:15340-15345.
12. Andreev OA, Engelman DM, Reshetnyak YK (2009) Targeting acidic diseased tissue: New technology based on use of the pH (Low) Insertion Peptide (pHLIP) *Chemistry Today* 27:10-13.
13. Merzlyakov M , Li E, Hristova K (2006) Directed assembly of surface-supported bilayers with transmembrane helices *Langmuir* 22:1247-1253.
14. Kiessling V, Tamm LK (2003) Measuring distances in supported bilayers by fluorescence interference-contrast microscopy: polymer supports and SNARE proteins *Biophysical J* 84:408-418.
15. Linke D et al (2004) Folding Kinetics and Structure of OEP16 *Biophysical J* 86:1479–1487.
16. Constantinescu I, Lafleur M (2004) Influence of the lipid composition on the kinetics of concerted insertion and folding of melittin in bilayers *Biochim Biophys Acta* 1667:26-37.
17. Tang J, Gai F (2008) Dissecting the membrane binding and insertion kinetics of a pHLIP peptide *Biochemistry* 47:8250-8252.

18. Hicks MR, Damianoglou A, Rodger A, Dafforn TR (2008) Folding and membrane insertion of the pore-forming peptide gramicidin occur as a concerted process *J Mol Biol* 383:358-366.
19. Reader JS et al (2001) A partially folded intermediate species of the β-sheet protein apo-pseudoazurin is trapped during proline-limited folding *Protein Sci* 10:1216–1224.
20. Balashov SP et al (1993) Effect of the arginine-82 to alanine mutation in bacteriorhodopsin on dark adaptation proton release and the photochemical cycle *Biochemistry* 32:10331-10343.
21. Balashov SP et al (1995) The two pKa's of aspartate-85 and control of thermal isomerization and proton release in the arginine-82 to lysine mutant of bacteriorhodopsin *Biochemistry* 34:8820-8834.
22. Ladokhin AS, White SH (2004) Interfacial folding and membrane insertion of a designed helical peptide *Biochemistry* 43:5782-5791.
23. Tucker MJ, Tang J, Gai F (2006) Probing the kinetics of membrane-mediated helix folding *J Phys Chem B* 110:8105-8109.
24. Tang J, Signarvic RS, DeGrado WF, Gai F (2007) Role of helix nucleation in the kinetics of binding of mastoparan X to phospholipid bilayers *Biochemistry* 46:13856-13863.
25. Milik M, Skolnick J (1993) Insertion of peptide chains into lipid membranes: an off-lattice Monte Carlo dynamics model *Proteins* 15:10-25.

26. Im W, Brooks CL (2005) Interfacial folding and membrane insertion of designed peptides studied by molecular dynamics simulations *Proced Natl Acad Sci USA* 102:6771–6776.
27. Nymeyer H, Woolf TB, Garcia AE (2005) Folding is not required for bilayer insertion: Replica exchange simulations of an alpha-helical peptide with an explicit lipid bilayer *Proteins-Structure Function and Bioinformatics* 59:783-790.
28. Ulmschneider MB, Ulmschneider JP (2008) Membrane adsorption folding insertion and translocation of synthetic trans-membrane peptides *Mol Membr Biol* 25:245-257.
29. Vāvere AL et al (2009) A novel technology for the imaging of acidic prostate tumors by positron emission tomography *Cancer Research* 69:4510-4516.

Tables

Temp.	k_1, s^{-1} (F_1, %)	k_2, s^{-1} (F_2, %)	k_3, s^{-1} (F_3, %)	k_4, s^{-1} (F_4, %)	*adj* R^2 / *RMSE*
7°C	>40 (13.0)	0.48 (13.7)	0.050 (39.4)	0.0110 (33.9)	0.99998 / 4.08E-4
11°C	>30 (18.0)	0.52 (14.2)	0.053 (37.8)	0.0131 (30.0)	0.99998 / 4.05E-4
18°C	>30 (21.2)	0.69 (16.8)	0.071 (32.4)	0.0196 (29.6)	0.99997 / 4.86E-4
25°C	>35 (23.1)	0.89 (16.3)	0.106 (27.5)	0.0242 (33.1)	0.99996 / 5.27E-4
37°C	>35 (23.0)	1.83 (18.2)	0.266 (27.7)	0.0454 (31.1)	0.99963 / 1.46E-3

Table 1. The transition rates, k_i, (fractional contributions, F_i) and goodness-of-fit (adjusted R-square, $adjR^2$, and root mean squared error, *RMSE*), were obtained by fitting the fluorescence kinetic curves measured at various temperatures presented in Figure 2a and using equation (3). The rates $k_2 - k_4$ have relative 95% confidence bounds of 1% or better. Due to an insufficient number of experimental points within first 50 ms, only a lower bound was estimated for the first rate (k_1).

	$I_1 \rightarrow I_2$ [a]	$I_2 \rightarrow I_3$	$I_3 \rightarrow I_4$	$I_4 \rightarrow I_5$
ΔE_a, kcal/mol	-0.4 ± 0.8	7.1 ± 0.8	9.1 ± 1.2	7.4 ± 0.4
$\Delta H^{\ddagger}$, kcal/mol	-1.0 ± 0.8	7.7 ± 0.8	9.7 ± 1.3	8.0 ± 0.4
$\Delta S^{\ddagger}$, cal/(K·mol)	-54.7 ± 2.9	-34.8 ± 2.7	-32.1 ± 4.3	-40.8 ± 1.3
$\Delta G^{\ddagger}$, kcal/mol at 25°C	15.4	17.5	18.7	19.6

Table 2. Activation thermodynamics parameters are presented for the transitions from one intermediate to another during the process of folding and insertion. The activation energy, E^a_i, was calculated from the Arrhenius plots (Figure 2b) according to the Arrhenius equation (6). The activation enthalpy $\Delta H_i^{\#}$ and the activation entropy $\Delta S_i^{\#}$ were calculated according to the Eyring equation (7). The activation Gibbs free energy, $\Delta G_i^{\#}$ at 25°C was calculated according to the formula (8).

[a]the data presented for the first transition are not statistically significant, since the correlation coefficient $R < 0.5$ and the p-level $p > 0.3$. All parameters calculated for other transitions are statistically significant, $R > 0.973$ and $p < 0.0053$.

Figures

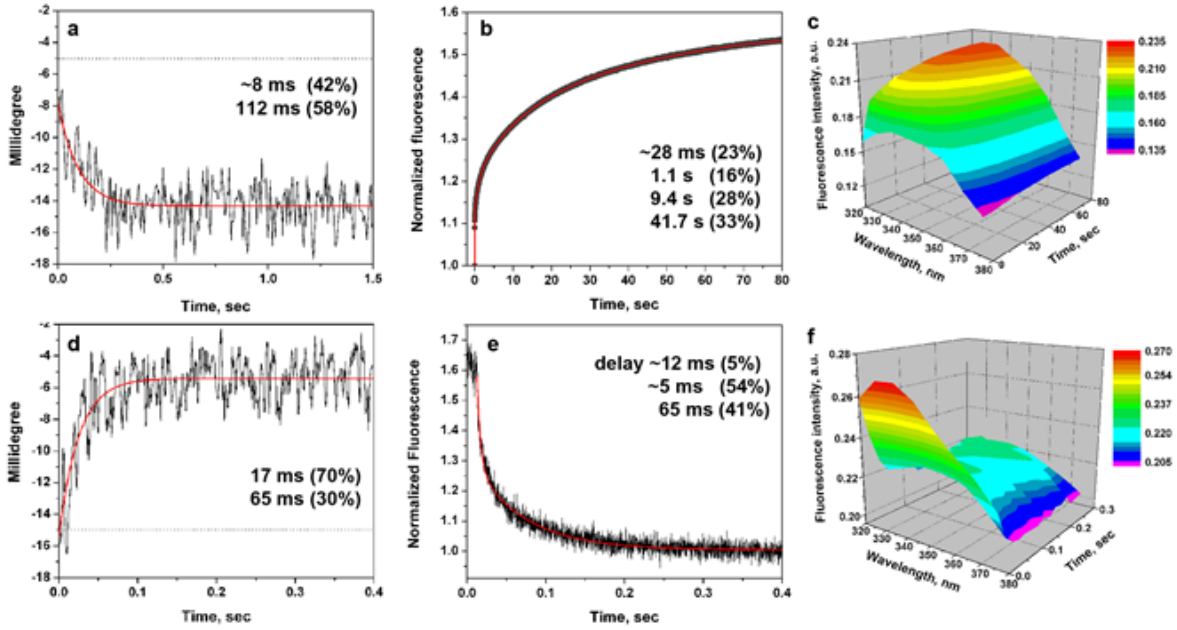

Figure 1. Membrane-associated pHLIP peptide folding and insertion across a POPC bilayer (a-c) and unfolding and exit (d-f) from the core of the bilayer were monitored by stopped-flow CD and fluorescence. Polypeptide folding and unfolding were induced by the rapid mixing of pHLIP-POPC solutions with diluted HCl or NaOH to give pH4 or pH8, respectively. The changes of intensity of CD (a, d) and fluorescence (b, e) were recorded at 225 nm (CD) and through a 320 nm cutoff filter using an excitation wavelength of 280 nm (fluorescence). The fluorescence signal recorded over 80 sec was corrected for photobleaching. The CD and fluorescence data were fitted by kinetic models with one and three intermediate states by using equations (3) and (4) (the fitting curves are red). The changes in the entire fluorescence spectrum during folding (c) and unfolding (f) were recorded in a global mode with the emission monochromator at the excitation wavelength of 275 nm to minimize the contribution of the scattered light component at short wavelengths (spectra were corrected for the

instrument sensitivity). The characteristic times (t_i) and fractional contributions (F_i) are obtained by the fitting of the experimental data using equations (3) and (4). The experiments were carried out at 25°C. The details of the experimental protocol can be found in the supplementary information.

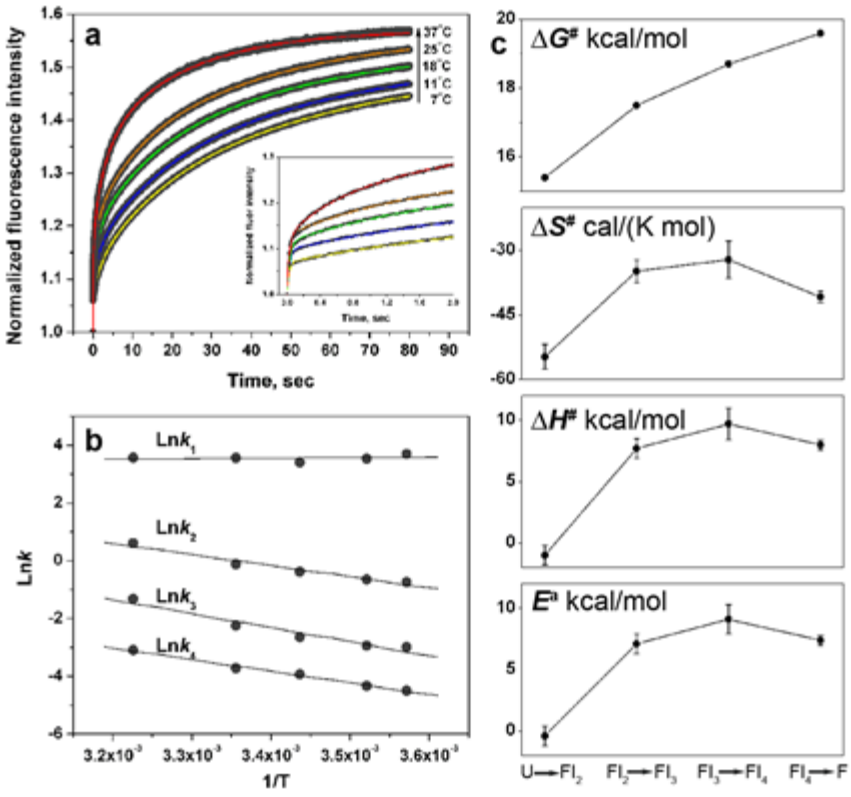

Figure 2. a) The membrane-associated pHLIP peptide insertion across the lipid bilayer of POPC vesicles was monitored by changes of the fluorescence signal through a 320 nm cutoff filter at an excitation wavelength of 280 nm and at various temperatures. The fitting curves obtained at various temperatures are color coded. The data were fitted by the kinetic model with three intermediates by using function (3). b) The Arrhenius plot was constructed according to the Arrhenius equation (6). c) The changes of the activation energy, E^a_i, enthalpy $\Delta H_i^{\#}$, entropy $\Delta S_i^{\#}$ and Gibbs free energy, $\Delta G_i^{\#}$ for each transition are plotted. The values of the thermodynamic activation parameters are presented in Table 2.

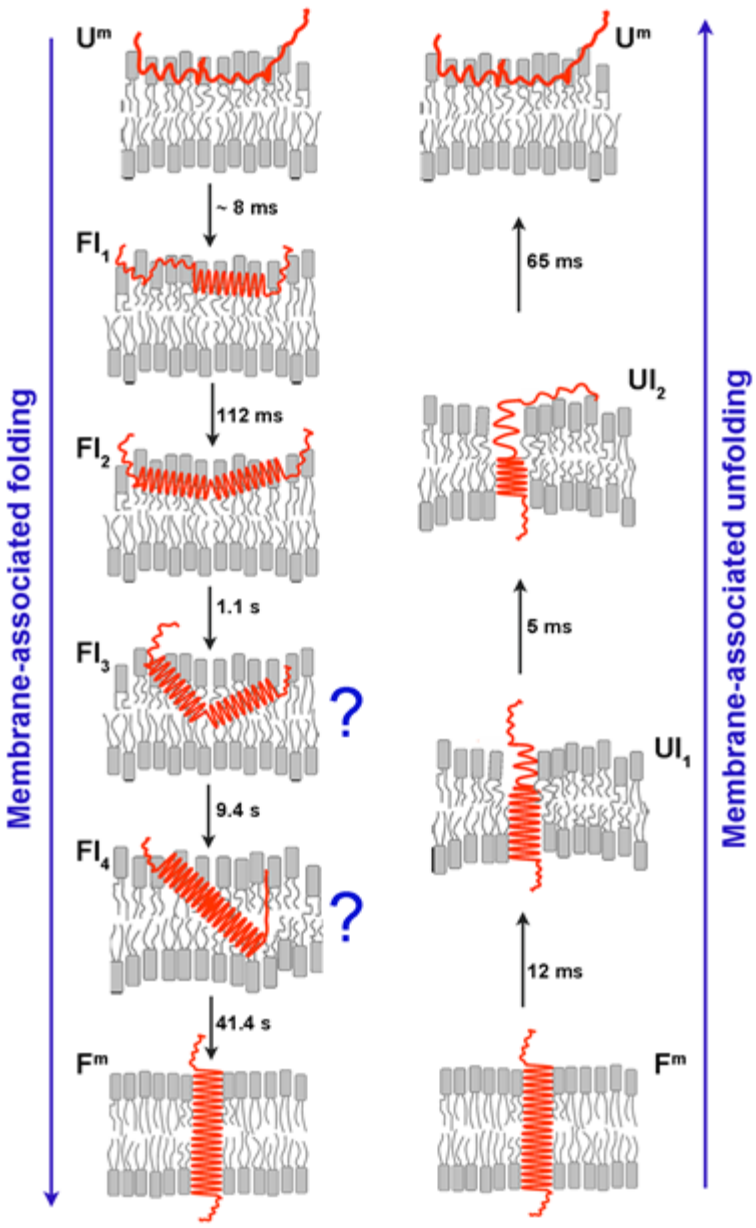

Figure 3. A schematic interpretation of the membrane-associated folding and unfolding events suggested by the kinetic data. The pHLIP peptide starts as a surface bound coil at pH8. A rapid drop of pH to 4 causes a rapid formation of helical structure on the surface, followed by a much slower insertion of the helix across the bilayer, with several kinetically distinct intermediates for which speculative models are shown. A sudden elevation of the pH from 4 to 8 results in the rapid unfolding and

exit of the peptide via a different pathway with different intermediates. The characteristic times ($t_i = 1/k_i$) were calculated from the rates presented in the Table 1. See discussion in the text.

Supplementary information

Methods

pHLIP peptide

The pHLIP sequences: AEQNPIYWARYADWLFTTPLLLLDLALLVDADEGT and its Pro to Ala variant AEQNPIYWARYADWLFTTALLLLDLALLVDADEGT were prepared by solid-phase peptide synthesis using Fmoc (9-fluorenylmethyloxycarbonyl) chemistry and purified by reverse phase chromatography at the W.M. Keck Foundation Biotechnology Resource Laboratory at Yale University. For use of the peptide, the lyophilized powder is dissolved in a solution containing 3 M urea and transferred to 10 mM phosphate buffer, pH8.0 using a G-10 size-exclusion spin column. The concentration of the peptide was determined by absorbance (ε_{280}=13,940 $M^{-1}cm^{-1}$).

Vesicle preparations

Large unilamellar vesicles (LUVs) were prepared by extrusion. 1ml of 25 mg POPC (1-Palmitoyl-2-Oleoyl-*sn*-Glycero-3-Phosphocholine, Avanti Polar Lipids, Inc.) in chloroform was desolvated on a rotary evaporator and dried under vacuum for several hours. The phospholipid film was rehydrated in 10 mM phosphate buffer, pH 8.0, vortexed for 2 hours, and repeatedly extruded through a 50 nm membrane to give small unilamellar vesicles.

Steady-state fluorescence and CD measurements

Steady-state fluorescence measurements were carried out on a PC1 spectrofluorometer (ISS, Inc.) under temperature control. Peptide fluorescence spectra were recorded from 310 nm to 400 nm with the spectral widths of excitation and emission slits set at 2-4

nm and 2 nm, respectively, using an excitation wavelength of 275, 280 and 295 nm. The changes of fluorescence signal in process of transition from one state to another are independent of the excitation wavelength, which indicate that the contribution of Tyr fluorescence into spectra is minimal. The polarizers in the excitation and emission paths were set at the "magic" angle (54.7^{o} from the vertical orientation) and vertically (0^{o}), respectively, in order to reduce Wood's anomalies from the reflecting holographic grating. Steady-state CD measurements were carried out on a MOS-450 spectrometer (Bio-Logic, Inc.) under temperature control. The CD spectra were recorded from 185 nm to 270 nm. All measurements were performed at 25^{o}C unless otherwise indicated.

OCD measurements

For oriented circular dichroism measurements we prepared the supported bilayer on quartz slides with spacers of 0.2 mm thickness on one side with special polish for far UV measurements (Starna). The cleaning slides included the following steps 1) soaking in cuvette cleaner solution for 5-10 min, 2) rinsing with de-ionized distilled water, 3) sonicating for 10 min in 2-propanol, 4) sonicating in acetone, 5) sonicating in 2-propanol once again, 6) rinsing with de-ionized water, 7) soaking for 30 min, first, in 30% hydrogen peroxide, 8) and, later, in 70% sulfuric acid, 9) rinsing with Milli-Q purified water. A POPC lipid monolayer was deposited on a quartz substrate by the Langmuir-Blodgett (LB) method using (KSV minitrough). For the LB deposition, a clean wet slide was immersed vertically into the clean subphase (Milli-Q purified water kept at 25 °C) of a Langmuir-Blodgett trough. Then small amount of POPC lipid in chloroform was spread on the surface of the subphase and allowed solvent to

evaporate for about 20 min. Next the monolayer was compressed to 32mN/m. When the surface pressure was stabilized the slide was pulled out form the subphase with speed of 10 mm/min. The second layer was created by fusion with POPC vesicles. About 60 μl of LUV vesicles (100 nm in diameter, lipid concentration of 2 mM) was spread on the slides for 30 min, then slides were rinsed carefully and filled with pH 4 phosphate buffer (80 μl of buffer for each slide).The slides were stacked together while filling with the buffer to have a complete set of 12 slides (24 bilayers). The spacers between slides kept them form the sticking to each other. The quality of the supported bilayers were accessed in separate experiment by using fluorescent vesicles for fusion, and analyzing roughness of the obtained supported bilayer under the fluorescent microscope (Olympus IX71). Once the blank OCD spectrum was measured the slides were carefully disassembled and filled with phosphate buffer pH4 containing 10 μM pHLIP peptide and the OCD spectrum of the sample was recorded. The blank spectrum was subtracted from the sample spectrum to get final line presented in Figure 1b supplementary information.

Stopped-flow fluorescence and CD measurements

The stopped-flow fluorescence and CD measurements were carried out on a SFM-300 mixing apparatus connected to a MOS-450 spectrometer (Bio-Logic, Inc.) under temperature control. The FC-20 and TS-100/15 observation cuvettes were used for the fluorescence and CD measurements, respectively. All solutions were degassed several minutes under vacuum before loading into the syringes to minimize air bubbles. The pHLIP was pre-incubated with POPC at pH8.0 to reach equilibrium and folding/insertion was induced by fast mixing (5.7 ms dead time) of equal volumes of

pHLIP-POPC pH8 and appropriately diluted HCl, to obtain a drop of pH from 8 to 4. In the unfolding experiments, pHLIP was pre-incubated with POPC at pH8.0, then HCl was added to lower the pH to 4.0, and time was allowed for equilibration (minutes). Unfolding was induced by mixing equal volumes of pHLIP-POPC pH4 and NaOH diluted to increase the pH from 4 to 8. The concentration of the peptide (7 μM), lipids (1 mM) and mixing conditions (6.5 ml/sec flow of each solution) were optimized to ensure i) the proper rapid mixing of the entire volume of the sample to get the target changes of pH (from pH8 to pH4 and vice versa); ii) the best signal to noise ratio and iii) the minimal disruption of liposomes, which was assessed by changes of the scattered light signal. At the peptide: lipid ratio of 1:142 we used in these experiments, the equilibrium binding strongly favors the membrane-bound state II (by 6-7 kcal/mol according to our previously published thermodynamic studies[11]). Changes of the pHLIP fluorescence signal were recorded through a 320 nm cutoff filter using an excitation wavelength of 280 nm. The fluorescence signal, recorded over 80 sec, was corrected for photobleaching. Changes of the scattered light signal from the liposomes were recorded through the 320 nm cutoff filter using an incident wavelength of 320 nm. Each kinetic curve was recorded several times and then averaged, excluding the first 3-4 shots. The shift of the entire fluorescence spectrum during folding/unfolding was also recorded in a global mode using an emission monochromator, with an excitation wavelength of 275 nm to minimize scattered light at short wavelengths (in a separate experiment the spectra were recorded with 280 nm of the excitation wavelengths). Each spectrum was recorded several times and averaged. All spectra were corrected for the spectral sensitivity of the instrument by

comparing the spectrum of a tryptophan solution obtained with the same instrument with a standard tryptophan spectrum. In a control experiment, the signal was measured from the liposomes in the absence of peptide. At an excitation of 275 nm the scattering signal was insignificant, even at short wavelengths of the spectra.

The most challenging measurement was to monitor the changes of the CD signal (at 225 nm), which occurred ~100 times faster than the fluorescence changes. About 15-20 shots were performed and signals were averaged. The sensitivity might be enhanced by increasing the peptide concentration. However, there are two serious obstacles to such an approach: i) at high peptide concentration the equilibrium in solution is shifted toward aggregated forms, which might differently interact with the lipid bilayer; ii) any increase of the peptide concentration must be accompanied with an increase of lipid concentration to fully favor the bound state and minimize amount of the unbound peptide, but high liposome concentrations result in the appearance of significant light scattering, which interferes with the CD signal. To reduce light scattering, small POPC vesicles (~50 nm in a diameter) were used in the study. In a separate experiment we confirmed that there is no significant difference between the fluorescence kinetics curves of pHLIP interacting with liposomes of 100 and 50 nm in diameter. In order to accurately establish the baseline in CD kinetics experiments, we recorded the signal alteration in response to the pH changes in a mode without triggering; in this mode the rapid changes could not be monitored and this mode was used only for the detection of the initial and final states of the process. Thus, the CD signal reproducibly varied from -5 to -14÷-15 millidegree and vice versa. The baseline and asymptotic values are important for accurate fitting of the experimental data.

Stopped-flow fluorescence measurements of the peptide insertion into the lipid bilayer were performed at various temperatures. All solutions were pre-equilibrated at each experimental temperature before the measurements.

Since the pHLIP peptide contains a Pro residue in the transmembrane part, we thought that proline isomerization might occur as part of the folding process. To test this possibility, a variant pHLIP was synthesized, where Pro was replaced by Ala. The steady-state fluorescence (excited at 295 nm) and CD spectra were measured in the absence of lipids at pH8.0 and in the presence of lipids at pH8.0 and 4.0. We observed that the mutated peptide forms some helical structure in solution, as might be understood from the role of proline as a helix breaker in some instances. The formation of helical structure is enhanced in the presence of vesicles. The fluorescence spectrum of the variant peptide in the presence of lipids at pH8.0 was blue shifted more (Lmax=338 nm) that for the normal membrane-attached state (Lmax = 342-343). Since replacement of the Pro residue led to alteration of the peptide-membrane interactions, we carried out experiments (folding/insertion) at various temperatures in the presence of prolyl isomerase (cyclophilin A), which catalyses the isomerization of Pro residues in peptides. pHLIP was preincubated with the cyclophilin A (Sigma) at a ratio of 1:100 for two hours before mixing with liposomes, and fluorescence (at various temperatures) and CD kinetics measurements were performed in presence of cyclophilin A. All data obtained were the same as in the absence of enzyme.

Data analysis

The kinetic equations were solved by integration of (1) in Mathematica 5 (Wolfram Research). Nonlinear least squares curve fitting procedures were carried out in Origin

7 and MatLab. The goodness-of-fit was assessed by the aadjusted R-square statistics (adjR^2) and root mean squared error (*RMSE*) according to the standard formula.

Figures for supplementary information

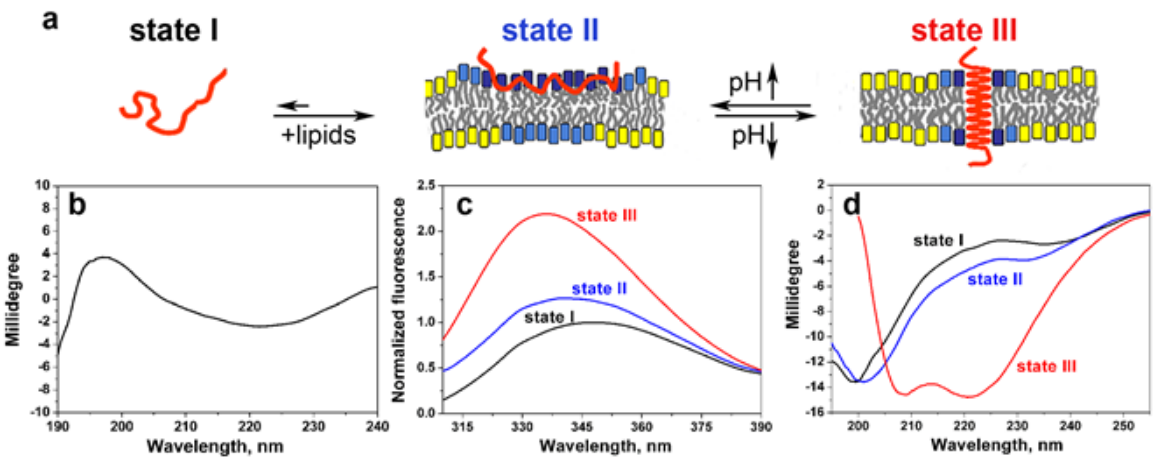

Figure 1 supplementary information

a) A schematic representation of pHLIP in solution and interacting with a lipid bilayer at neutral and low pHs. State (I) corresponds to the peptide in solution at normal and basic pHs. By addition of vesicles, the unstructured peptide is adsorbed on the membrane surface, raising the local concentration (State II). A drop of pH leads to the protonation of Asp residues, increasing peptide hydrophobicity, and resulting in the insertion and formation of a transmembrane alpha-helix (State III). Lipids interacting with the peptide directly are marked with blue head groups, lipids influenced by the interaction but not interacting with the peptide directly have cyan head groups, and lipids that are not involved in the interaction with pHLIP have yellow head groups. b) The transmembrane orientation of the helix has been confirmed by OCD. Transitions between states can be monitored by changes of fluorescence (c) and circular dichroism (CD) (d) spectral signals. The fluorescence and CD spectra of pHLIP at pH8 (black lines) indicate an unstructured configuration with tryptophan residues fully exposed to

solvent. Incubation of pHLIP with liposomes at pH8 (blue lines) induces the partial burial of tryptophan residues inside the lipid bilayer without helix formation. Decreasing the pH to 4.0 by the addition of HCl (red lines) induces the insertion of pHLIP and helix formation

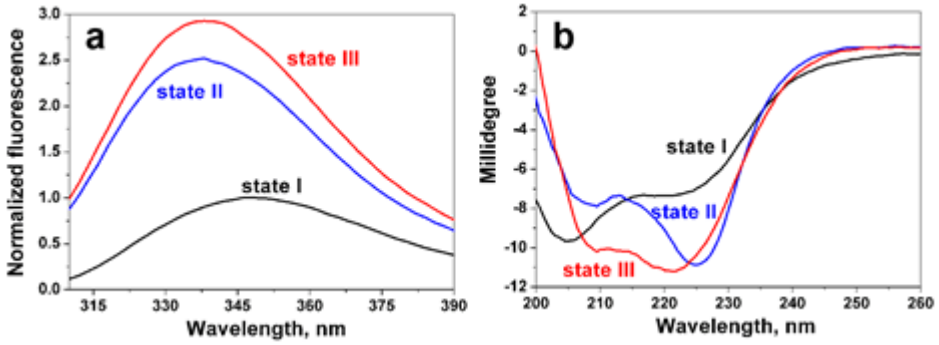

Figure 2 supplementary information

The fluorescence (a) and CD (b) spectra of variant pHLIP with the Pro located in the middle of the transmembrane part replaced by Ala. Spectra are presented at pH8.0 in the absence (black lines) and presence (blue lines) of vesicles and at pH4.0 in the presence of vesicles (red line).

CHAPTER 2

Published in Journal of Molecular Biology on

21th of October, 2011

Roles of Carboxyl Groups in the Transmembrane Insertion of Peptides

Francisco N. Barrera[1], Dhammika Weerakkody[2], Michael Anderson[2], Oleg A. Andreev[2], Yana K. Reshetnyak[2], Donald M. Engelman[1]

[1] Department of Molecular Biophysics and Biochemistry, Yale University, PO Box 208114, New Haven, CT 06520, USA

[2] Physics Department, University of Rhode Island, Kingston, RI 02881, USA

Research Highlights

pHLIP forms a TM helix at acidic pH. We mutate all aspartic acid residues. His residues do not prevent pH-dependent peptide membrane insertion. The number of residues that protonate correlates with insertion cooperativity.

Abbreviations

TM, transmembrane; wt, wild type; POPC, 1-palmitoyl-2-oleoyl-*sn*-glycero-3-phosphocholine; OCD, oriented circular dichroism; PEG, polyethylene glycol; pH, extracellular pH

Keywords

membrane protein folding; pHLIP; pH trigger; carboxyl titration; transmembrane helix

Abstract

We have used pHLIP® [*pH* (*l*ow) *i*nsertion *p*eptide] to study the roles of carboxyl groups in transmembrane (TM) peptide insertion. pHLIP binds to the surface of a lipid bilayer as a disordered peptide at neutral pH; when the pH is lowered, it inserts across the membrane to form a TM helix. Peptide insertion is reversed when the pH is raised above the characteristic pK_a (6.0). A key event that facilitates membrane insertion is the protonation of aspartic acid (Asp) and/or glutamic acid (Glu) residues, since their negatively charged side chains hinder membrane insertion at neutral pH. In order to gain mechanistic understanding, we studied the membrane insertion and exit of a series of pHLIP variants where the four Asp residues were sequentially mutated to nonacidic residues, including histidine (His). Our results show that the presence of His residues does not prevent the pH-dependent peptide membrane insertion at ~ pH 4 driven by the protonation of carboxyl groups at the inserting end of the peptide. A further pH drop leads to the protonation of His residues in the TM part of the peptide, which induces peptide exit from the bilayer. We also find that the number of ionizable residues that undergo a change in protonation during membrane insertion correlates with the pH-dependent insertion into the lipid bilayer and exit from the lipid bilayer, and that cooperativity increases with their number. We expect that our understanding will be used to improve the targeting of acidic diseased tissue by pHLIP.

Introduction

Extracellular acidification is a hallmark of different pathologies, including cancer, inflammation, ischemic stroke, and atherosclerotic plaques. Acidosis might be a useful biomarker for diagnosis or treatment if means can be found to target tissue acidity. We have found that a peptide derived from helix C of bacteriorhodopsin,[1] named pHLIP® [**pH** (**l**ow) **i**nsertion **p**eptide], is capable of targeting acidic tissues and inserting into the cell plasma membrane.[2] pHLIP is able to target mouse tumors **in vivo** with high specificity,[2] opening the possibility of its use for cancer imaging. Additionally, pHLIP has a promising therapeutic potential, as it is able to translocate cell-impermeable cargo molecules, such as organic dyes, peptides, peptide nucleic acids, and toxins, across the plasma membrane into the cytoplasm of tumor cells. [2 and 3] pHLIP itself does not have obvious acute toxicity in cells[3] or in mice.[2]

pHLIP is monomeric at low concentrations, with a mostly unstructured conformation in neutral and basic solutions (state I). If lipid vesicles or membranes are present at neutral pH, pHLIP binds to their external surface with an energy of 6–7 kcal/mol (state II).[4] In the membrane-attached state, pHLIP remains largely unstructured.[1] However, if the solution pH is lowered, pHLIP inserts to form a transmembrane (TM) α-helix (state III). The insertion is fully reversible and unidirectional, with the C-terminus being translocated across the membrane.[3] The p$\mathbf{K}_a$ of peptide insertion into lipid bilayers is 6.0, and the energy difference between the attached state and the inserted state is 1.8 kcal/mol at 37 °C.[4]

The pHLIP sequence is relatively rich in acidic residues (Table 1). At neutral pH, the combined negative charges of these residues, together with the carboxy terminus, constitute a large energetic barrier to pHLIP insertion across the membrane. The estimated energetic cost of the transfer of a single aspartic acid residue from water to the hydrophobic core of the membrane is unfavorable by 3.6 kcal/mol for the unprotonated (negatively charged) state, but only by 0.4 kcal/mol for the protonated (noncharged) state.[5] Simultaneously moving four charged Asp residues, one Glu residue, and the carboxy terminus into the membrane would cost 21.6 kcal/mol, assuming 3.6 kcal/mol for each carboxyl group, and peptide partitioning into the membrane at equilibrium would be about $1{:}10^{16}$. Thus, for pHLIP to be able to insert into membranes, protonation of a large fraction of the acidic residues can be expected, and knowledge of the protonation pattern of the acidic residues of pHLIP is an essential part of understanding the molecular mechanism of the membrane insertion process for any peptide containing carboxyl groups. Two classes of carboxyl groups are of interest: those that remain buried in the membrane after pHLIP is inserted into the membrane and those that traverse the hydrophobic core of the membrane during insertion.[6] Accordingly, we have studied both the pH-driven membrane insertion and the exit process for a series of peptides where the key aspartic acid residues are sequentially mutated.

Results

Previous studies in our laboratories revealed that sequence variations in the TM region of pHLIP can disrupt the delicate balance that preserves its water solubility. For example, a simultaneous change in the two aspartic acid residues at positions 14 and 25 to the homologous glutamic acid (Asp14/25Glu) resulted in a loss of pH-dependent membrane insertion due to aggregation of the peptide in aqueous solution[7] (we have recently developed new pHLIP variants with several Glu residues, which preserve pH-dependent properties; unpublished data). In order to reduce the likelihood that the introduced variations in the peptides used in this work could cause aggregation, we decided to follow a dual strategy to increase their water solubility: (i) we added an Asp tag to the N-terminus (noninserting end) to increase the number of charges in the molecule, which typically improves the solubility of hydrophobic peptides[8 and 9]; this resulted in the replacement of the N-terminal sequence AAEQ with DDDED (Table 1); and (ii) we used the TANGO algorithm[10] to define the region of the pHLIP sequence with the highest aggregation tendency and found this to be the stretch from residue 21 to residue 30 (coinciding with the most hydrophobic region of the peptide). We then mutated Leu26 to Gly, which greatly reduced the predicted aggregation tendency.

We incorporated these modifications into a series of pHLIP variants, where four aspartic acid residues were sequentially mutated to nonacidic polar residues. The aspartic acid residues at the C-terminus of the peptide that transitorily traverse the core of the membrane upon insertion (Asp31 and Asp33) were replaced with polar but

uncharged asparagine residues. On the other hand, for the Asp residues that are located in the core of the membrane after insertion (in positions 14 and 25), histidine was chosen as the replacement residue, as it is expected to be partially charged at neutral pH (thus improving water solubility) while being only slightly polar in its uncharged state (the transfer energies from water to the bilayer interior are 0.43 and 0.11 kcal/mol for the neutral forms of Asp and His,[5] respectively) so that the insertion properties of pHLIP may not be altered. The peptides were named D0–D3 according to the number of aspartic acid residues present in the regions of interest (TM and C-terminus; the positively charged N-terminus is not expected to interact with the membrane). For the variants with three aspartic acids, two alternatives were studied: one that kept Asp14 (D3a peptide) and the other that kept Asp25 (D3b peptide).

We conducted experiments to test the state of the variants in solution, where pHLIP is largely found as an unstructured monomer.[11] Sedimentation velocity experiments were conducted to determine the oligomerization state of the different peptide variants in aqueous buffer. Previous analysis of wild-type (wt) pHLIP (at 7 μM in 10 mM phosphate buffer and 100 mM NaCl, pH 8)[11] showed that pHLIP is mostly monomeric, but a small oligomer population is observed (~ 6%). We performed our sedimentation velocity experiments under the same conditions, but without NaCl in the solution. For each peptide, we observed a peak with a sedimentation coefficient of 0.72 ± 0.12 S (Table 2 and Fig. 1), which corresponds to a molecular mass of 3.4 ± 0.8 kDa. This is in agreement with the expected monomer masses of the different peptides (4126 Da for wt and ~ 4300 Da for the different variants), with the differences being ascribed to shape effects from the extended peptide. In the case of

D1 and D0, a minor peak with a sedimentation coefficient of 3.3 ± 0.3 S was also observed. This component represents $5 \pm 2\%$ of the total population, and its sedimentation coefficient corresponds to a molecular mass of 43 kDa (roughly consistent with the presence of an octameric or decameric particle). Comparison of our results with the previous report for wt suggests that the presence of oligomers is reduced at lower ionic strength. For the particular case of the D1 and D0 peptides, they seem to have a slightly higher oligomerization tendency in solution, but they are still 95% monomeric. Thus, our results suggest that all the peptide variants remain soluble and are essentially monomeric. For the rest of the experiments, we employed peptide concentrations (1.5–5 μM) lower than that used for sedimentation analysis (7 μM); thus, the level of oligomers present for D1 and D0 is expected to be lower.

Fluorescence spectra of the peptides in aqueous solution at neutral pH showed that, in all cases, the emission maximum is centered around 347–349 nm (Fig. 2, black lines, and Table 2), indicating that the two tryptophan residues of the peptides are largely exposed to aqueous solution, as in fully unfolded proteins, and consistent with the slightly low sedimentation coefficient. This finding represents an improvement over the previously studied Asp14/25Glu mutant peptide, where peptide aggregation shifts the emission maximum to 342 nm in buffer at pH 8.[7] A similar fluorescence maximum was also observed for the Asp14/25Asn mutant under the same conditions.[2] The presence of mostly unstructured species in aqueous solution for each of the studied peptides was confirmed by circular dichroism (CD) experiments, since the observed CD spectra were characterized by a minimum at 203 nm (Fig. 3, black lines), as observed for pHLIP in state I.

The two lipid-interacting states of the pHLIP variants were then examined: state II, where wt pHLIP is mostly unstructured and attached at the bilayer surface, and state III, where wt pHLIP forms a TM helix at low pH.[1 and 6] Fluorescence experiments in the presence of 1-palmitoyl-2-oleoyl-**sn**-glycero-3-phosphocholine (POPC) liposomes revealed that for the two D3 variants, the characteristic fluorescence signatures for states II and III were evident: (i) in the presence of liposomes at neutral pH (Fig. 2, blue lines), the fluorescence emission maxima of the peptides were slightly shifted from 348.7 ± 1.0 to 346.2 ± 1.2 nm, accompanied by a small fluorescence increase (Table 2); and (ii) when the pH was lowered to pH 4, we observed a large fluorescence increase and a spectral blueshift to 336.2 ± 1.1 nm (red lines), which are typically observed when the Trp side chain is buried in the membrane hydrophobic core. To complement the fluorescence data, we performed CD experiments under the same conditions (Fig. 3). The CD signature of the pHLIP membrane insertion process consists of the appearance of the characteristic signals associated with the formation of α-helix: minima at 208 and 222 nm and positive ellipticity at 190 nm. Both D3 variants showed spectral changes very similar to those observed for wt upon acidification. Thus, we concluded that replacement of one of the Asp residues in the TM region of the peptide does not lead to changes in the peptide's ability to interact with the membrane in a pH-dependent manner.

The D2 variant, where both Asp residues are replaced by His residues, also demonstrates a pH-dependent membrane interaction. However, the spectral pattern is slightly different from those for wt and D3 variants: the fluorescence intensity of D2 in the presence of POPC decreases in the pH range 8–6, with no significant changes in

the spectral maximum at pH 8–7 and with a small shift to lower wavelengths at pH 6 (Fig. S1). The amount of the helical structure of D2 at neutral pH is slightly higher than those of wt and D3 (Fig. 2 and Table 2), while no change is seen in the pH range 8–6. As an explanation, we suggest that D2 partitions somewhat more deeply into the membrane lipid bilayer than wt and D3 at neutral pH values, since His residues are expected to be only partially charged at neutral pH values, enhancing the hydrophobicity of the peptide TM and its affinity for the lipid bilayer. The decrease in fluorescence signal in the pH range 8–6 might be attributed to the partial quenching of emission of at least one of the Trp residues by one of the partially protonated His residues. At the same time, at neutral pH values, the peptide C-terminus containing four negative charges (two Asp, one Glu, and the C-terminus) does not partition into the membrane, keeping the peptide at the membrane surface. A further drop of the pH to pH 3–4 is associated with a fluorescence spectral maximum blueshift, an increase in fluorescence intensity (Fig. 2), and the appearance of a more pronounced negative band at 222 nm on CD spectra (Fig. 3), which is usually an indication of peptide insertion into the bilayer.[1] Reduction of pH leads to the protonation of negatively charged groups at the C-terminus and peptide insertion into the membrane. At the same time, we expect that protonation of His residues at low pH should occur; this might lead to the peptide's exit from the lipid bilayer or, alternatively, the formation of a pore channel in the lipid bilayer, where positively charged His residues would be pointed toward the channel. Calcein encapsulation control experiments that rule out the formation of pores in the membrane by the D2 and D3 peptides were performed (Fig. S2). Thus, most probably, the p$\mathbf{K}_a$ for the protonation of His is shifted to very

low pH values when it is embedded in a lipid bilayer. We carried out fluorescence pH titrations to compare the behaviors of D2 and wt peptides at pH values lower than 3.5 (Fig. S3). While no fluorescence change was detected for wt at acidic pH values, we observed that an additional process was present for D2 (with an apparent p$\mathbf{K}_a$ of 2.5), characterized by a fluorescence decrease and a redshift of the spectral maximum, which might be associated with peptide exit from the lipid bilayer.

To establish the orientation of each helix in the membrane, we performed oriented circular dichroism (OCD) measurements in which the light beam is oriented perpendicular to the planes of a stack of oriented lipid bilayers containing the peptides of interest. Theoretical calculations and experimental data indicate that helices oriented with axes parallel with the membrane surface (perpendicular to the incident light) give CD signals distinctly different from those of helices oriented across the bilayer (parallel with the incident light).[12, 13 and 14] In the range of 190–240 nm, the peptide CD spectrum is dominated by π–π* and n–π* transitions.[15] The π–π* transition in a helix splits into three components, one of which gives rise to a negative Gaussian band near 205 nm, with its electric transition dipole parallel with the helical axis. When the incident light propagates parallel with the helical axis, the electric field vector is orthogonal to the 205-nm π–π* dipole transition, and there is no interaction between the electromagnetic wave and the dipole, leading to the disappearance of the negative band at 205 nm in a CD spectrum. Thus, when the supported bilayers are oriented perpendicular to the light propagation, a helix with a TM orientation will have a CD spectrum that contains a positive 190-nm band and a negative 225-nm band. If the helix adopts a membrane surface orientation on the supported bilayer, then

all transitions are seen, and the OCD spectrum is the same as for a peptide CD spectrum in solution, with randomly oriented helices. Our data clearly indicate that D2 adopts a TM orientation at pH 3.5–4.5, while increasing the pH leads to peptide exit and the appearance of a membrane surface orientation of the helix (Fig. 4). The OCD spectrum at pH 1.9 does not correspond to a TM helix. Thus, we conclude that the p$\mathbf{K}_a$ of both or at least one of the His residues is significantly shifted from 6.3–6.9[16] to a lower value (2.5) due to their location at the bilayer interface in state II, emphasizing the important influence of bilayer surface properties on the p**K** values of dissociating groups in interacting peptides. A similar trend was previously observed for peptides that insert into membranes **via** the deprotonation of His residues, [17 and 18] although the magnitude of the p$\mathbf{K}_a$ shift was smaller. However, large changes in p$\mathbf{K}_a$ are typically observed when the side chains are in different environments, as the protonation of titratable amino acids depends on the dielectric properties of their environment.[19] A fitting example of large p$\mathbf{K}_a$ changes is found in the native environment of pHLIP, bacteriorhodopsin, where Asp14 and Asp25 have p$\mathbf{K}_a$ values of 7.5 and > 9, respectively,[20] significantly higher than the p$\mathbf{K}_a$ values of 3.7–4.0 found for fully solvated aspartic acid side chains.[16]

D1 has one less Asp residue at the C-terminus than D2. The slightly larger blueshift of fluorescence emission (Fig. 2) and the higher content of helicity observed in the presence of POPC at neutral pH values (Fig. 3) could be associated with an even deeper position of the peptide in the membrane. Fluorescence spectral blueshift and intensity increase, together with an increase in ellipticity at 222 nm, occur upon acidification; this might indicate protonation of Asp33, Glu34, and the C-terminus, as

well as peptide insertion into the lipid bilayer. The OCD spectrum obtained for D1 at pH 3.3 (Fig. 4) does not show a clear TM orientation of the helix: some decrease in ellipticity at 205–225 nm—which might indicate the existence of a mixture of TM and surface-parallel orientations of helices or the appearance of a significantly tilted TM helix—is observed. D0, in contrast to all other pHLIP variants described above, has a blueshifted maximum of fluorescence emission (Fig. 2) at neutral pH values in the presence of POPC, with a high content of helical structure (Fig. 3). Virtually no changes in spectral signal occur for D0 upon acidification (Figs. 2 and 3). The OCD data primarily reveal a surface orientation of the helix at low pH values (Fig. 4), as expected for a peptide with no aspartic acids.

To study the magnitude and directionality of the membrane insertion of the peptides, we used a biotin–avidin binding assay. A biotin moiety was attached to the C-terminus of each peptide. The level of binding to avidin was measured, and the protection of the biotin molecule from avidin interaction was used to assess the translocation of the peptide C-terminus into the liposome interior. The biotin moiety was linked to the C-terminal Cys of the peptides **via** a long polar polyethylene glycol (PEG) linker. The linker has a double purpose. It facilitates biotin access to the avidin binding site and—more critically for our experiments—helps to delineate between an intraliposomal location and an extraliposomal location of the biotin, since the polarity of the moiety makes a location inside the hydrophobic region of the bilayer unlikely. We quantified the amount of biotin that binds to avidin molecules present exclusively outside the liposomes (see Materials and Methods for details). We did not detect avidin binding to biotin for the D2 peptide at low pH (Fig. 5a) due to the biotin translocation across the

membrane, which complements our data (suggesting complete insertion of this peptide across the lipid bilayer) and confirms that the directionality of insertion is the same as for wt. Only partial translocation and no translocation of biotin across the membrane were seen for D1 and D0, respectively (Fig. 5a), in agreement with our results indicating partial (or tilted) insertion and no insertion into the lipid bilayer of D1 and D0, respectively. Additionally, the translocation of biotin (which can be considered as a cargo) across the membrane does not appear to significantly hinder the membrane insertion of the peptides. This might be explained by its small size (526 Da) and its moderate polarity ($\log \boldsymbol{P} = -1.4$; see Materials and Methods for details), which are both well within the range of cargo properties that pHLIP has been reported to effectively translocate.[21] However, as the biotin assay used here is responsive to changes in the level of binding to avidin present outside of the liposomes, we cannot rule out the possible influences of different processes such as peptide aggregation, although we have no reason to suspect them.

How does the number of carboxyl groups affect the p$\boldsymbol{K}$ and cooperativity of insertion? We monitored the pH-induced changes in the position of the fluorescence emission maximum of the peptides, which provide details about peptide insertion into the lipid bilayer, in the presence of POPC (Fig. 6). A plot of the positions of the spectral maxima follows a sigmoid behavior as a function of pH, corresponding to the transition between the interfacial state and the inserted state for all variants (except for D0). Fitting the experimental data provides the two main parameters that describe the insertion process: p$\boldsymbol{K}_a$ and cooperativity (**m**). The p$\boldsymbol{K}_a$ of membrane insertion obtained for wt pHLIP is 5.94 ± 0.09, which is in agreement with previous reports. [1 and 7] For the

different variants, shifts of the p$\boldsymbol{K}_a$ to lower values (~ 5.2) were detected (Fig. 7a). The reason for this decrease is unclear, but it might be related to the lower number of aspartic residues or to the presence of histidines in the TM region of the pHLIP variants. We do not think that the N-terminal DDDED sequence will influence the p$\boldsymbol{K}_a$ values of the peptides in our study, since its polarity should preclude hydrophobic interaction with the lipid bilayer; thus, it is not expected to be involved in the insertion process. However, we cannot rule out that it might reduce the overall membrane affinity of the peptide. While the p$\boldsymbol{K}_a$ values for the variants changed very little, we observed a gradual decrease in the cooperativity of the insertion process (**m** parameter) for peptides with fewer Asp residues, as the titration occurred progressively over a wider pH range (~ 1 pH unit for wt and ~ 2 pH units for D1) (Figs. 6 and 7b). Our data indicate that the cooperativity of insertion is linked to the number of protonatable residues. Cooperativity and p$\boldsymbol{K}_a$ might also respond to the position of protonatable groups in the peptide sequences and their proximity to each other. When pHLIP is at the surface of the vesicle and the pH is lowered, the protonation of one Asp residue might facilitate the protonation of other protonatable residues, shifting their p$\boldsymbol{K}_a$ values. The protonation of the first Asp residue might induce partial insertion of the peptide into the membrane. In this scenario, the protonation of the neighboring Asp residues would be energetically favored to shield the negative charge (i.e., the p$\boldsymbol{K}_a$ value of the neighboring Asp is shifted to higher values in a more hydrophobic environment) and then a positive feedback would be established, triggering membrane insertion.

How do the number and the location of Asp residues affect peptide exit from the membrane? The CD and fluorescence changes associated with wt pHLIP lipid insertion at acidic pH are completely reversible.[11] Here we also followed changes in the CD and fluorescence signals and in the reversibility of biotin translocation across the membrane. The ellipticity increase associated with each peptide insertion into the membrane was found to be essentially reversible for wt and D3b (Fig. 3, broken blue lines overlap with continuous blue lines), while for D3a, D2, and D1, the reversibility was only partial. Since changes in the CD signal upon acidification for D2–D0 are less pronounced than those for wt and D3, the reversibility of the D2–D0 membrane insertion was also assessed by changes in the fluorescence signal (Fig. S4). It is interesting to note the different levels of reversibility of the two D3 peptides: the insertion process is significantly more reversible in D3b (90%) than in D3a (70%) (Fig. 5b), suggesting nonequivalence of the two buried positions. We observed an overall linear relationship between the number of aspartic acid residues interacting with the membrane and the degree of α-helix formation reversibility (Fig. 5b). The results obtained for the reversibility of the biotin translocation (exit process) were also in agreement (Fig. 5b).

An important consideration in the interpretation of the exit data is the time course of equilibration of the pH inside the liposomes, so we encapsulated the membrane-impermeable fluorescent probe 5(6)-carboxy-2′,7′-dichlorofluorescein in POPC liposomes to follow the pH changes. The fluorescence of the probe is pH-sensitive, with a p$\boldsymbol{K}_a$ of 5.1. When we varied the pH of the solution outside the liposomes, the fluorescence of the encapsulated probe changed in a sigmoid fashion, with an apparent

p$\boldsymbol{K}_a$ of 5.05 (data not shown). A relatively high proton permeation through unilamellar POPC liposomes in the minute timescale has been reported elsewhere. [22 and 23] On the other hand, our kinetic data suggest that the time of wt peptide exit (with two TM groups and four C-terminal protonatable groups) is in the range of milliseconds.[6] Thus, peptides exit from the lipid bilayer much faster such that the pH is completely equilibrated inside the liposomes and, most probably, C-terminal residues cross the membrane in their noncharged form. The question is: 'Why is the reversibility of D3a, D2, and, to some degree, D1 only partial?' To provide an explanation, we take into account the location of the Asp residues. For the peptide exit from the lipid bilayer to take place, the deprotonation of Asp residues must energetically destabilize the inserted state. Destabilization of the inserted state is mainly caused by the charges resulting from the deprotonation of groups deeply buried in the hydrophobic core of the membrane. Therefore, the exit of wt and D3b, which have two Asp or one Asp in the hydrophobic core of the membrane, is fully reversible. The reason for the difference in peptide insertion reversibility between D3a and D3b might be related to the presence of an arginine residue at position 11. Accordingly, the deprotonation of Asp25 in D3b would strongly destabilize the membrane-inserted state due to the presence of a negative charge in the hydrophobic core of the membrane, favoring the exit process. However, the negative charge of Asp14 in D3a might be forming a salt bridge with the neighboring side chain of Arg11, which would result in a weaker destabilization of the inserted state. Another potential explanation is an altered position of the TM domain, which was mentioned above. There is a possibility that the TM domain in variants is shifted toward the C-terminal residues, leading to a greater

exposure of the amino acid in position 14 (with His in D3a) to the aqueous environment and a shift to the hydrophobic core of amino acids at positions 31 and 33. As a result, the deprotonation of His14 in D3a might be associated with less destabilization of the helix than deprotonation of His25 in D3b. The side chains of Asp31 and Asp33 most probably are interacting with the headgroup region of the bilayer. The destabilization energy associated with their deprotonation is not enough to cause a complete exit from the membrane. Our results suggest that the deprotonation of acidic residues located in the hydrophobic core of the membrane ensures complete exit of the peptide.

Discussion

We have previously observed that even conservative changes in the pHLIP sequence can lead to peptide aggregation in solution at neutral pH.[7] Our results show that all the peptides in this study are soluble in solution, being essentially monomeric (the addition of a D-tag at the N-terminus and the L26G mutation appear to favor peptide solubility). Spectral data obtained with D3–D0 peptides indicate that the lower is the number of negatively charged groups in the peptide sequence, the deeper are the peptide partitions into a lipid bilayer and the greater is the helicity. At the same time, TM orientation (at least for the D3–D2 peptides) requires protonation of the Asp/Glu residues and the terminal carboxyl group at the C-terminus, which can readily go across a membrane in its noncharged form. We confirmed our previous finding[2] suggesting that TM Asp residues are not essential for peptide insertion. Interestingly, we have observed here that membrane insertion upon acidification occurs in our peptides in the presence of two His residues in the predicted TM region. Histidines

have been used in the past to drive the insertion of peptides into membranes at neutral pH values.[17 and 18] However, in these examples, acidic residues were completely absent in the sequence. For the peptides described in this article, the establishment of states II and III is driven by acidic residues. Since the protonated (charged) state of the side chains of His14 and His25 in the hydrophobic core of the membrane would be energetically very unfavorable, in the peptides, their p$\boldsymbol{K}_a$ values are expected to shift to lower values in the membrane-inserted state (favoring the unprotonated state). Further acidification eventually causes their protonation, resulting in a strong destabilization of the inserted TM helix and peptide exit. We cannot rule out that the diminished membrane insertion of the D1 and D0 peptides might be influenced by the hydrophobicity change concomitant to the Asp-to-Asn mutations at the C-terminus. The free energy of membrane transfer of the Asn side chain is 0.42 kcal/mol, which is a less favorable value than the free energy of transfer of the neutral state of Asp (− 0.07 kcal/mol)[5]; thus, the membrane translocation of the C-terminus would be less favorable. A similar effect might occur in the insertion reversibility of D1.

We conclude that protonation of negatively charged residues located in the TM or in the C-terminal inserting end must occur in order to preserve the pH-dependent ability of pHLIP to interact with the membrane. These residues act as switches for pHLIP membrane insertion, as the negative charges of their side chains block membrane insertion. Acidification causes the protonation of these side chains, resulting in an increase in the overall hydrophobicity of the peptide, which leads to TM helix formation, shielding the hydrophobic residues of pHLIP from water molecules. When the pH is raised to near neutrality, the negatively charged state of the carboxyl groups

is again favored, decreasing the peptide hydrophobicity and resulting in exit from the TM position. Peptide exit from the lipid bilayer is completed when deprotonation of Asp/Glu residues located in the hydrophobic core of the membrane occurs and the TM helix is destabilized.

The knowledge gained from our experiments can be used as a guide to improve the imaging and therapeutic properties of pHLIP. For the specific case of tumor targeting, the pHLIP insertion characteristics should be finely tuned to exploit the low extracellular pH (pH_e) of tumors. Tumor targeting by wt pHLIP conjugated to a Cu^{64}–1,4,7,10-tetraazacyclododecane-1,4,7,10-tetraacetic acid chelate for positron emission tomography imaging correlates with the pH_e of tumors, where the contrast index was higher for LNCaP tumors (pH_e 6.78 ± 0.29) than for PC-3 tumors (pH_e 7.23 ± 0.10[24]). Thus, pHLIP variants where Asp14/Asp25 were replaced by Glu, with a higher pK_a ($pK_a = 6.5$),[7] might be more effective for targeting tumors with higher pH_e values. Our present results suggest that the number of Asp residues in the TM region can also modulate the pK_a value. Thus, a peptide containing an extra Asp in the TM region might have a higher pK_a and might be directed to tumors more effectively. Another important factor to be considered is the broadness of the pH transition of the peptide, which is dictated by the cooperativity of the transition. On one hand, for the case where the peptide pK_a is lower than the tumor pH_e but the transition is broad (**m** value is low), a significant part of the pH transition could intercept the pH_e value, resulting in a significant pHLIP tumor insertion. However, such a scenario will also lead to more accumulation in healthy tissue. Since it is usually desirable to have a high tumor/organ ratio, an insertion transition of high cooperativity might be best. This

would ensure greater differentiation between the amount of inserted peptides and the amount of noninserted peptides over a narrow range of pH values, favoring selective tumor targeting, since the difference in pH between normal tissue and cancerous tissue may be only 0.5–0.7 units. However, we must bear in mind that the measured pH_e provides an indication of the average acidity outside the cell for a given tumor and can vary between different tumor regions. Furthermore, pH_e may not reflect the precise pH on the exterior surface of the cells, since the cells pump protons to the extracellular medium and ΔpH will lead to proton accumulation at the membrane surface.[25] Another feature that is expected to shift the equilibrium toward the membrane-inserted form is the presence of Asp/Glu residues at the C-terminus of the peptide. After being translocated across the plasma membrane into the cytoplasm, where the pH is neutral, these groups would be deprotonated. Since the translocation of charges across membranes is unfavorable, the inserted form would be stabilized.

pHLIP shows promise as a means of targeting cells in acidic tissues and delivering agents for therapy and imaging. At the same time, we are learning more about the binding and insertion of peptides at the membrane surface. Here we have shown that variation in the positions and numbers of carboxyl group titrations modulates the p***K*** and cooperativity of insertion.

Materials and methods

Peptide synthesis and assessment of monomeric state

Peptides were made by solid-phase synthesis, using standard 9-fluorenylmethyloxycarbonyl chemistry, at the W. M. Keck Foundation Biotechnology Resource at Yale University (New Haven, CT) and were purified by reverse-phase chromatography (C18 column, using a water/acetonitrile gradient in 0.01% trifluoroacetic acid). Purity was checked by matrix-assisted laser desorption/ionization time-of-flight mass spectrometry. Peptides were quantified by absorbance spectroscopy using a molar extinction coefficient of 13,940 M^{-1} cm^{-1}. Some peptides contain a single Cys residue in the C-terminus and thus have the potential to form intermolecular disulfide bonds, leading to the formation of dimers. To rule out the possibility that this might occur under our experimental conditions, we ran HPLC on peptide samples incubated (at room temperature for 3 h) at concentrations higher than those used in our experiments and in the absence and in the presence of POPC. No dimer band could be detected, and concentrations in the range of 0.1 mM peptide and overnight incubation were required to detect a significant amount of dimer (~ 10%). The peptides described in Table 1 were used in the experiments, except for some experiments with D2–D0, where a Cys-less version was employed (similar results were obtained for both results; data not shown).

Analytical ultracentrifugation

Sedimentation velocity experiments were performed at 25 °C in a Beckman Optima XL-I analytical centrifuge at 35,000 rpm. Peptides at a concentration of 7 μM were

dissolved in 5 mM phosphate buffer (pH 8) after 1 h of incubation at room temperature. Absorbance at 280 nm was used to monitor centrifugation, and analysis was performed using SEDFIT.[26]

Liposome preparation

The required amount of chloroform-dissolved POPC (Avanti Polar Lipids) was placed in a glass tube, dried with argon, and then held under vacuum overnight. The dried film was resuspended in water or 10 mM phosphate buffer (pH 8) and vortexed. Extrusion to make unilamellar vesicles was performed using a Mini-Extruder (Avanti Polar Lipids), with Nuclepore polycarbonate membranes of 0.1 or 0.05 μm pore size (Whatman). To obtain the final large unilamellar vesicles, we performed 15–25 extrusion steps, depending on the lipid concentration.

Fluorescence spectroscopy

Peptides were dissolved in 5 or 10 mM phosphate buffer (pH 8) and incubated with POPC vesicles prepared in water, resulting in a molar lipid/peptide ratio of 250:1. The incubation time with POPC liposomes varied from 90 min to 18 h. The pH of the samples was adjusted with a 10 mM concentration of the buffers for the indicated pH ranges (H_3PO_4, pH 1.0–3.5; sodium acetate, pH 3.5–5.5; Na_2HPO_4/NaH_2PO_4, pH 5.5–8.0; sodium borate, pH 8.0–10.5) or by addition of concentrated HCl. The final peptide concentration was varied from 1.5 to 5 μM in different experiments. Emission spectra were measured in SLM-Aminco 8000C and PC2 ISS spectrofluorometers at

room temperature (controlled temperature), with excitation at 295 nm. The appropriate blanks were subtracted in all cases.

For determination of spectral maxima, we used the FCAT mode of the PFAST software, which fits the experimental spectra to log-normal components.[27 and 28] The spectral maxima values for each point of the pH curve were plotted and analyzed according to[29]:

$$F = \frac{\left(F_a + F_b 10^{m(pH-pKa)}\right)}{(1+10^{m(pH-pKa)})} \qquad \text{Equation(1)}$$

where $\boldsymbol{F}_a = (\mathbf{f}_A + \mathbf{S}_A pH)$ and $\boldsymbol{F}_b = (\mathbf{f}_B + \mathbf{S}_B pH)$; $\mathbf{f}_A$ and $\mathbf{f}_B$ are the spectral maxima for the acidic and basic forms, respectively; $\mathbf{S}_A$ and $\mathbf{S}_B$ are the slopes of the acidic and basic baselines, respectively; and **m** is the cooperativity parameter. Fitting by nonlinear least squares analysis was carried out with Origin software.

Circular dichroism

Samples were prepared as in the fluorescence experiments, but the final molar lipid/peptide ratio was 300:1, with the final peptide concentration varying from 2 to 5 μM. CD spectra were recorded in Jasco J-810 and MOS450 Biologic spectropolarimeters interfaced with a Peltier system. Spectra were recorded at 25 °C using 2- or 5-mm cuvettes, the scan rate was 50 nm/min, and 10–30 averaging steps were performed. Raw data were converted into mean residue ellipticity according to[30]:

$[\Theta]=\Theta/(10\boldsymbol{lcN})$

where Θ is the measured ellipticity, $\boldsymbol{l}$ is the path length of the cell, $\boldsymbol{c}$ is the protein concentration, and $\boldsymbol{N}$ is the number of amino acids.

For the study of membrane attachment, insertion, and its reversibility, the typical procedure was as follows: The samples were incubated with POPC vesicles at pH 8 for 90 min, the spectra were recorded, the pH was lowered to 4.0, and the measurements were performed after 30 min. Finally, the pH of the sample was increased with sodium borate buffer (pH 10.2) to a final pH of 7.5. After 30 min, 90 min, and 24 h, the spectra were recorded, and similar results were obtained in all cases. The degree of reversibility was established from the recovery of the signal at 222 nm. The final buffer concentration for the different experiments was in the range of 3–15 mM. Appropriate blanks were subtracted in all cases.

OCD measurements

For OCD measurements, supported bilayers were prepared on quartz slides with 0.2-mm-thick spacers on one side and with a special polish for far-UV measurements (Starna). Slides were cleaned by sonication for 10 min in cuvette cleaner solution (Decon Contrad 70, 5% in water), 2-propanol, acetone, and 2-propanol, and rinsed with deionized water. Then the slides were immersed in a mixture of concentrated sulfuric acid and hydrogen peroxide (3:1) for 5–10 min to completely remove any remaining organic material from the slides. The slides were then thoroughly rinsed with and stored in deionized water (Milli-Q purified water kept at 25 °C). A POPC lipid monolayer was deposited on a quartz substrate by the Langmuir–Blodgett

method using a KSV mini-trough. For the Langmuir–Blodgett deposition, a cleaned slide was vertically immersed in the clean subphase (Milli-Q purified water kept at 25 °C) of a Langmuir–Blodgett trough. A POPC lipid solution in chloroform was spread on the subphase, and chloroform was allowed to evaporate for about 30 min, followed by monolayer compression to 32 mN/m. The first layer was deposited by retrieving the slide from the subphase at a rate of 15 mm/min. The second layer of the bilayer was created by fusion. For this step, the monolayer on the slide was incubated with a solution of POPC vesicles (50 nm in diameter, obtained by extrusion) mixed with peptide solution at the required pH (0.5 mM POPC and 10 μM peptide). The fusion occurred for about 6 h under 100% humidity. Then, excess vesicles were carefully removed, and the slides were stacked to make a pile while filling up the spaces between them with a peptide solution (5 μM) at the required pH. The bilayers with the peptide solution were allowed to equilibrate for about 6 h. Measurements were taken in three steps during the process: when the monolayers were incubated with an excess of liposomes, soon after the spaces between the bilayers had been filled with the peptide solution and 6 h after the second measurement. Fourteen slides (28 bilayers) were assembled, and the OCD spectrum was recorded on a MOS-450 spectrometer at a sampling time of 2 s.

Biotin translocation assay

HABA dye (4′-hydroxyazobenzene-2-carboxylic acid) binds to avidin at a 1:1 stoichiometry and absorbs at 510 nm only in the avidin-bound state. This interaction is strongly displaced by the binding of biotin to avidin, resulting in a quantitative

reduction in HABA absorbance. This property was used to probe the location of the C-terminus of different peptides with regard to the liposome (inside or outside) (method modified from Nicol **et al.**[31]). The C-terminus of each of the peptide variants was labeled with biotin (see the text below). The rationale for the assay is that pH-driven insertion of the C-terminus would result in biotin translocation inside the liposome, causing shielding of the biotin from the medium outside the liposome, where a preformed HABA/avidin complex (Thermo Scientific) is added. If the biotin is inside the liposome, no change in absorbance is expected. On the other hand, if pHLIP lies at the exterior surface of the liposome, the C-terminal biotin would be accessible to the solution outside the liposome (as the biotin group is polar, it is expected not to be protected by the membrane) and would be able to bind to avidin and displace the HABA/avidin complex, with a consequent reduction in absorbance at 510 nm. Liposomes were prepared in 150 mM NaCl, and ionic strength was carefully maintained during all steps to avoid liposome osmotic shock. Biotin-labeled peptides were incubated in the presence of POPC at pH 8 for 2 h at room temperature (150:1 lipid/peptide ratio). For studies of C-terminal translocation, acetate buffer was added to the samples, resulting in a final pH of 4.3 prior to 1 h of incubation with the peptide. The HABA/avidin complex was added to the solution only after the final conditions had been established. The final peptide concentration for the measurement conditions was 3 μM. To determine the reversibility of the biotin translocation, we increased the pH by the addition of 10 mM sodium borate buffer (pH 10.2) to give a final pH of 7.4. Absorbance was measured after 1 h of incubation. For quantitation of the level of reversibility, the recovery of absorbance obtained for pHLIP labeled with

biotin at its C-terminus was taken as 100% reversibility, and that of pHLIP labeled at its N-terminus was taken as 0%.

Peptides were labeled at the C-terminal Cys residues using the membrane-impermeable compound maleimide–PEG_2–biotin (Thermo Scientific), which has a long polar spacer arm of 29.1 Å to allow adequate biotin binding to avidin. The synthesis reaction was performed in 10 mM phosphate buffer (pH 7.5; overnight incubation at 4 °C). Reaction products were purified by HPLC, and the mass of the biotin-labeled peptides was checked by matrix-assisted laser desorption/ionization time-of-flight mass spectrometry. The octanol/water partition coefficient of maleimide–PEG_2–biotin was determined experimentally by measuring the absorbance at 300 nm in the aqueous and octanol (previously preequilibrated with water) phases after 2 h of vortexing. A log***P*** value of − 1.07 ± 0.02 was obtained. As this value does not take into account the chemical changes in the cross-linking reaction (formation of a thioether bond between the maleimide moiety and the Cys side chain), the QikProp 3.0 software was employed to predict the log**P** value of the reacted form, resulting in a value of − 1.4, which is in the range of molecules that can be translocated by pHLIP.[21]

Acknowledgements

The authors are thankful to Miriam Alonso, Ming An, Justin Fendos (Yale University), and José Luis Neira (Universidad Miguel Hernández) for stimulating discussions and insightful comments on the manuscript. D.M.E. was supported by National Institutes of Health grant GM073857-04. O.A.A., D.M.E., and Y.K.R. were

supported by National Institutes of Health grant CA133890-03. F.N.B. was the recipient of a postdoctoral fellowship from the Fundación Alfonso Martín Escudero.

References

1. Hunt, J. F., Rath, P., Rothschild, K. J. & Engelman, D. M. (1997). Spontaneous, pH-dependent membrane insertion of a transbilayer alpha-helix. Biochemistry. 36, 15177-15192.

2. Andreev, O. A., Dupuy, A. D., Segala, M., Sandugu, S., Serra, D. A., Chichester, C. O., Engelman, D. M. & Reshetnyak, Y. K. (2007). Mechanism and uses of a membrane peptide that targets tumors and other acidic tissues in vivo. Proc. Natl Acad. Sci. U. S. A. 104, 7893-7898.

3. Reshetnyak, Y. K., Andreev, O. A., Lehnert, U. & Engelman, D. M. (2006). Translocation of molecules into cells by pH-dependent insertion of a transmembrane helix. Proc. Natl. Acad. Sci. U. S. A. 103, 6460-6465.

4. Reshetnyak, Y. K., Andreev, O. A., Segala, M., Markin, V. S. & Engelman, D. M. (2008). Energetics of peptide (pHLIP) binding to and folding across a lipid bilayer membrane. Proc. Natl. Acad. Sci. U S A 105(40):15340-5.

5. White, S. H. & Wimley, W. C. (1999). Membrane protein folding and stability;Physical principles. Annu. Rev. Biophys. Biomol. Struct. 28, 319-365.

6. Andreev, O. A., Karabadzhak, A. G., Weerakkody, D., Andreev, G. O., Engelman, D. M. & Reshetnyak, Y. K. (2010). pH (low) insertion peptide (pHLIP) inserts across a lipid bilayer as a helix and exits by a different path. Proc. Natl. Acad. Sci. U. S. A 107, 4081-4086.

7. Musial-Siwek, M., Karabadzhak, A., Andreev, O. A., Reshetnyak, Y. K. & Engelman, D. M. (2009). Tuning the insertion properties of pHLIP. Biochim. Biophys. Acta. 1798(6):1041-6

8. Melnyk, R. A., Partridge, A. W., Yip, J., Wu, Y., Goto, N. K. & Deber, C. (2003) Polar residue tagging of transmembrane peptides. Biopolymers.71(6):675-85.

9. Cunningham, F. & Deber, C. M. (2007). Optimizing synthesis and expression of transmembrane peptides and proteins. Methods 41, 370-380.

10. Fernandez-Escamilla, A. M., Rousseau, F., Schymkowitz, J. & Serrano, L. (2004). Prediction of sequence-dependent and mutational effects on the aggregation of peptides and proteins. Nat. Biotechnol. 22, 1302-1306.

11. Reshetnyak, Y. K., Segala, M., Andreev, O. A. & Engelman, D. M. (2007). A monomeric membrane peptide that lives in three worlds: in solution, attached to, and inserted across lipid bilayers. Biophys. J. (7); 2363-72.

12. Kuyper C.L., Kuo J.S., Mutch S.A. & Chiu D.T. (2006) Proton permeation into single vesicles occurs via a sequential two-step mechanism and is heterogeneous. J. Am. Chem. Soc. 128(10), 3233-40.

13. Deamer D.W. & Nichols J.W. (1989). Proton flux mechanisms in model and biological membranes. J. Membr. Biol. 107(2),91-103.

14. Thevenin, D., An, M. & Engelman, D. M. (2009). pHLIP-mediated translocation of membrane-impermeable molecules into cells. Chem. Biol 16, 754-762.

15. Pace, C. N., Grimsley, G. R. & Scholtz, J. M. (2009). Protein ionizable groups: pK values and their contribution to protein stability and solubility. J Biol Chem. 284, 13285-13289.

16. Bechinger, B. (1996). Towards membrane protein design: pH-sensitive topology of histidine-containing polypeptides. J. Mol. Biol. 263, 768-775.

17. Ladokhin, A. S. & White, S. H. (2004). Interfacial folding and membrane insertion of a designed helical peptide. Biochemistry 43 (19):5782 -91.

18. Harms, M. J., Castaneda, C. A., Schlessman, J. L., Sue, G. R., Isom, D. G., Cannon, B. R. & Garcia-Moreno, E. B. (2009). The pK(a) values of acidic and basic residues buried at the same internal location in a protein are governed by different factors. J Mol. Biol 389, 34-47.

19. Lanyi, J. K. (2006). Proton transfers in the bacteriorhodopsin photocycle. Biochim. Biophys. Acta 1757, 1012-1018.

20. Vavere, A. L., Biddlecombe, G. B., Spees, W. M., Garbow, J. R., Wijesinghe, D., Andreev, O. A., Engelman, D. M., Reshetnyak, Y. K. & Lewis, J. S. (2009). A novel technology for the imaging of acidic prostate tumors by positron emission tomography. Cancer Res. 69, 4510-4516.

21. Bränden, M., Sanden, T., Brzezinski, P. & Widengren, J. (2006). Localized proton microcircuits at the biological membrane-water interface. Proc. Natl. Acad. Sci. U. S. A 103, 19766-19770.

22. Schuck, P. (2000). Size-distribution analysis of macromolecules by sedimentation velocity ultracentrifugation and lamm equation modeling. Biophys. J. 78, 1606-1619.

23. Burstein, E. A., Abornev, S. M. & Reshetnyak, Y. K. (2001). Decomposition of protein tryptophan fluorescence spectra into log-normal components. I. Decomposition algorithms. Biophys. J 81, 1699-1709.

24. Shen, C., Menon, R., Das, D., Bansal, N., Nahar, N., Guduru, N., Jaegle, S., Peckham, J. & Reshetnyak, Y. K. (2008). The protein fluorescence and structural

toolkit: Database and programs for the analysis of protein fluorescence and structural data. Proteins 71, 1744-1754.

25. Ionescu, R. M. & Eftink, M. R. (1997). Global analysis of the acid-induced and urea-induced unfolding of staphylococcal nuclease and two of its variants. Biochemistry 36, 1129-1140.

26. Kelly, S. M. & Price, N. (2000). The use of Circular Dichroism in the investigation of protein structure and function. Current Protein and Peptide Letters 1, 349-384.

27.Nicol, F., Nir, S. & Szoka, F. C., Jr. (1999). Orientation of the pore-forming peptide GALA in POPC vesicles determined by a BODIPY-avidin/biotin binding assay. Biophys.
J 76, 2121-2141.

Tables

Table 1. Sequence of the peptides.

wt[a]	AAEQNPIYWARYADWLFTTPLLLLDLALLVDADEGTCG
D3a[b]	*DDDED*NPIYWARYADWLFTTPLLLL**H***G*ALLVDADECT
D3b	*DDDED*NPIYWARYA**H**WLFTTPLLLLDGALLVDADECT
D2[c]	*DDDED*NPIYWARYA**H**WLFTTPLLLL**H***G*ALLVDADECT
D1[c]	*DDDED*NPIYWARYA**H**WLFTTPLLLL**H***G*ALLV**N**ADECT
D0[c]	*DDDED*NPIYWARYA**H**WLFTTPLLLL**H***G*ALLV**N**A**N**ECT
	14 25 31 33

[a] The pHLIP sequence is referred to as wt.

[b] The variant peptides are named by a D followed by the number of aspartic acid residues in the TM and C-terminal regions. Two different D3 peptides were studied, D3a and D3b, each with different transmembrane aspartic acid residues mutated. The acidic residues that are expected to interact with the hydrophobic core of the membrane at some stage of the insertion process (Asp 14, 25, 31 and 33, in red) were mutated to the polar residues marked in bold. The N-terminal Asp-tag and the Leu26Gly mutation are highlighted in italics. The transmembrane region of pHLIP was predicted, using the octanol scale[5], to be located between residues Ile7 and Leu29 (marked with inverted blue triangles). N- and C-terminus were not capped.

[c] A version of D2-D0 without cysteine were employed in experiments except of biotin translocation assay.

Table 2. Parameters describing the studied peptides.

	AUC [a]	Fluorescence					Circular Dichroism		
	Sed. Coef.	Spectral maximum, nm			Area curve		MRE 218 nm		
	State	State			State		State		
	I	I	II	III	II	III	I	II	III
wt	0.80±0.17[b]	347.7±0.6	347.2±1.6	336.7±0.1	1.04	2.10	-7.4	-7.4	-16.3
D3a	0.67±0.08	349.9±0.1	347.4±1.3	337.0±0.1	1.12	2.61	-7.6	-6.8	-15.4
D3b	0.66±0.09	349.1±1.0	345.5±0.7	334.6±0.2	1.08	2.11	-5.3	-6.1	-16.4
D2	0.84±0.16	348.2±0.1	344.9±1.4	336.5±0.7	1.09	1.53	-7.9	-9.3	-14.1
D1	0.88±0.18	346.2±3.6	343.7±1.6	337.4±1.0	1.10	1.46	-7.0	-10.5	-15.6
D0	0.75±0.20	347.2±1.0	341.0±0.6	338.0±0.9	1.71	1.21	-6.5	-13.5	-12.8

[a] The sedimentation coefficient for the peak corresponding to the monomer is showed.

[b] The averages and the standard deviations are provided.

[c] The spectral maxima were calculated with PFAST (see Methods).

Figures

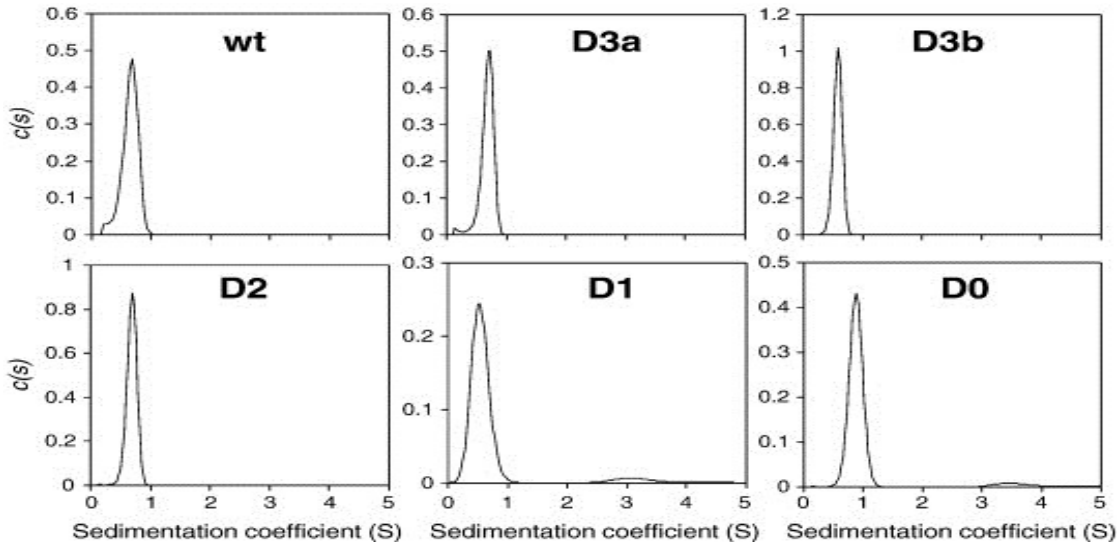

Figure 1. Sedimentation velocity of the different peptide variants. Apparent sedimentation coefficient distribution derived from sedimentation velocity profiles of the peptides(7 μM)) in 5 mM phosphate buffer at pH 8.

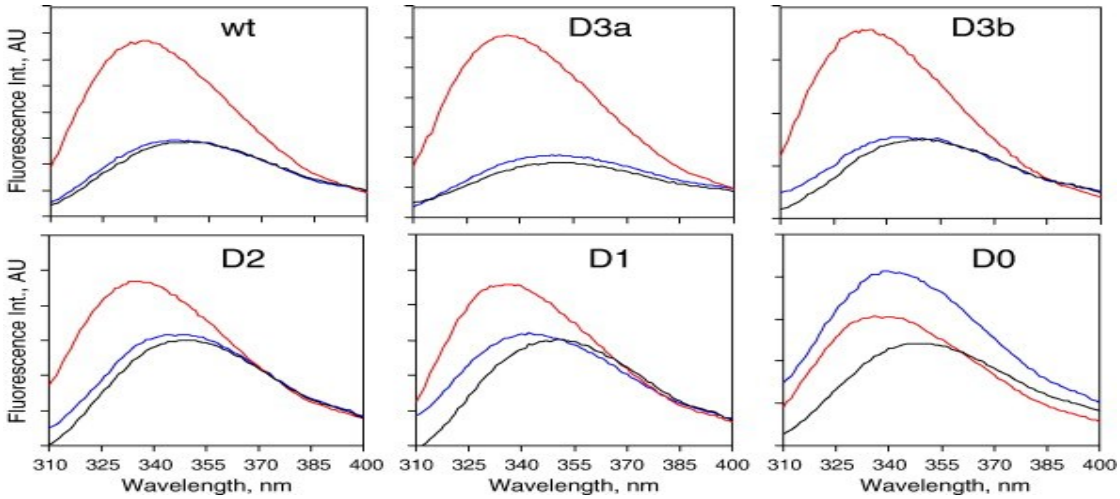

Figure 2. Fluorescence spectra of peptides in buffer and with POPC vesicles. Emission spectra of each variant were recorded under the following conditions: buffer at pH 7.5 (black lines), POPC at neutral pH (blue lines), and POPC at pH 4 (red lines). The pH values for the different POPC samples at neutral pH were selected according to the midpoint and slope of the transitions shown in Figure 6: wt, pH 7.5; D3a, pH 7.5; D3b, pH 7.1; D2, pH 6.5; D1, pH 6.2; D0, pH 8. The peptide concentration was 1.5 μM, and the lipid concentration was 375 μM. Fluorescence intensity is given in arbitrary units (AU).

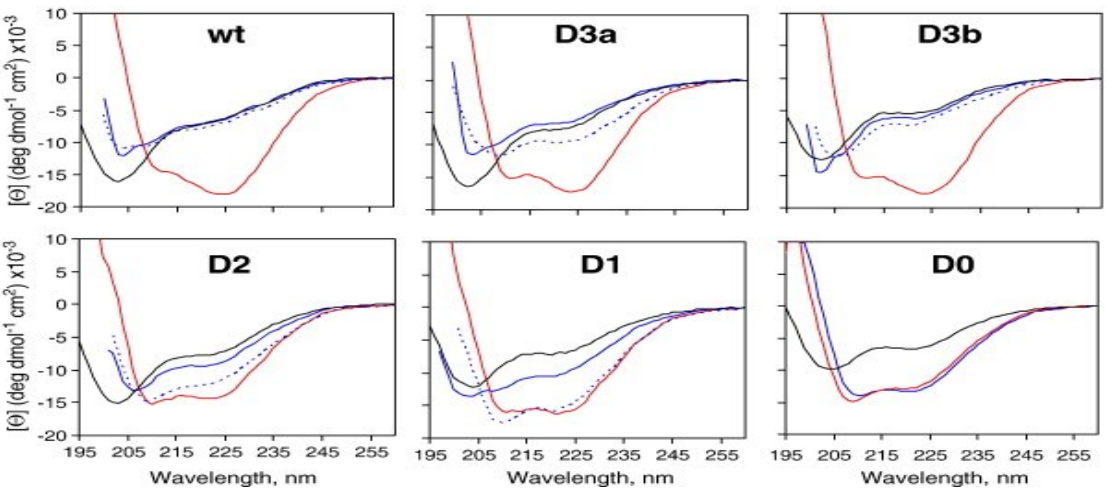

Figure 3. CD of peptides in buffer and with POPC vesicles. Far-UV CD spectra were recorded for all variants under different conditions: buffer at pH 7.5 (black lines), POPC at pH 7.4 (blue lines), and POPC at pH 4 (red lines). The reversibility of the insertion process was studied by raising the pH of the samples from pH 4 (broken blue line) to pH 7.4. Reversibility for D0 was not studied, as the ellipticity changes between the states at pH 7.5 and pH 4 were negligible. In all samples, the final peptide and lipid concentrations were 5 μM and 1.5 mM, respectively.

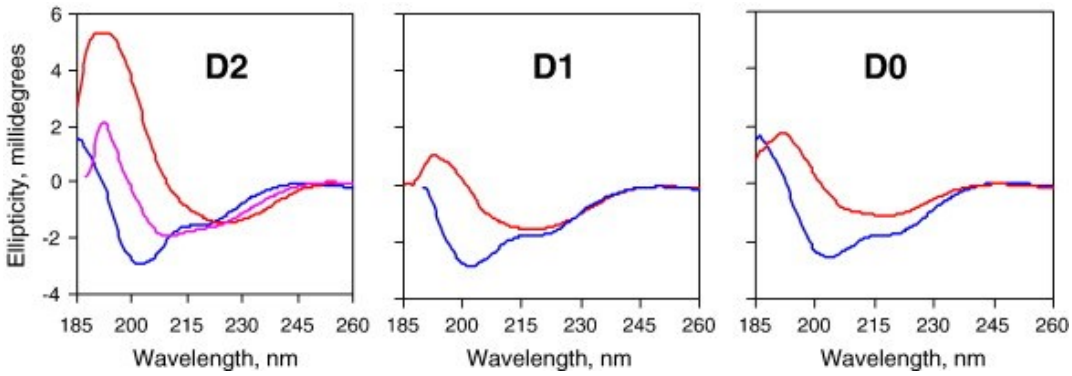

Figure 4. OCD spectra of D2, D1, and D0 measured on oriented POPC-supported bilayers at neutral (blue lines) and acidic (red lines) pH values. The OCD spectrum of D2 at pH 1.9 was also recorded (purple line). The experimental spectra are corrected for the lipid background.

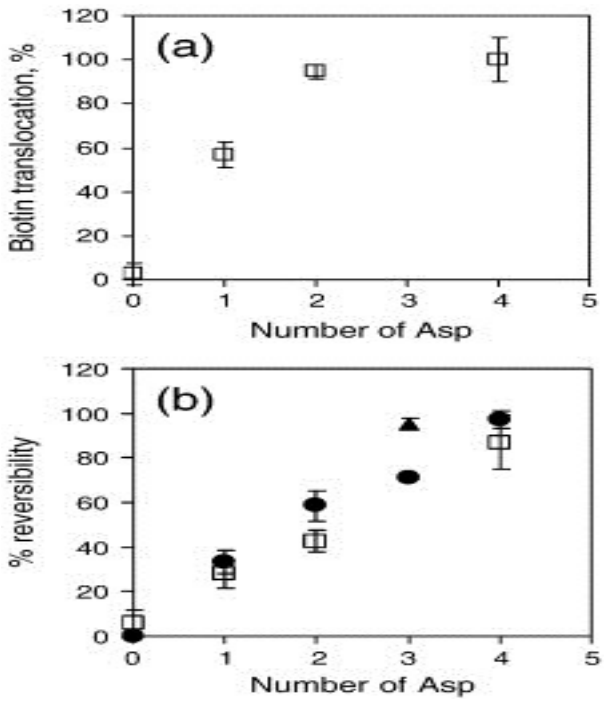

Figure 5. Quantification of membrane insertion (biotin translocation) and reversibility. Data corresponding to the biotin translocation assay (open squares) and CD (black symbols) were plotted against the number of Asp residues in the TM and C-terminal regions. (a) Degree of normalized biotin translocation (open squares). For data normalization, the translocation levels of wt pHLIP labeled with biotin at the C-terminus and N-terminus were used as 100% and 0%, respectively. Results from D3a and D3b are not shown for the biotin translocation assay, as the biotin labeling for these peptides affected the interaction with lipids (data not shown). No adverse effects of labeling were observed for the rest of the peptides tested. Averages and standard deviations are shown. (b) The percent reversibility of the biotin translocation of the samples used in (a) is shown (open squares). For CD experiments (Fig. 3), the degree of reversibility was determined by monitoring the relative changes in ellipticity at

222 nm (black symbols). Averages and standard deviations are shown. Data corresponding to D3b appear as a triangle, while the rest of the CD data appear as circles. All data points were used for linear fitting ($\mathbf{R}^2 = 0.95$).

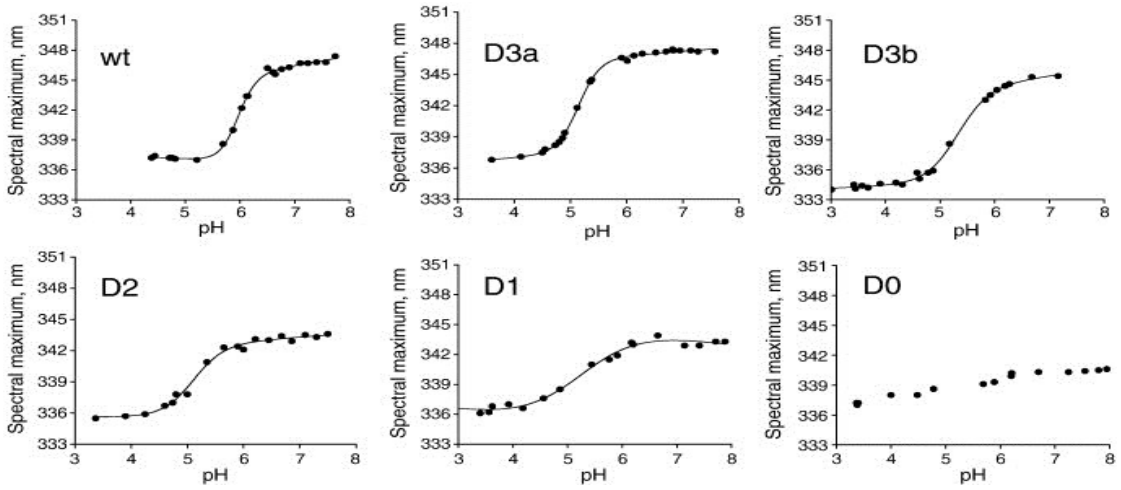

Figure 6. Fluorescence spectral maximum changes upon pH titration. The pH-controlled transitions of the peptides in POPC were followed by monitoring the variations in the spectral maxima. The experimental data for the different peptides were fitted to Eq. (1) (black lines). Representative experiments are shown.

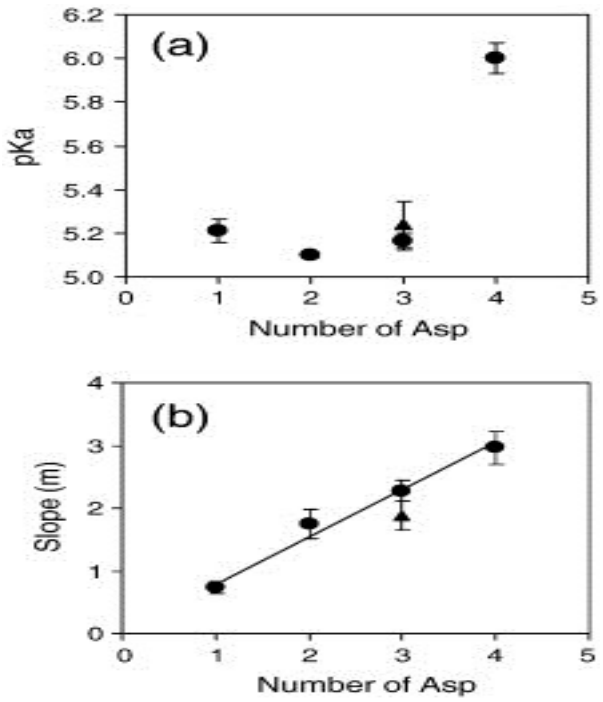

Figure 7. Parameters obtained from the fitting of fluorescence pH transitions. The p$\mathbf{K}_a$ (a) and **m** parameter (b) values obtained from the fitting of the data in Figure 6 to Eq. (1) are shown in black symbols. Data from the D3b variant are shown as triangles (to maintain the representation as in Fig. 5). The line corresponds to the fitting of all data points ($\mathbf{R}^2 = 0.93$). Averages and standard deviations are shown.

Supplementary information

Roles of carboxyl groups in the transmembrane insertion of peptides.

Francisco N. Barrera, Dhammika Weerakkody, Michael Anderson, Oleg A. Andreev,

Yana K. Reshetnyak and Donald M. Engelman

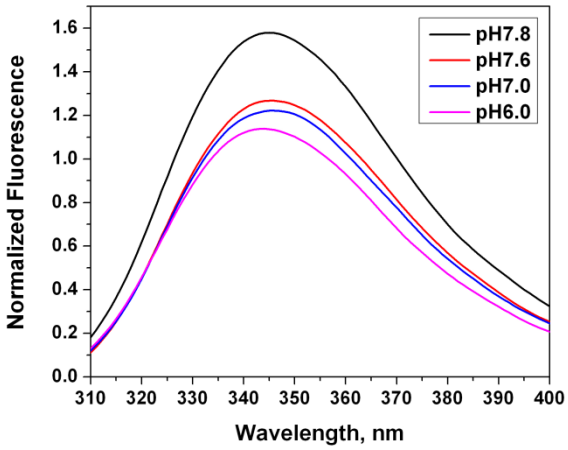

Figure S1. Fluorescence of D2 in presence of POPC at various pH values**.**

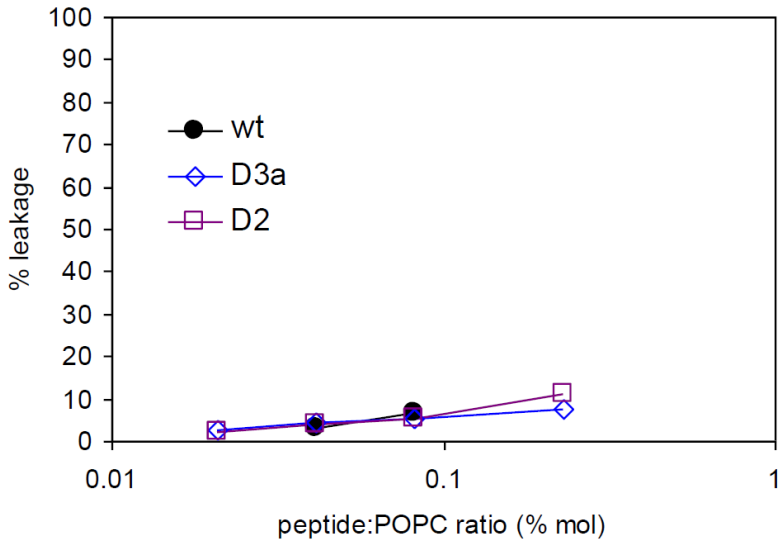

Figure S2. Leakage of encapsulated calcein. The release of calcein encapsulated in large unilamellar POPC liposomes was measured by following the fluorescence at 515 nm in the presence of different concentrations of peptides. Little disruption by peptide interaction is seen. The level of 100% disruption of liposomes was determined by addition of 0.05% Triton X-100

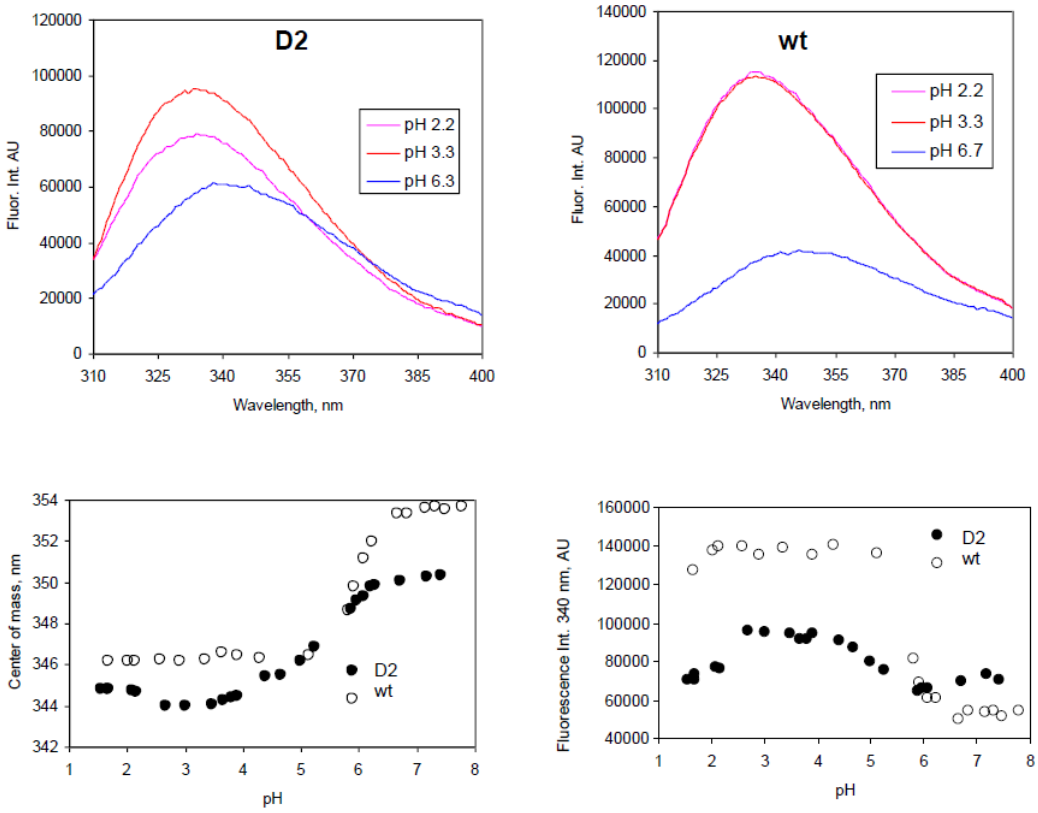

Figure S3. Fluorescence of wt and D2 at low pHs. The usual range of pHs was extended to lower values to study the protonation state of His residues. D2 was employed as an example of peptide containing two His residues. *Upper panels:* Emission spectra in POPC liposomes at pH 2.2, 3.3 and 6.3. *Lower panels:* the fluorescence intensity and center of mass were calculated for the complete pH range studied for D2 and wt pHLIP.

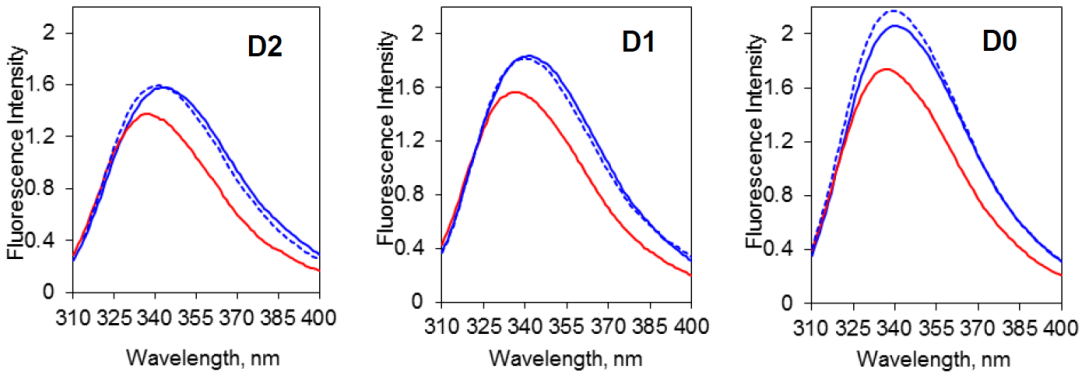

Figure S4. Fluorescence studies of the reversibility of the membrane insertion for D2, D1 and D0. Spectra were measured of the peptides in the presence of POPC at pH 4.1 (red lines) and 7.8 (straight blue lines). The pH of the samples at pH 4.1 was increased back to 7.8 (dashed blue lines) to study reversibility. For D2, where acidification caused TM helix formation occurs, the two blue lines have a good overlap, suggesting a high degree of reversibility. For D1 and D0, a TM helix is not formed in a pH-dependent fashion, so the interpretation of the reversibility data is less straightforward.

CHAPTER 3

Published in Biophysical Journal on 18th of April 2012

Modulation of the pHLIP transmembrane helix insertion pathway

Alexander G. Karabadzhak[1], Dhammika Weerakkody[1], Dayanjali Wijesinghe[1], Mak S. Thakur[1], Donald M. Engelman[2], Oleg A. Andreev[1], Vladislav S. Markin[3], Yana K. Reshetnyak[1]

[1]Physics Department, University of Rhode Island, 2 Lippitt Rd., Kingston, RI, 02881, USA

[2]Department of Molecular Biophysics and Biochemistry, Yale, P.O. Box 208114, New Haven, CT 06520, USA

[3] Department of Neurology, University of Texas Southwestern Medical Center, Dallas, TX, 75390, USA

Running title: Insertion/folding and exit/unfolding of membrane peptides

Keywords*:* kinetics, fluorescence, CD, pH-dependent insertion, acidity, cargo translocation, single peptide molecular transporter

Corresponding author:

Yana Reshetnyak, Physics Department, University of Rhode Island, 2 Lippitt Rd., Kingston, RI, 02881, USA, Phone: (401) 874-2060, Fax: (401) 874-2380, E-mail: reshetnyak@mail.uri.edu

Abstract

The membrane-associated folding/unfolding of pHLIP® (pH (Low) Insertion Peptide) provides an opportunity to study how sequence variations influence the kinetics and pathway of peptide insertion into bilayers. Here we present the results of steady-state and kinetics investigations of several pHLIP variants with different numbers of charged residues, with attached polar cargoes at the peptide's membrane inserting end, and with three single-Trp variants placed at the beginning, middle and end of the transmembrane helix. Each pHLIP variant exhibits a pH-dependent interaction with a lipid bilayer. While the number of protonatable residues at the inserting end does not affect the ultimate formation of helical structure across a membrane, it correlates with the time for peptide insertion, the number of intermediate states on the folding pathway, and the rates of unfolding and exit. The presence of polar cargoes at the peptide's inserting end leads to the appearance of intermediate states on the insertion pathway. Cargo polarity correlates with a decrease of the insertion rate. We conclude that the existence of intermediate states on the folding and unfolding pathways are not mandatory and, in the simple case of a polypeptide with a non-charged and non-polar inserting end, the folding and unfolding appears as an all-or-none transition. A model for membrane-associated insertion/folding and exit/unfolding is proposed, and the importance of these observations for the design of new delivery agents for the direct translocation of polar therapeutic and diagnostic cargo molecules across cellular membranes is discussed.

Introduction

The molecular mechanism of spontaneous polypeptide folding and insertion into a membrane as well as its exit and unfolding is of interest from several standpoints, including the action of antimicrobial peptides, the folding and degradation of membrane proteins, and the medical applications of the pH triggered insertion peptides. Most helical membrane proteins insert into a lipid bilayer with the assistance of the translocon machinery (1, 2). While they are assisted in their pathways by the Get proteins (3), tail-anchored membrane proteins can spontaneously insert and fold themselves across the lipid bilayer of a membrane, and may do so when released by the Get complex *in vivo* (4, 5). The stability and folding of membrane proteins are strongly constrained by the formation of secondary structures in the lipid bilayer environment, driven by the hydrophobic effect and hydrogen bonding (6-8). When helical membrane proteins are degraded, their TMs must exit the bilayer as they become destabilized by cleavages (9). Peptide insertion into a bilayer can be triggered by a pH jump if it leads to the protonation/de-protonation of charged groups to render them uncharged and so to increase peptide hydrophobicity and affinity for the nonpolar region of a membrane. One example of a synthetic peptide with pH dependent membrane-insertion properties has been investigated by White and Ladokhin (10). Another example, which is the subject of this study, is the pH Low Insertion Peptide (pHLIP®) family. At neutral and high pHs, pHLIP is monomeric and largely unstructured, and equilibrates between aqueous solution and the surface of a lipid bilayer. Lowering the pH shifts the equilibrium towards transmembrane insertion and the formation of a TM helix (11). A subsequent increase of pH promotes

unfolding of the TM and exit from the bilayer. The process of binding of the peptide to the membrane surface is accompanied by an energy release of 6-7 kcal/mol and the process of insertion is accompanied by an additional energy release of about 1.8-2.0 kcal/mol (12). We previously showed that pHLIP insertion is associated with the protonation of Asp/Glu residues, which leads to an increase of hydrophobicity that triggers the folding and insertion of the peptide across a lipid bilayer (13, 14). The insertion of the pHLIP is unidirectional: the C-terminus crosses the lipid bilayer, and the N-terminus stays outside (11, 15). The energy of membrane associated-folding can be used to favor the movement of cell-impermeable polar cargo molecules across the hydrophobic membrane bilayer when they are attached to the inserting end of pHLIP (15-17). Both pH-targeting behavior and molecular translocation have been demonstrated in cultured cells and *in vivo* (16-21). Thus, there is an opportunity to develop a novel concept in drug delivery, which is based on the use of a monomeric, pH-sensitive peptide molecular transporter to deliver agents that are significantly more polar than conventional drugs.

In our initial kinetic study we found that pHLIP inserts into a POPC phospholipid bilayer in several steps: first, an interfacial helix is rapidly formed (~100 ms), which is then followed by a slow transmembrane insertion pathway (~1 minute) that contains several intermediates. The exit of the peptide from the bilayer core proceeds ~800 times faster and through different intermediates (22). It remained unclear why it takes 1000 times longer for the helix to insert across a bilayer after it is formed on the surface, and what the intermediates are on the insertion/exit pathways. Another

question we wanted to address is how polar cargo might affect the process of insertion, and thus, translocation of cargo across the bilayer.

Materials and methods

Due to the limit of space, a detailed description of experiments could be found "in the Supporting Material".

Results

Design of pHLIP variants

Our previous data indicated that the pHLIP peptide forms a helix, after a pH drop, 1000 times faster than it inserts into a lipid bilayer, and insertion occurs through several steps. The insertion time and nature of the intermediates might result from the presence of four protonatable groups at the C-terminus of the peptide, which have to cross the membrane to complete the process of insertion. In order to cross the energy barrier presented by the hydrophobic membrane core at any appreciable rate, it is reasonable to hypothesize that these charged groups should be at least partially protonated. To test the idea, we asked if the number of protonatable groups at the C-terminus would correlate with the rates of insertion and exit, as well as examining the number of intermediate states along the insertion/exit pathways. Two truncated pHLIP variants were designed: pHLIP-2 and pHLIP-1, where the number of protonatable groups (shown below in red) was reduced to two and one, respectively. Additional Asp residues were placed at the N-terminus to preserve peptide solubility.

pHLIP-4: AE-QN-PI YWARYADWLFTTPLLLLDLALLV DADEGTCOOH

pHLIP-2: AEDQN-P- YWARYADWLFTTPLLLLDLALLV D---G-COOH

pHLIP-1: AEDQNDP- YWARYADWLFTTPLLLLDLALLV ----G-COOH

To gain insights into the structural nature of the intermediates along the insertion and exit pathways, we studied three single-Trp variants of pHLIP-4 peptide (pHLIP-W1, pHLIP-W2 and pHLIP-W3), where a Trp residue was positioned at the beginning, middle, and end of the TM helix.

pHLIP-W1: AEQNPI YWARYADFLFTTPLLLLDLALLV DADET-COOH

pHLIP-W2: AEQNPI YFARYADWLFTTPLLLLDLALLV DADET-COOH

pHLIP-W3: AEQNPI YFARYADFLFTTPLLLLDLALLW DADET-COOH

The following pHLIP sequences were selected for the conjugation of polar cargoes to the inserting end to probe cargo effects on kinetics:

pHLIP-4: AE-QN-PI YWARYADWLFTTPLLLLDLALLV DADEGCTCOOH

pHLIP-2: AEDQN-PI YWARYADWLFTTPLLLLDLALLV D---GCTCOOH

pHLIP-2E: AEDQNDPI YWARYADWLFTTPLLLLELALLV E---GCTCOOH

pHLIP-2E is a pHLIP-2 where the two Asp residues are replaced by Glu to increase the pKa of peptide insertion, which is desirable for the translocation of polar cargo into cytoplasm. Each of the last three pHLIP variants had a free SH group at its C-terminus for conjugation with maleimide-cargo. As cargo we chose biotin and biotin-Peg mainly based on their Log *P* values (chosen to be slightly polar), the convenience of conjugation to the peptides, the low level of absorbance, and the absence of fluorescence in the UV range (in contrast to fluorescent dyes and phallatoxins). The measured Log *P* of biotin-maleimide and biotin-Peg-maleimide are -0.3 and -1.4, respectively (for comparison, the Log *Ps* of phalloidin-rhodamine and phalloidin are -0.05 and -1.5, respectively (16). Information about Log *P* measurements can be found in the supporting material. We have shown previously that the pHLIP-4 is capable of

translocating biotin-Peg (23). All constructs were purified to remove unreacted peptide and cargo.

Steady-state study of pHLIP variants

We employed fluorescence and CD/OCD spectroscopic techniques to demonstrate that pHLIP variants and their cargo conjugates preserve pH dependent membrane-inserting properties (Fig. S1-4). The data clearly indicate that all peptides preserve ability to interact with lipid bilayer of membrane in a pH-dependent manner. The data also suggest that the peptides may be partly pulled away from the membrane core by the polar cargo molecules attached to their C-termini (especially pHLIP-2 and pHLIP-2E, which are more hydrophobic and partition more deeply into the membrane and have higher helix content at pH8 compared to pHLIP-4) (Fig. S3 and Table S1). Because we had moved protonatable residues from the C to the N-terminus and attached polar (non-charged) cargo, we checked for effects on the pH-dependencies of the insertion (Fig. 1*c*, *f* and 4S). The perturbation of the insertion pKa by truncation of the C-terminus and attachment of the polar cargoes is small.

Mathematical models for fitting of kinetics data

In our earlier kinetic studies, we used a sequential mathematical model to fit the kinetic data and to find the rates and contributions of individual components (22). To simplify the mathematical model, only forward reactions were taken into consideration. In the present work we have made an attempt to describe the processes by taking into account both forward and backward reactions. We have considered several linear models: two-state (no intermediates):

$$A \underset{k_1^-}{\overset{k_1}{\rightleftharpoons}} B$$

three-state (single intermediate):

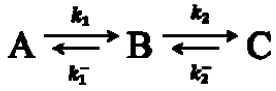

and four-state (two intermediates) models:

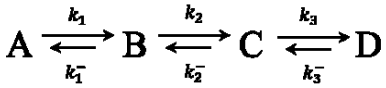

The transitions between states are described by a set of differential equations (Appendix S1-3), which can be solved, but the functions obtained are very complex and will contain a number of variable parameters increasing with the complexity of the applied model. It is not practical to perform fitting of the experimental data using such complex functions: a slight variation in input data dramatically affects the solution, thus making it unreliable. However, the solution for fluorescence varation with time can be presented in a general form as a sum of the exponential functions:

$$F(t) = f_0 + f_1 \exp(-t/\tau_1) \quad \text{for the (II) model} \quad (1)$$

$$F(t) = f_0 + f_1 \exp(-t/\tau_1) + f_2 \exp(-t/\tau_2) \quad \text{for the (III) model} \quad (2)$$

$$F(t) = f_0 + f_1 \exp(-t/\tau_1) + f_2 \exp(-t/\tau_2) + f_3 \exp(-t/\tau_3) \quad \text{for the (IV) model} \quad (3)$$

where τ_i are the characteristic times for each transition or $\nu_i = 1/\tau_i$ are the characteristic rates of the transitions, and f_i are the characteristic contributions. Thus fitting of the measured curves can be performed using exponential functions and the characteristic rate constants ν_i can be found directly from the experiment. However, we wish to emphasize that the characteristic rates (or times) and contributions need to be related to the rate constants (k_i) and contributions for the transition from one

intermediate to another, which fully reflect the transitions. Due to the complexity of the problem, we proposed to establish relations only between the characteristic rates and the real rate constants without considering the contributions. By making a few reasonable assumptions, simple approximate relations between k and v can be established. Thus, for the two-state model (see Appendix S1):

$$k_1 \sim 0.91 v_1 \tag{4}$$

for the three-state model (see Appendix S2):

$$k_1 \sim \frac{v_1}{1.1} - \frac{v_2}{12.21}, \qquad k_2 \sim 1.0091 v_2 \tag{5}$$

and for the four-state model (see Appendix S3):

$$k_1 \sim v_1, \qquad k_2 \sim \frac{v_2}{1.1} - \frac{v_3}{12.21}, \qquad k_3 \sim 0.991 v_3 \tag{6}$$

The experimental kinetic data were fitted by the single, or double, or triple exponential functions (eqs. 1-3), which are general solutions for the two-, three- or four-state models, respectively.

Kinetics of insertion of pHLIP variants with truncated C-terminus at various temperatures

The insertion of each of the pHLIP-4, -2, -1 peptides into a lipid bilayer was triggered by a drop of pH from 8 to 3.6 and was monitored at various temperatures (7, 11, 18, 25ºC) by the increase of tryptophan fluorescence (Fig. 1 *a*-*c*). The pHLIP-4 peptide inserts across the bilayer as a helix within 30-50 sec (at various temperatures), the pHLIP-2 – within 3-8 sec, and for the pHLIP-1 the process is completed in 80-400 ms, which is about the same as the time of helix formation (90-100 ms) (Table 1). Thus the processes of helix formation and insertion occur practically simultaneously in the absence of protonatable side chains at the C terminal tail, and the number of

protonatable residues at the inserting end does not affect the formation of helical structure, but correlates with the time of peptide insertion into the lipid bilayer.

To ensure that the addition of Asp residues to the N-terminus of truncated pHLIP variants does not alter the kinetics, we tested the following sequence:

pHLIP-6: **AEDQNDPIYWARYADWLFTTPLLLLDLALLVDADEGTCOOH**

where an additional two Asp residues (total 6 Asp) were placed at the N-terminus of pHLIP-4. The steady-state and kinetics data obtained for pHLIP-6 were very similar to the data obtained with pHLIP-4 (Fig. S5), which confirms our suggestion that the modification of the N-terminus does not interfere with the process of insertion.

Activation energies of pHLIP variants insertion into bilayer

Arrhenius plots were constructed to establish activation energies (E_a) and frequency factors (A) for the transitions between the states for each pHLIP variant (Fig. 1*d*). The points were fitted by the Arrhenius equation:

$$\ln k = -E_a/RT + \ln A \qquad (7)$$

A global fit was used in the analysis of the second transition for pHLIP-2 and -1, and for the second and third transitions for pHLIP-4, since slopes of the corresponding curves are very similar to each other (established by separate fitting of each data set). In the global fitting we used activation energy as a shared parameter to establish differences in the frequency factors for various transitions. The activation energy barrier for the pHLIP-1 and -2 is 13.2 kcal/mol. The frequency factor for the pHLIP-1 transition to the final state is 4.2×10^{10}, which is an order of magnitude higher than the frequency factor for the pHLIP-2 (1.9×10^{9}): we reason that this finding may reflect the lower probability of simultaneous protonation of both COO^- groups of Glu and C-terminus on the pHLIP-2, relative to the probability of protonation of the single

carboxyl terminus of pHLIP-1. Insertion of the helical structure of the pHLIP-4 into the lipid bilayer occurs in two steps, with an activation barrier of about 4.6 kcal/mol each (9.2 kcal/mol combined), but with frequency factors ($1.1x10^3$ for B→C transition) more than a million times lower than for the pHLIP-2 and -1. An especially low frequency factor of 80 (for the transition of C→D) was obtained for the transition to the final TM state for the pHLIP-4.

Kinetics of insertion of pHLIP variants with cargoes

The attachment of biotin or biotinPeg cargoes to the peptides slows down the process of insertion. The overall insertion time of the pHLIP-4 increases from 30-35 sec to 400 sec and 500 sec, when the biotin and the biotin-Peg are attached to the inserting end, respectively (Fig. 2, Table 2). For the pHLIP-2 and pHLIP-2E the processes of insertion slows down from 1-2 sec to 100-200 sec, and from 0.2 sec to 80-90 sec, respectively. At the same time, the first (fast) rate of the insertion is very similar for all pHLIP variants with and without cargo, and coincides with the rate of helix formation. The higher the polarity of cargo attached to the inserting end, the slower the final steps to adopt TM orientation and "flip" cargo across a membrane. It is interesting to note that the biggest change of the fluorescence signal for pHLIP-4 is observed for the peptide with no cargo. The steady-state measurements (Fig. S3) indicate that state II (membrane-bound) is not affected significantly by the attachment of cargoes. At the same time, when cargoes are attached, fewer pHLIP-4 peptides are reaching state III (TM orientation), and smaller changes of fluorescence signal are observed. In contrast to pHLIP-4, in the cases of pHLIP-2 and especially pHLIP-2E, the increase of fluorescence is higher for peptides with the cargo compared to the peptides with no

cargo. Truncated pHLIP-2s partition more deeply into the membrane and exhibit formation of elements of secondary structure already in the state II, which is reflected by the shift of the position of maximum and increase in emission (Table S1). The cargo "pulls" the peptides to the membrane surface, affecting their state II positions. Thus pHLIP-2 and pHLIP-2E with cargoes start their journey into the membrane to adopt TM configuration from a more superficial membrane surface configuration than peptides with no cargo, which are more membrane-embedded at high and neutral pHs.

Insertion/folding transitions to intermediate pHs

To further study the intermediate states of insertion, we compared transitions from pH8 to 3.6 and intermediate pHs (pH8→6, pH8→5) (Fig. S6). When the size of the pH jump is reduced, both peptide folding and bilayer insertion slow down. The first (fast) rate of the insertion is very similar for all pHLIP variants (Table 3), and coincides with the rate of helix formation; however, after the first 100-300 ms the behaviors of the pHLIP variants are significantly different. The pHLIP-1 forms helical structure and partitions into the lipid bilayer slightly slower when the pH is jumped from 8 to 6 in comparison with the 8→3.6 pH jump. All processes are completed within the first 200-300 ms for pHLIP-1 at any pH jump. It appears that the absence of several protonatable groups at the inserting end makes the peptide less dependent on the variations of the pH-jumps. In contrast, pHLIP-2 and pHLIP-4 insertion into the membrane are more dependent on the final pH. Thus, the more protonatable groups there are on the inserting end, the slower the process of insertion is at the intermediate pH jumps. Interestingly, about 85% of the CD signal changes for both peptides occur within the first 80 ms for all pH-transitions, while the rate constants for the remaining

15% of the CD signal changes correlate very well with the rate constant of the fluorescence changes at the final step of the insertion and depend on the pH-jump magnitude. It seems that the final adjustment of the content of helical structure occurs at the final stage of insertion, when the peptides adopt TM orientations.

We observed an interesting behavior of pHLIP-4 when the pH was dropped from 8 to 6, and a "kink" in the fluorescence and CD kinetic curves appeared (Fig. 3). The kinetic curves of the insertion and folding at the pH8→6 jump were fitted by three-exponential functions with negative amplitudes for the second component (shown in red in Table 3). The physical meaning of a negative amplitude is that the spectral signal changes in the opposite direction. These changes indicate that after the pH is dropped, pHLIP-4 first partitions into the lipid bilayer with helical structure formation, but later comes out of the membrane with a reduction of helical content, and then finally "dives" into the membrane slowly with an increase of helical content.

Exit/unfolding of pHLIP variants

We also investigated the reverse processes of exit/unfolding of the pHLIP variants when the pH is changed from 3.6 to 5, 6 and 8 (Fig. S7, Table 4). Our CD and fluorescence data show very fast 50-150 ms exit transitions for each variant when the pH is raised to 8. With a reduction of the sizes of the pH jumps, both unfolding and exit from the bilayer slow down. As in the case of insertion/folding, the pHLIP-1 kinetics is less sensitive to the magnitude of the pH jumps than pHLIP-2 or -4. The pHLIP-2's exit/unfolding slows down from 200 ms for a pH3.6→8 jump to 60-80 sec for a pH3.6→6 jump. Dramatic changes are observed for the pHLIP-4 with different pH jumps: the exit/unfolding slows down from 200 ms to 150-170 sec.

Insertion/folding and exit/unfolding of single-Trp pHLIP variants

Wishing to better understand the intermediates, we used tryptophan residues positioned along the sequence to follow insertion and exit of different parts of pHLIP-4 into and out of a lipid bilayer (Fig. 4, Table 5). The characteristic times of the transitions for the single-Trp variants are similar to those of pHLIP-4, while double the time is required for the pHLIP-W2 and -W3 to insert and adopt its final TM configuration when the pH is dropped from 8 to 3.6. For the pH8→6 transition, a "kink" is observed similar to that of pHLIP-4 within the same time scale of 4-7 sec. The most pronounced kink is observed for the pHLIP-W3, and a less pronounced kink is seen for pHLIP-W1 and -W2. As mentioned above, the kink is interpreted as a partial exit and unfolding of the pHLIP-4 peptide in the path to the inserted and folded state when the pH is dropped from 8 to 6. Based on this view, we infer that the C-terminal end of the peptide, which has four protonatable groups, tends to exit the bilayer to a greater extent than other parts of the peptide.

Exit and unfolding for the pH3.6→8 transition happens fast for all single-Trp variants (within 350 ms), but much more slowly for the intermediate transition driven by the pH3.6→6 jump. (Fig. 4 *c-d*). Interesting changes were observed for pHLIP-W3 with a pH increase from 3.6 to 6: while the fluorescence decays progressively for pHLIP-W1 and –W2, pHLIP-W3 exhibits an initial increase of fluorescence, which then decays slowly. Our interpretation is that the changes are related to the movement of Trp residues across the bilayer as the pHLIP-W3 peptide exits from the membrane.

Rates of pH equilibration in POPC liposomes

It is known that the pH inside a liposome equilibrates progressively with the external pH after a pH jump (24). However, the rate of equilibration depends on the magnitude of the pH changes, the concentrations of other ions present, the charges on the lipid headgroups, the buffering capacities inside and outside of the vesicles, and other factors. One of the widely used methods to follow changes is to monitor fluorescence changes of the pH-sensitive dye fluorescein (FITC) encapsulated into the liposomes. FITC carries 2 negative charges at pH9 that are protonated as the pH is lowered. Since some of the charged residues of pHLIP peptides are located near the bilayer surfaces (on inner or outer leaflets), we chose to use lipid bound FITC to probe pH changes near the inner leaflet rather than bulk pH changes. We followed pH equilibration after the addition of acid or base using liposomes containing 1% FITC labeled phospholipids. Biphasic kinetics were seen for a pH jump from pH8→3.6 with characteristic rates of about 0.04 and 0.003 sec^{-1} (Fig. S8*a*), the data are in a good agreement with the rates measured previously (25). Thus the fastest component of the pH changes inside a liposome is of the same order of magnitude as the slowest component of pHLIP-4 insertion, while pHLIP-2, -2E and -1 peptides fold and insert into the lipid bilayer much faster than the pH equilibrates on the bilayer inner leaflet. In the case of a pH jump from pH8→6, the first component slows down to 110 sec (0.009 sec^{-1}) and the second component is not detectable within 20 min.

We also measured the FITC fluorescence changes when the solution pH is raised from 3.6 to pH 8 and to pH 6 by addition of NaOH (the solution already contained H^+ and Cl^- ions to mimic our unfolding experiments). In both cases, the characteristic time of

the first increase of FITC fluorescence associated with the pH changes on the inner leaflet of the bilayer is about 20 sec (Fig. S8 *c*-*d*), after which it takes tens of minutes for the pH to be fully equilibrated.

Discussion

In this study we designed several pHLIP variants and examined how elements of the pHLIP peptide and polar cargoes attached to the inserting end determine the pathways and kinetics of peptide insertion across and exit from a lipid bilayer. Based on our results, we have developed a model that describes our current view of the polypeptide membrane entry and exit pathways, as well as cargo translocation across the bilayer (Fig. 5). The model assumes a sequential pathway for the processes of insertion and exit, and takes the state II as a starting point, where the peptide is bound to the surface of the lipid bilayer in predominantly unstructured configuration. A drop of pH leads initially to the protonation (or partial protonation) of the carboxyl groups located in the TM part of the peptide, which are positioned closer to the hydrophobic core of the bilayer and, most probably, have the highest values in the sequences for the pK_a of protonation, since the other titratable groups are not as constrained by nearby side chain hydrophobicity to lie near the interface. It is known that the pK_a of the protonation/deprotonation of residues depends on the dielectric properties of their environment (26, 27), and it was shown previously that buried Asp residues in the C-helix of bacteriorhodopsin, from which pHLIP is derived, have higher pK_a's of protonation than those exposed to a more polar aqueous environment (28). Protonation of the carboxyl groups in the TM parts of pHLIP peptides induces a deeper penetration of the peptide into the membrane, which is accompanied by the formation of

secondary structure within the first 20-90 ms, stabilized by the formation of internal H-bonds that result from the depletion of water in their environment. As a result, an effective force directed toward the bilayer core ($\vec{F}_{in}$) is created at the center of the TM region where the hydrophobic Leu and protonated Asp residues are located. On the other hand, at the negatively charged C-terminus (which most probably hasn't been protonated yet) and positively charged N-terminus, the net forces ($\vec{F}_{out}$) are directed away from the bilayer core. This force became even stronger if polar cargo is attached to the inserting end of the peptide. The difference in folding/insertion between pHLIP-4, -2 and -1 peptides and peptides with and without polar cargoes corresponds to the strength of the force pulling these sequences away from the membrane, which is the greatest for pHLIP-4 with cargo (pHLIP-4 itself has four charged groups at its C-terminus), and smallest for pHLIP-1, which has only its C-terminal carboxyl group. These forces account in part for the observation that the insertions of pHLIP-2 and -1 into a lipid bilayer are completed 10 and 100 times faster than the insertion of pHLIP-4, since they bias the position of the peptide away from the energy barrier that must be crossed. Moreover, the existence of a large pulling force at the C-terminus of pHLIP-4 may account for the stabilization of an additional intermediate on the insertion pathway, which is most probably transient in the case of insertions of pHLIP-2 and -1. In the case of the intermediate pH jump from 8 to 6 the probability of protonation of the C-terminal carboxyl groups is even lower so the $\vec{F}_{out}$ force becomes more significant, which may lead to partial exit of the pHLIP-4 peptide from the bilayer and the reduction of helical content observed experimentally. Experiments with the single-Trp pHLIP-4 variants allowed us to demonstrate that the C-terminal part of the TM

helix moves away from the membrane more than the N-terminal part, while the middle of the TM helix does not move much.

The process of unfolding/exit is induced by a pH jump from acid to base, which most probably leads to the de-protonation (or at least partial de-protonation) of Asp residues located in the TM parts of the peptides. It results in the presence of charges that are unstable in the membrane interior, and an outward force appears. As a peptide exits from the bilayer, it progressively unfolds. We note that the folding/insertion experiments, which are performed on liposomes, may mimic the real processes of a polypeptide's interaction with cellular membranes quite well, but have the shortcoming that the pH difference that is present across the plasma membrane of a living cell is absent. For a cell in a diseased tissue, the intracellular pH is around 7.2-7.4, while the extracellular pH is low. We expect that carboxyl groups translocated across a bilayer are in their non-charged form, since the pH is equilibrated inside liposomes. For a large pH jump, all pHLIP variants, regardless of the number of protonatable groups at their C-termini, exit and unfold at least 100 times faster than the pH starts to be equilibrated inside a liposome (about 20 sec), so the protonatable groups can make the journey before they see the higher pH inside of liposome. However, for the intermediate pH jumps the probability of deprotonation of carboxyl groups in TM part is much lower, and the pH inside the liposome starts to equilibrate faster (within 20 sec) than peptides exit (77-175 s). We assume that at least partial protonation of the carboxyl groups at the inserted C-terminus would occur, and as a result, a force directed toward the inside of a liposome ($\overrightarrow{F_{in}}$) is created. As with insertion, the more charges there are at the C-terminus, the more time it takes for the

process of the C-terminus translocation across a bilayer during exit. Our results are consistent with this view, and also confirm our assumption that the peptides exit to the surface of the outside leaflet. Otherwise, if the peptides were able to exit to the inside of a liposome, then the exit rate would not depend on the number of protonatable residues at the C-terminus, rather it would be affected by the N-terminus of the peptides and would be highest for pHLIP-4, with fewer charged residues at its N-terminus.

In contrast to other known peptide-based delivery technologies, the selective direct delivery of polar molecules across a membrane by the pHLIP peptide is achieved by the pH-dependent folding and insertion of a monomer across a bilayer, enabling the targeting of acidic tissues. By using variants of the pHLIP peptide and by attaching polar cargoes to the inserting end, we have advanced our understanding of the mechanism of membrane-associated folding/unfolding, providing mechanistic insights on the formation of helical structures and the existence of intermediates, and the mechanism of cargo translocation across the lipid bilayer of a membrane. Here we summarize the main conclusions:

- The existence of intermediate states on the folding and unfolding pathways is not mandatory and, in the simple case of a polypeptide with a non-charged and non-polar inserting end, the folding and unfolding is seen as an all-or-none transition.

- If the peptide inserting end has charges or a polar cargo attached, an interfacial helical intermediate will occur before a peptide propagates into the hydrophobic core of a membrane.

- The origin of the driving force for the interfacial helix to insert into a bilayer to adopt a TM orientation might include the distortion of lipids by the partial surface insertion of the peptide. When a polypeptide forms a rigid helical structure and propagates deeply into one monolayer of a lipid bilayer, membrane tension and instability are created (29).

- A consistent and significant experimental observation is that the formation of secondary structure accompanies the partitioning of a polypeptide into a lipid bilayer, and that peptide exit from a membrane occurs simultaneously with unfolding on this timescale. The energetic cost of breaking backbone H-bonds inside a bilayer appears higher than the cost of the membrane distortion created by an asymmetric inclusion of helices in one leaflet of a membrane lipid bilayer.

- Our study provides useful principles for the design of drug delivery agents for the translocation of molecules across membranes into the cells in acidic diseased tissues. There are both thermodynamic and kinetic limitations for the direct translocation of polar cargo across membrane by pHLIP. The following parameters correlate inversely with increasing polarity of cargo attached to the peptide inserting end: i) the depth of peptide partitioning onto the membrane surface at neutral pH (state II) that increases the effective concentrations of cargo molecules near the membrane surface, ii) the proportion of peptide molecules in the membrane-inserted state (state III) associated with cargo translocation, and iii) the rate of peptide insertion into a bilayer (transition from state II to III) that moves cargo from the extracellular to the intracellular space.

Acknowledgements

This work was supported by NIH grants CA133890 and GM073857 to OAA, DME, YRK and NIH grants CA138468 to YRK. We thank Michael Anderson and Dr. Lan Yao for fruitful discussions and comments on the manuscript.

References

1. Van den Berg, B., W. M. Clemons, Jr., I. Collinson, Y. Modis, E. Hartmann, S. C. Harrison, and T. A. Rapoport. 2004. X-ray structure of a protein-conducting channel. Nature 427:36-44.
2. Osborne, A. R., T. A. Rapoport, and B. van den Berg. 2005. Protein translocation by the Sec61/SecY channel. Annu Rev Cell Dev Biol 21:529-550.
3. Simpson, P. J., B. Schwappach, H. G. Dohlman, and R. L. Isaacson. 2010. Structures of Get3, Get4, and Get5 provide new models for TA membrane protein targeting. Structure 18:897-902.
4. Brambillasca, S., M. Yabal, M. Makarow, and N. Borgese. 2006. Unassisted translocation of large polypeptide domains across phospholipid bilayers. J Cell Biol 175:767-777.
5. Renthal, R. 2010. Helix insertion into bilayers and the evolution of membrane proteins. Cell Mol Life Sci 67:1077-1088.
6. White, S. H., and W. C. Wimley. 1999. Membrane protein folding and stability: physical principles. Annu Rev Biophys Biomol Struct 28:319-365.
7. Engelman, D. M., Y. Chen, C. N. Chin, A. R. Curran, A. M. Dixon, A. D. Dupuy, A. S. Lee, U. Lehnert, E. E. Matthews, Y. K. Reshetnyak, A. Senes, and J. L. Popot. 2003. Membrane protein folding: beyond the two stage model. FEBS Lett 555:122-125.
8. Minetti, C. A., and D. P. Remeta. 2006. Energetics of membrane protein folding and stability. Arch Biochem Biophys 453:32-53.

9. Urban, S. 2010. Taking the plunge: integrating structural, enzymatic and computational insights into a unified model for membrane-immersed rhomboid proteolysis. Biochem J 425:501-512.

10. Ladokhin, A. S., and S. H. White. 2004. Interfacial folding and membrane insertion of a designed helical peptide. Biochemistry 43:5782-5791.

11. Reshetnyak, Y. K., M. Segala, O. A. Andreev, and D. M. Engelman. 2007. A monomeric membrane peptide that lives in three worlds: in solution, attached to, and inserted across lipid bilayers. Biophys J 93:2363-2372.

12. Reshetnyak, Y. K., O. A. Andreev, M. Segala, V. S. Markin, and D. M. Engelman. 2008. Energetics of peptide (pHLIP) binding to and folding across a lipid bilayer membrane. Proc Natl Acad Sci U S A 105:15340-15345.

13. Andreev, O. A., A. D. Dupuy, M. Segala, S. Sandugu, D. A. Serra, C. O. Chichester, D. M. Engelman, and Y. K. Reshetnyak. 2007. Mechanism and uses of a membrane peptide that targets tumors and other acidic tissues in vivo. Proc Natl Acad Sci U S A 104:7893-7898.

14. Musial-Siwek, M., A. Karabadzhak, O. A. Andreev, Y. K. Reshetnyak, and D. M. Engelman. 2010. Tuning the insertion properties of pHLIP. Biochim Biophys Acta 1798:1041-1046.

15. Reshetnyak, Y. K., O. A. Andreev, U. Lehnert, and D. M. Engelman. 2006. Translocation of molecules into cells by pH-dependent insertion of a transmembrane helix. Proc Natl Acad Sci U S A 103:6460-6465.

16. An, M., D. Wijesinghe, O. A. Andreev, Y. K. Reshetnyak, and D. M. Engelman. 2010. pH-(low)-insertion-peptide (pHLIP) translocation of membrane impermeable phalloidin toxin inhibits cancer cell proliferation. Proc Natl Acad Sci U S A 107:20246-20250.

17. Wijesinghe, D., D. M. Engelman, O. A. Andreev, and Y. K. Reshetnyak. 2011. Tuning a polar molecule for selective cytoplasmic delivery by a pH (Low) insertion peptide. Biochemistry 50:10215-10222.

18. Andreev, O. A., A. D. Dupuy, M. Segala, S. Sandugu, D. A. Serra, C. O. Chichester, D. M. Engelman, and Y. K. Reshetnyak. 2007. Mechanism and uses of a membrane peptide that targets tumors and other acidic tissues in vivo. Proc. Natl. Acad. Sci. U. S. A. 104:7893-7898.

19. Andreev, O. A., D. M. Engelman, and Y. K. Reshetnyak. 2010. pH-sensitive membrane peptides (pHLIPs) as a novel class of delivery agents. Mol Membr Biol 27:341-352.

20. Vavere, A. L., G. B. Biddlecombe, W. M. Spees, J. R. Garbow, D. Wijesinghe, O. A. Andreev, D. M. Engelman, Y. K. Reshetnyak, and J. S. Lewis. 2009. A novel technology for the imaging of acidic prostate tumors by positron emission tomography. Cancer Res 69:4510-4516.

21. Reshetnyak, Y. K., L. Yao, S. Zheng, S. Kuznetsov, D. M. Engelman, and O. A. Andreev. 2011. Measuring tumor aggressiveness and targeting metastatic lesions with fluorescent pHLIP. Mol Imaging Biol 13:1146-1156.

22. Andreev, O. A., A. G. Karabadzhak, D. Weerakkody, G. O. Andreev, D. M. Engelman, and Y. K. Reshetnyak. 2010. pH (low) insertion peptide (pHLIP)

inserts across a lipid bilayer as a helix and exits by a different path. Proc Natl Acad Sci U S A 107:4081-4086.

23. Barrera, F. N., D. Weerakkody, M. Anderson, O. A. Andreev, Y. K. Reshetnyak, and D. M. Engelman. 2011. Roles of carboxyl groups in the transmembrane insertion of peptides. J Mol Biol 413:359-371.

24. Elamrani, K., and A. Blume. 1983. Effect of the lipid phase transition on the kinetics of H+/OH- diffusion across phosphatidic acid bilayers. Biochimica et biophysica acta 727:22-30.

25. Kuyper, C. L., J. S. Kuo, S. A. Mutch, and D. T. Chiu. 2006. Proton permeation into single vesicles occurs via a sequential two-step mechanism and is heterogeneous. Journal of the American Chemical Society 128:3233-3240.

26. Petkova, A. T., J. G. Hu, M. Bizounok, M. Simpson, R. G. Griffin, and J. Herzfeld. 1999. Arginine activity in the proton-motive photocycle of bacteriorhodopsin: solid-state NMR studies of the wild-type and D85N proteins. Biochemistry 38:1562-1572.

27. Harris, T. K., and G. J. Turner. 2002. Structural basis of perturbed pKa values of catalytic groups in enzyme active sites. IUBMB Life 53:85-98.

28. Kawase, Y., M. Tanio, A. Kira, S. Yamaguchi, S. Tuzi, A. Naito, M. Kataoka, J. K. Lanyi, R. Needleman, and H. Saito. 2000. Alteration of conformation and dynamics of bacteriorhodopsin induced by protonation of Asp 85 and deprotonation of Schiff base as studied by 13C NMR. Biochemistry 39:14472-14480.

29. Bohinc, K., D. Lombardo, V. Kraljiglic, M. Fosnaric, S. May, F. Pernus, H. Hagerstrand, and A. Iglic. 2006. Shape variation of bilayer membrane daughter vesicles induced by anisotropic membrane inclusions. Cell Mol Biol Lett 11:90-101.

Tables

	25ºC	**18ºC**	**11ºC**	**7ºC**
pHLIP-1	0.02 (44.4 – 45.3) for various temperatures			
	0.08 (12.6)	0.15 (6.72)	0.31 (3.26)	0.48 (2.10)
pHLIP-2	0.04 (22.70 – 22.72) for various temperatures			
	2.7 (0.37)	3.7 (0.27)	6.0 (0.17)	7.5 (0.13)
pHLIP-4	0.09 (11.1) for various temperatures			
	2.0 (0.45)	2.1 (0.43)	2.8 (0.32)	3.5 (0.26)
	32 (0.031)	33 (0.030)	38 (0.026)	50 (0.020)

Table 1. **Insertion at different temperatures** (characteristic times, $\boldsymbol{\tau}$, sec, and rate constants, $\boldsymbol{k}$, sec^{-1} (shown in parentheses)). The first, second and third raw, for each pHLIP variant, contain kinetics parameters for the fastest, slow and the slowest transitions, respectively.

	no cargo	**biotin**	**biotin-Peg**
pHLIP-4	0.07 – 0.15 (14.2 – 6.7) for various cargo		
	2 (0.45)	17 (0.05)	16 (0.05)
	32 (0.03)	385 (0.0026)	416 (0.0024)
pHLIP-2	0.1 –0.6 (10 – 1.7) for various cargo		
	2.7 (0.37)	3.6 (0.25)	10.0 (0.09)
	-	102 (0.0097)	253 (0.0039)
pHLIP-2E	0.04 (22 – 25) for various cargo		
	0.2 (0.45)	1.4 (0.65)	3.4 (0.27)
	-	80 (0.012)	90 (0.011)

Table 2. **Insertion with cargoes** (characteristic times, $\boldsymbol{\tau}$, sec, and rate constants, $\boldsymbol{k}$, sec^{-1} (shown in parentheses)). The first, second and third raw, for each pHLIP variant, contain kinetics parameters for the fastest, slow and the slowest transitions, respectively.

	pH 8-3.6	**pH 8-5**	**pH 8-6**
pHLIP-1 fluoresc.	0.02 (44.6 - 45.0) for various pHs 0.09 (10.3)	0.18 (5.6)	0.20 (5.0)
pHLIP-1, CD	0.09 (10.1) for various pHs		
pHLIP-2 fluoresc.	0.08 (11.3 – 11.4) for various pHs 2.8 (0.36)	4.5 (0.22)	13.0 (0.08)
pHLIP-2 CD	0.08 (11.3 – 11.4) for various pHs 2.2 (0.46)	5.0 (0.20)	13.0 (0.08)
pHLIP-4 fluoresc.	0.09 (11.1) for various pHs 2.0 (0.45) 32 (0.031)	3.4 (0.27) 102 (0.0097)	5.0 (0.18) 138 (0.0072)
pHLIP-4 CD	0.09 (11.1) for various pHs 2.0 (0.45) 32 (0.031)	5.0 (0.18) 102 (0.0097)	5.0 (0.18) 138 (0.0072)

Table 3. Insertion and folding at different pH transitions (characteristic times, $\boldsymbol{\tau}$, sec, and rate constants, $\boldsymbol{k}$, sec^{-1} (shown in parentheses)). The first, second and third raw, for each pHLIP variant, contain kinetics parameters for the fastest, slow and the slowest transitions, respectively.

	pH 3.6-8	**pH 3.6-7**	**pH 3.6-6**
pHLIP-1 fluoresc.	0.14 (7.14)	0.40 (2.5)	0.85 (1.18)
pHLIP-1, CD	0.02 (45.5) for various pHs		
pHLIP-2 fluoresc.	0.03(29.9) 0.21 (4.81)	0.3 (3.01) 4.8 (0.21)	8.1 (0.11) 67.7 (0.015)
pHLIP-2 CD	0.02 (50)	0.3 (3.01) 3.9 (0.26)	8.0 (0.11) 77.0 (0.013)
pHLIP-4 fluoresc	0.03 (29.9) 0.2 (5.05)	0.22 (4.12) 11 (0.092)	16.8 (0.054) 175 (0.0058)
pHLIP-4 CD	0.02 (50)	0.22 (4.12) 6.5 (0.16)	16.8 (0.054) 149 (0.0068)

Table 4. Exit and unfolding at different pH transitions (characteristic times, $\boldsymbol{\tau}$, sec, and rate constants, $\boldsymbol{k}$, sec^{-1} (shown in parentheses)). The first and second raw, for each pHLIP variant, contain kinetics parameters for the fastest and slowest transitions, respectively.

	pHLIP-W1	pHLIP-W2	pHLIP-W3
pH 8-3.6	0.09 (11.1) for various pHLIPs 2.5 (0.36) 35 (0.028)	76 (0.013)	71 (0.014)
pH 8-6	0.01 (100) for various pHLIPs 4.0 (0.22)	2.6 (0.35)	6.2 (0.14) 200 (0.005) for various pHLIPs
pH 3.6-8	0.04 (22.5)	0.05 (18.0)	0.06 (14.9) 0.35 (2.88) for various pHLIPs
pH 3.6-6	4.2 (0.21) 54.9 (0.02)	- -	- -

Table 5. Insertion and exit of single-Trp pHLIP variants at various pH transitions (characteristic times, $\boldsymbol{\tau}$, sec, and rate constants, $\boldsymbol{k}$, sec^{-1} (shown in parentheses)). The first, second and third raw, for each pHLIP variant, contain kinetics parameters for the fastest, slow and the slowest transitions, respectively.

Figures

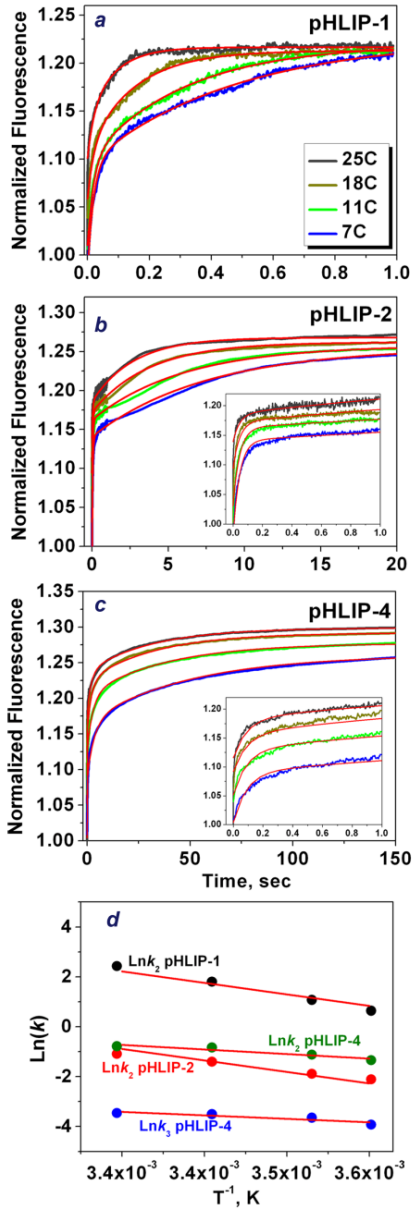

Figure 1

Figure 1. Insertion kinetics of pHLIP-4, -2, -1 at different temperatures, with Arrhenius plots. Arrhenius plots are shown for the second and third rates. The data were fitted by the Arrhenius equation, the fitting curves are colored in red.

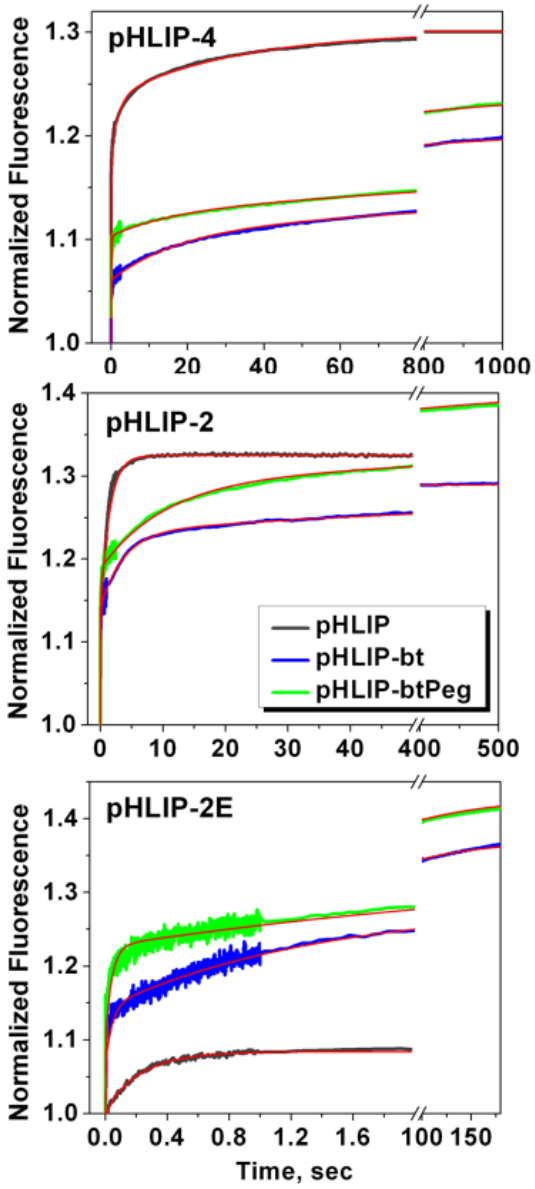

Figure 2

Figure 2. Insertion of pHLIP-4, -2, -2E with no cargo and with biotin and biotinPeg cargoes attached to the inserting ends of the peptides. The fitting curves are colored in red.

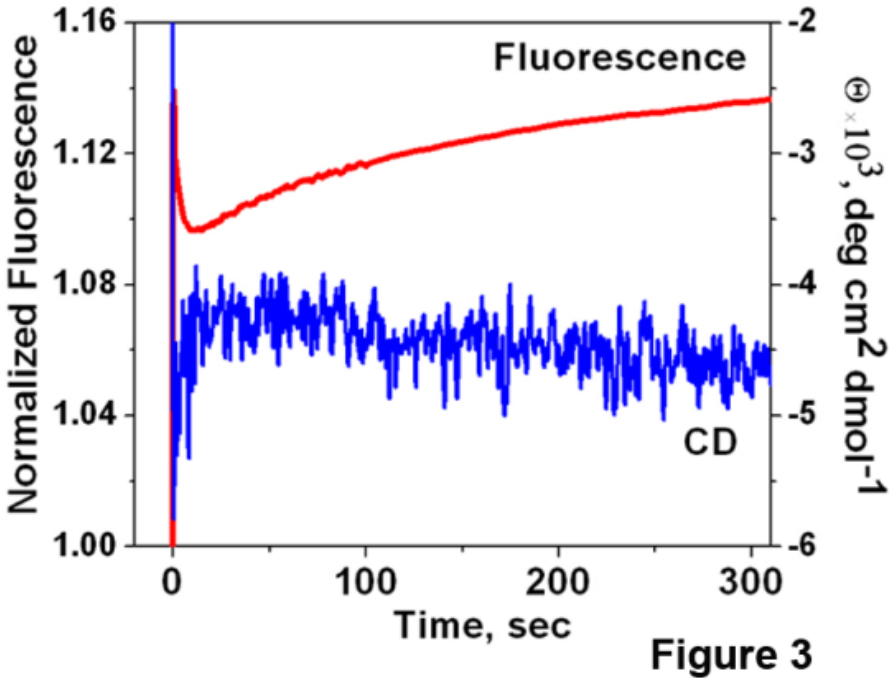

Figure 3. "Kink" in the fluorescence and CD kinetic curves at the pH8→6 transition for the pHLIP-4 variant.

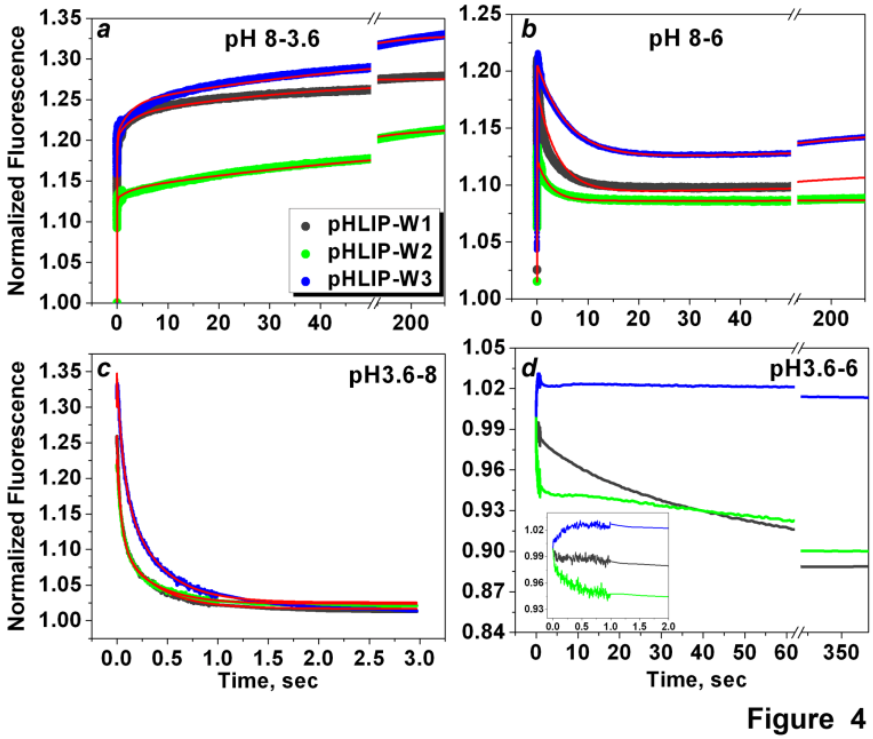

Figure 4. Insertion/exit of single-Trp pHLIP variants at different pHs. The fitting curves are colored in red.

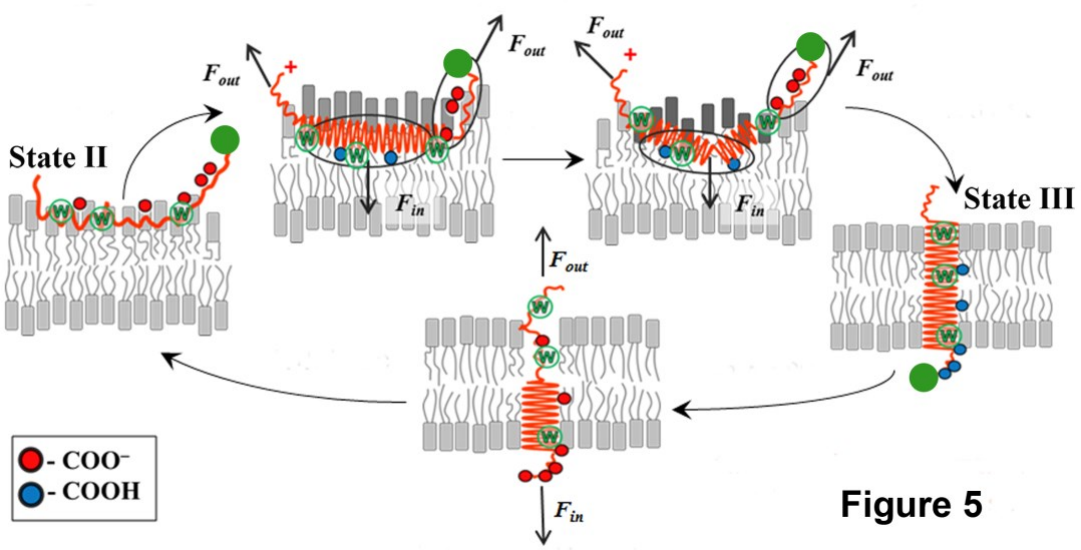

Figure 5. Model of membrane-associated folding and unfolding. The schematic presentation of the insertion/folding and exit/unfolding of pHLIP polypeptides. The letter "W" indicates approximate positions of Trp residues in the single-Trp pHLIP-4 variants. Small red and blue circles represent the approximate positions of the protonatable carboxyl groups of Asp, Glu and the C-terminus. The green circle represents polar cargo attached to the inserting end of the peptide. Membrane distortion is shown schematically by lipids with darker headgroups. In the case of pHLIP peptides with no cargo and a non-protonatable C-terminal end, the insertion and folding appears without intermediates as an all-or-none transition.

Supporting material

Modulation of the pHLIP transmembrane helix insertion pathway

Alexander G. Karabadzhak[1], Dhammika Weerakkody[1], Dayanjali Wijesinghe[1], Mak S. Thakur[1],

Donald M. Engelman[2], Oleg A. Andreev[1], Vladislav S. Markin[3], Yana K. Reshetnyak[1]

Materials and methods

Synthesis of peptides

All variants were prepared by solid-phase peptide synthesis using Fmoc (9-fluorenylmethyloxycarbonyl) chemistry and purified by reverse phase chromatography at the W.M. Keck Foundation Biotechnology Resource Laboratory at Yale. The lyophilized powder of each of the peptides was dissolved in a solution containing 3M urea, and the peptides were transferred to buffer using a G-10 size-exclusion spin column. The concentrations of the peptides were determined by absorbance (for pHLIP-4, -2, -2E and -1: $\varepsilon_{280} = 13{,}940\ M^{-1}\ cm^{-1}$; for pHLIP-W1 and -W2: $\varepsilon_{280} = 8{,}520\ M^{-1}\ cm^{-1}$; and for pHLIP-W3: $\varepsilon_{280} = 8{,}700\ M^{-1}\ cm^{-1}$).

Conjugation of biotin and biotin-Peg to the pHLIPs

For conjugation with biotin and biotinPeg, pHLIP peptides were mixed with biotin-maleimide or biotin-dPeg$_3$-maleimide (Quanta Biodesign Ltd) in DMSO at a ratio of 1:10 and incubated at room temperature for about 8 hrs and then at 4ºC until the conjugation reaction was completed. The reaction progress was monitored by HPLC.

The product was purified using reverse phase C18 HPLC, lyophilized and characterized by SELDI-TOF mass spectrometry.

Liposome preparation

Large unilamellar vesicles were prepared by extrusion. 25 mg POPC (1-palmitoyl-2-oleoyl-sn-glycero-3-phosphocholine, Avanti Polar Lipids, Inc.) or 99 mol% of POPC and 1 mol% of fluorescein (FITC) DHPE (*N*-(fluorescein-5-thiocarbamoyl)-1,2-dihexadecanoyl-*sn*-glycero-3-phosphoethanolamine, triethylammonium salt, Invitrogen) lipids were dissolved in 2.5 ml chloroform and desolvated on a rotary evaporator and dried under high vacuum for several hours. The phospholipid film was then rehydrated in 10 mM phosphate buffer, pH 8.0, vortexed for 2 hours, and repeatedly extruded through a membrane with either 100 or 50 nm pore sizes. The concentration of the fluorescein lipids was determined by absorbance of FITC-DHPE ε_{496} = 89,000 M^{-1} cm^{-1}.

Steady-state fluorescence and circular dichroism measurements

Tryptophan fluorescence and circular dichroism (CD) measurements were carried out on a PC1 ISS spectrofluorometer (ISS, Inc.) and a MOS-450 spectrometer (Biologic, Inc.), respectively, under temperature control. All measurements were performed at 25^{o}C. Peptide fluorescence spectra were recorded from 310 nm to 410 nm with the spectral widths of excitation and emission slits set at 4 and 2 nm, respectively, using excitation wavelengths of 295 nm (excitation of 280 nm was selected for study pHLIP-biotin constructs to reduce contribution of biotin). The polarizers in the

excitation and emission paths were set at the "magic" angle (54.7° from the vertical orientation) and vertically (0°), respectively, to reduce Wood's anomalies from the reflecting holographic grating. Peptide CD spectra were recorded from 190 to 270 nm with 0.5 nm increment using a cuvette with an optical path length of 0.5 cm. The concentration of the peptides and POPC were 7 μM and 1.5 mM, respectively.

pH-dependence

pH-dependent partitioning of the peptides into a lipid bilayer of membrane was investigated by the shift of the position of the fluorescence spectral maximum for the pHLIP variants in the presence POPC liposomes induced by a drop of pH from 8 to 3 by addition of HCl. 3 μM of the peptide was incubated overnight with 2 mM of 100-nm POPC liposomes, and pH decrease was achieved by the addition of aliquots of 4, 2, 1 and 0.1 M HCl. pH was measured by micro-electrode probe (Thermo Electron Corporation, Orion Ross Micro pH electrode). Fluorescence spectra were recorded at each pH value. The spectra were analyzed by the decomposition algorithms (40) using on-line PFAST toolkit (Protein Fluorescence And Structural Toolkit: http://pfast.phys.uri.edu/) (41). The position of the fluorescence maxima (λ_{max}) of single-component solutions obtained in a result of decomposition were plotted versus pH and the Henderson–Hasselbalch equation was used to fit the data (using Origin 8.5 software):

$$\lambda_{max} = \lambda_{2\,max} + \frac{(\lambda_{1\,max} - \lambda_{2\,max})}{1 + 10^{n\cdot(pH-pKa)}}$$

where $\lambda_{1\,max}$ and $\lambda_{2\,max}$ are the beginning and end of the transition, n is the cooperativety parameter, and pKa – is the midpoint of the transition. It is assumed that there is a linear relation between the position of maximum and contribution of the state II (or state III). However, due to the fact that the quantum yield in the states II and III is different it contributed to slight non-linearity. We performed completed analysis by estimating the contributions of states for pHLIP-4, which demonstrates the biggest difference in fluorescence between states II and III and found out that the apparent pK shifts no more than on 0.05 pH units toward lower pHs. Since the shift is non-significant (less than the experimental error) we present values of pKa of transitions from the state II to III, which were calculated based on the analysis of the position of maximum of single-component decomposition of original spectra.

Oriented circular dichroism measurements

Oriented circular dichroism was measured from supported bilayers deposited on a stack of quartz slides with special polish for far UV measurements, with spacers of 0.2 mm thickness on one side of each slide (Starna). Quartz slides were cleaned by sonication for 10 min in cuvette cleaner solution (Decon Contrad 5% in water), 2-propanol, acetone, 2-propanol and rinsed with deionized water. Then the slides were immersed in a mixture of concentrated sulfuric acid and hydrogen peroxide (ratio 3:1) for 5-10 min to completely remove any remaining organic material form the slides. Slides were then thoroughly rinsed with and stored in deionized water (Milli-Q purified water kept at 25 °C). A POPC lipid monolayer was deposited on the clean quartz substrate by the Langmuir-Blodgett (LB) method using a KSV minitrough. For

the LB deposition, a POPC lipid solution in chloroform was spread on the subphase and allowed to evaporate chloroform for about 30 min, followed by monolayer compression to 32 mN/m. An initial layer was deposited by retrieving the slide from the subphase at a rate of 15 mm/min. The second layer of the bilayer was created by fusion. For this step, the monolayer on the slide was incubated with a solution of POPC vesicles (50 nm in diameter obtained by extrusion) mixed with the peptide solution at pH 4 (0.5 mM POPC and 10 μM peptide). The fusion occurred during 6 hour incubation at 100% humidity. Then, excess vesicles were carefully removed and the slides were stacked to make a pile filled with the peptide solution (5 μM) at pH 4. Bilayers with the peptide solution were allowed an additional 6 hour equilibration. Measurements were taken at 3 steps during the process: when the monolayers were incubated with the excess of liposomes, soon after spaces between slides were filled with the peptide solution and 6 hours after the second measurement. 14 slides (28 bilayers) were assembled and OCD spectra were recorded on a MOS-450 spectrometer with 2 s sampling time. Control measurements were carried out of the peptide between slides with and without supported bilayers and in the presence of an excess of POPC liposomes.

Octanol-water partition coefficient measurements

The polarity of biotin-maleimide and Peg-biotin-maleimide was determined by the assessment of the relative partitioning between aqueous and octanol liquid phases. The biotin and biotin-Peg was dissolved in a 10 mM phosphate buffer pH8 (0.5 ml) followed by the addition of *n*-octanol (0.5 ml). The solutions were mixed by vortexing for 24 hrs at room temperature and then left for another 48 hrs in order to reach

equilibrium. After the phase separation, the absorption maximum of biotin at 300 nm was recorded for each phase. The molar extinction coefficients in *n*-octanol and phosphate buffer are assumed to be the same, and the ratio of the OD readings was used directly to calculate the partition coefficients, P = OD*n*-octanol/ODwater, and Log_{10} P values, which reflect the relative polarity of the cargoes.

Stopped–flow fluorescence and CD measurements

Stopped–flow fluorescence and CD measurements were carried out on a SFM-300 mixing apparatus connected to a MOS-450 spectrometer (Biologic, Inc.) under temperature control. The FC-20 and TS-100/15 observation cuvettes were used for the fluorescence and CD measurements, respectively. All solutions were degassed several minutes under a vacuum before loading into the syringes to minimize air bubbles. pHLIP variants (7 μM) were pre-incubated with POPC (1.5 mM) at pH 8.0 to reach binding equilibrium and folding/insertion was induced by fast mixing (5 ms dead time) of equal volumes of pHLIP-POPC variants at pH 8.0 and appropriately diluted HCl, to obtain a drop of pH from 8 to the desired value. At peptide (pHLIP-4) and lipid concentrations of 7 μM and 1.5 mM, respectively, more than 95% of the peptide is bound to the lipid bilayer of POPC liposomes according to our previous thermodynamic studies (15, 16). In the case of pHLIP-2, -2E and -1, stronger binding of the peptides to the membrane at pH8 is expected and therefore a smaller amount of the unbound peptide. In a separate control experiment we assessed changes of tryptophan fluorescence of the peptide in solution as a result of a pH drop in the absence of liposomes. Reduction of the pH is accompanied by a blue shift of the fluorescence emission of the peptide in solution (due to partial aggregation), but no

increase of fluorescence intensity is observed. Therefore, increase of fluorescence signal observed in the presence of liposomes reflects only the process of peptide partition into the bilayers. In the unfolding experiments, pHLIP variants were pre-incubated with POPC at pH 8.0, then HCl was added to lower the pH to 3.6, and half an hour was allowed for equilibration. Unfolding was induced by rapidly mixing equal volumes of pHLIP-POPC variants at pH 3.6 and diluted NaOH to increase the pH from 3.6 to the desired value. The mixing conditions and the concentrations of the peptide and lipids were optimized to ensure i) the proper rapid mixing of the entire volume of the sample to get the target changes of pH; ii) the best signal to noise ratio and iii) a minimal disruption of liposomes, which was assessed by changes of the scattered light signal. In the majority of cases, samples were collected after the stopped-flow shots and the steady-state fluorescence spectra were recorded on a PC1 spectrofluorometer. Changes of the pHLIP fluorescence signal were recorded through a 320 nm cutoff filter using an excitation wavelength of 295 nm (280 nm in case of pHLIP-biotin to minimize absorbtion of biotin). The fluorescence signal was corrected for photobleaching. Each kinetic curve was recorded several times (~10) and then averaged, excluding the first 2-3 shots. Changes of the pHLIP CD signal were recorded at 225 nm. About 20 shots were performed and CD signals were averaged. Kinetics signals were recorded with increasing step. It allows reducing number of points at long time scale. As a result, the signal at short time scale is noisier compared to the signal at long time scale.

Probing pH changes on the lipid bilayer inner leaflet by FITC fluorescence changes

To probe the kinetics of pH changes on the inner leaflet of vesicle lipid bilayers when the external pH is suddenly changed, we used POPC liposomes containing 1 mol% of FITC-DHPE. FITC-DHPE is a pH-sensitive fluorescent dye conjugated with lipid headgroups, and the dye absorbance and fluorescence decreases with a decrease of the pH from 9 to 4. The pH8→3.6 transition was induced by fast mixing (5 ms dead time) of 1.5 mM of POPC-FITC liposomes and HCl. To raise the pH, we rapidly mixed fluorescent liposomes, which were pre-mixed with HCl and had equilibrated at pH4 inside and outside the vesicles, with diluted NaOH. Different ratios were used to induce pH3.6→6 and pH3.6→8 transitions. FITC fluorescence emission changes were recorded at 519 nm using an excitation wavelength set at 496 nm.

Data analysis

The kinetic equations were solved in Mathematica 7 (Wolfram Research). Nonlinear least squares curve fitting procedures using Levenberg-Marquardt algorithm were carried out in Origin 8.5.0 SR1 and MatLab 2009b (7.9.0.529 version). The aim of curve fitting was to find the best fit of the experimental data to minimize the deviations of the theoretical curve from the experimental points (chi-square minimization). In each case we selected the solution with the minimal number of exponents that provide a fit of the experimental data within experimental error, the results are obtained within 95% confidence interval. We carried out global fitting when some characteristic times were used as shared parameters in the common fitting of kinetic curves obtained at different temperatures or different pHs. The global fitting

allows reduction of the number of variable parameters and gives a more reliable solution. An F-test was used to compare fits of different models to select the best one.

Tables

		State I	State II	State III
Increase of Area for pHLIP-4 is 1.54 and 2.15 in states II and III				
pHLIP-4-bt	λ_{max} ***S*** θ_{225} **x10^3**	351.3 nm 1.0 -1.43	349.5 nm 1.23 -1.56	340.9 nm 1.48 -6.05
pHLIP-4-btPeg	λ_{max} ***S*** θ_{225} **x10^3**	351.5 nm 1.0 -1.44	349.7 nm 1.24 -1.76	341.3 nm 1.53 -6.04
Increase of Area for pHLIP-2 is 1.86 and 2.20 in states II and III				
pHLIP-2-bt	λ_{max} ***S*** θ_{225} **x10^3**	351.5 nm 1.0 -1.39	345.6 nm 1.51 -2.41	340.0 nm 1.96 -6.33
pHLIP-2-btPeg	λ_{max} ***S*** θ_{225} **x10^3**	350.3 nm 1.0 -0.99	347.5 nm 1.28 -1.43	338.6 nm 1.99 -5.05
Increase of Area for pHLIP-2E is 2.54 and 2.64 in states II and III				
pHLIP-2E	λ_{max} ***S*** θ_{225} **x10^3**	349.0 nm 1.0 -1.10	341.3 nm 2.54 -4.42	339.2 nm 2.64 -6.36
pHLIP-2E-bt	λ_{max} ***S*** θ_{225} **x10^3**	350.7 nm 1.0 -1.89	344.7 nm 1.71 -3.96	340.1 nm 2.41 -6.09
pHLIP-2E-btPeg	λ_{max} ***S*** θ_{225} **x10^3**	350.9 nm 1.0 -1.61	347.9 nm 1.50 -2.27	340.1 nm 2.26 -5.05

Table S1. Three states of the pHLIP-cargo constructs. The spectral parameters of the pHLIP-4, -2 and 2E conjugated to the biotin and biotin-Peg cargoes in the states I, II and III are presented. The parameters were obtained from the analysis of the

fluorescence and CD spectra shown on the Figure 3 supporting material: the maximum position of the fluorescence spectrum λ_{max}, ***S*** – the normalized area under the spectra (normalization was done on the area under the spectrum in the state I); $\theta_{225} \times 10^3$, deg cm^2 $dmol^{-1}$ – the molar ellipticity at 225 nm.

Figures

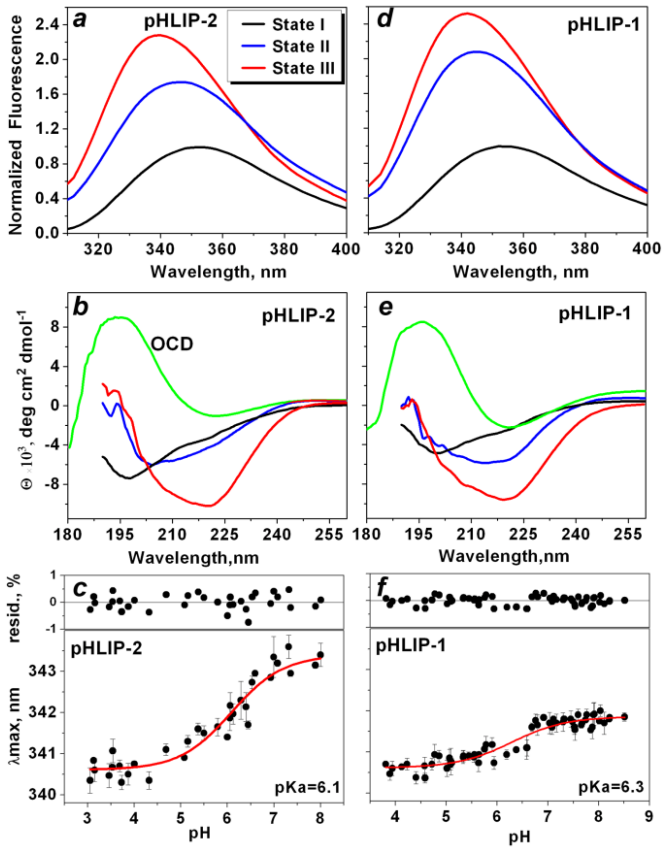

Fig. S1. pHLIP-2 and -1 variants show three states and pH-dependent insertion into a membrane. Three states of the pHLIP-2 and -1 variants monitored by the changes of the steady-state tryptophan fluorescence (***a***, ***d***) and CD (***b***, ***e***) spectroscopic signals are presented (state I is the peptide in solution at pH8; state II is the peptide in the presence of POPC liposomes at pH8; state III represents the peptide with POPC, when the pH was dropped from 8 to 3.6 by the addition of an aliquot of HCl). OCD signals (green lines on the ***b***, ***e***) demonstrate the transmembrane orientation of the helices at low pH. The pH-dependent insertion into the lipid bilayer of the membrane for the pHLIP-2 and -1 is shown on ***c*** and ***f***, respectively. The experimental points were fitted by the Henderson–Hasselbalch equation, the fitting curves are colored in red.

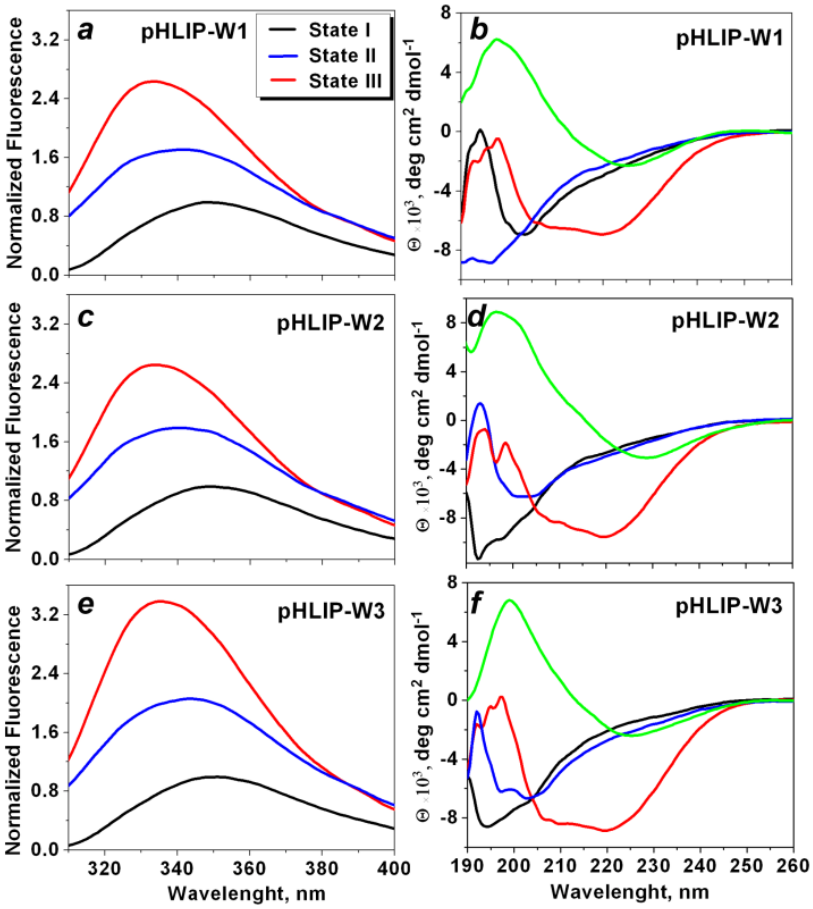

Fig. S2. Single-Trp pHLIP variants show three states. Three states of the single-Trp pHLIP variants (pHLIP-W1, -W2, -W3) were seen as monitored by the changes of the steady-state tryptophan fluorescence (***a***, ***c,*** ***e***) and CD (***b***, ***d,*** ***f***) spectroscopic signals. OCD signals (green lines on the ***b***, ***d***, ***f***) demonstrate the transmembrane orientation of the helices at low pH.

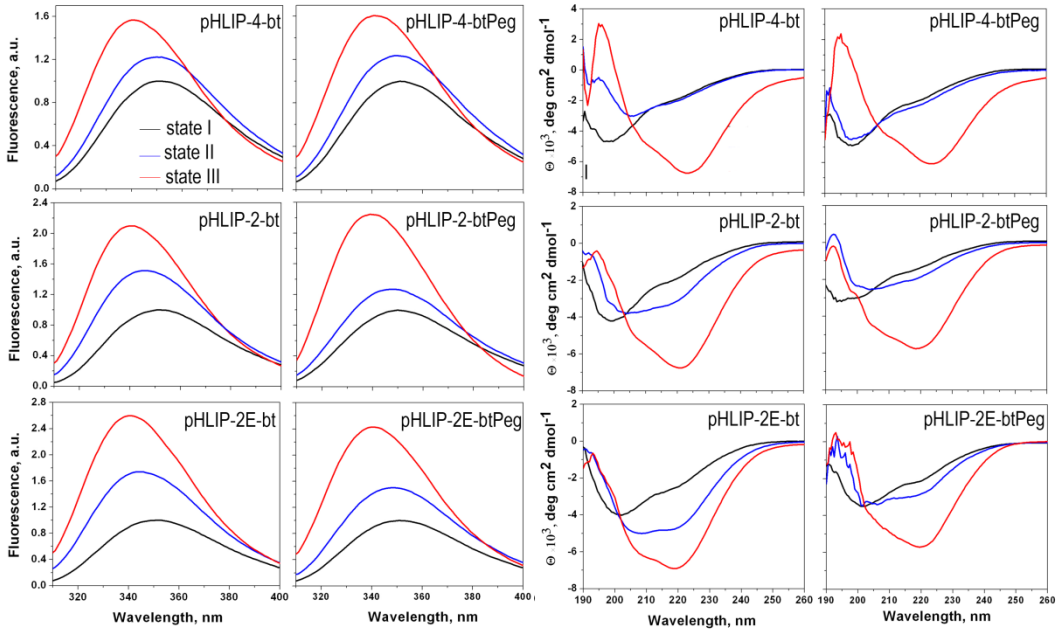

Fig. S3. Three states monitored by the changes of fluorescence and CD for pHLIP-cargo constructs. Three states of the pHLIP-4, pHLIP-2 and pHLIP-2E with the biotin and biotingPeg cargoes monitored by the changes of the steady-state peptide fluorescence and CD are presented (state I corresponds to the peptide-cargo in solution at pH8; state II corresponds to the peptide-cargo in the presence of POPC liposomes at pH8; state III corresponds to the peptide-cargo with the POPC, when the pH was dropped from 8 to 3.6 by addition of aliquot of HCl).

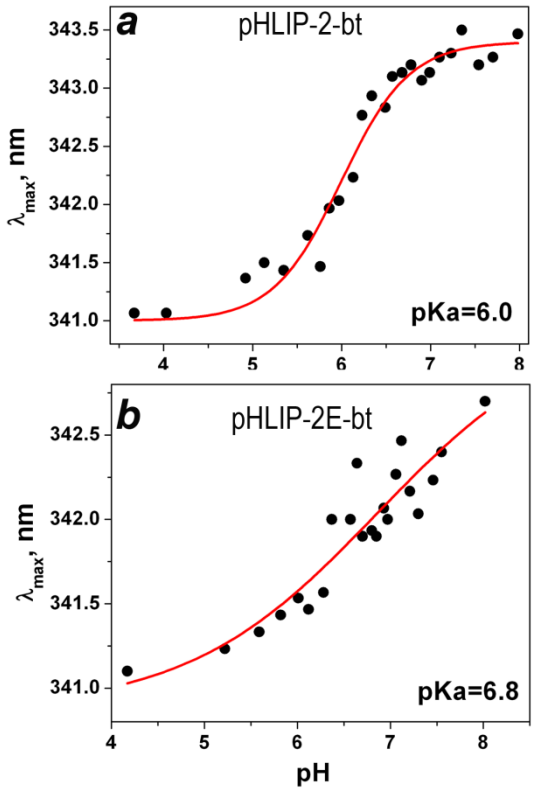

Fig. S4. pH-dependent insertion into lipid bilayer of the membrane of the pHLIP-2-bt (***a***) and the pHLIP-2E-bt **(*b*)** is shown. The pKa of the transitions were found by the fitting of the curves with the Henderson–Hasselbalch equation. The fitting curves are colored in red.

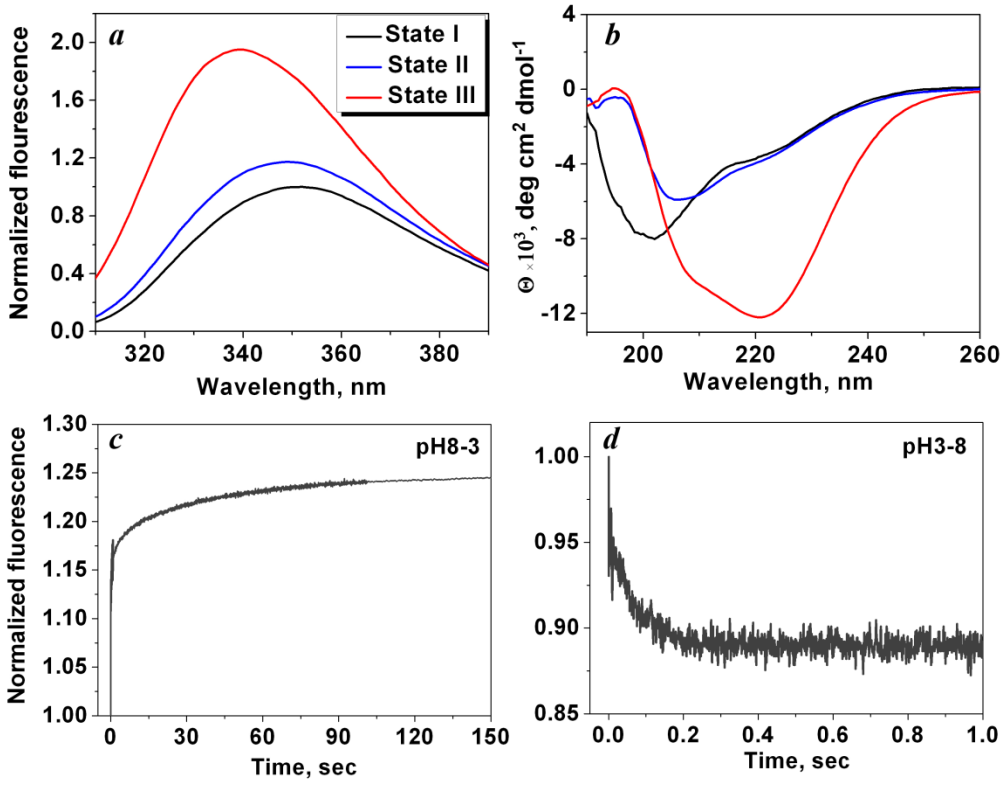

Fig. S5. pHLIP-6 show three states and pH-dependent insertion and exit from a membrane. Three states of the pHLIP-6 monitored by the changes of the steady-state tryptophan fluorescence (***a***) and CD (***b***) spectroscopic signals are presented (state I is the peptide in solution at pH8; state II is the peptide in the presence of POPC liposomes at pH8; state III represents the peptide with POPC, when the pH was dropped from 8 to 3.6 by the addition of an aliquot of HCl). Kinetics of the insertion into membrane (***c***) and exit from the lipid bilayer (***d***) for the pHLIP-6 are shown.

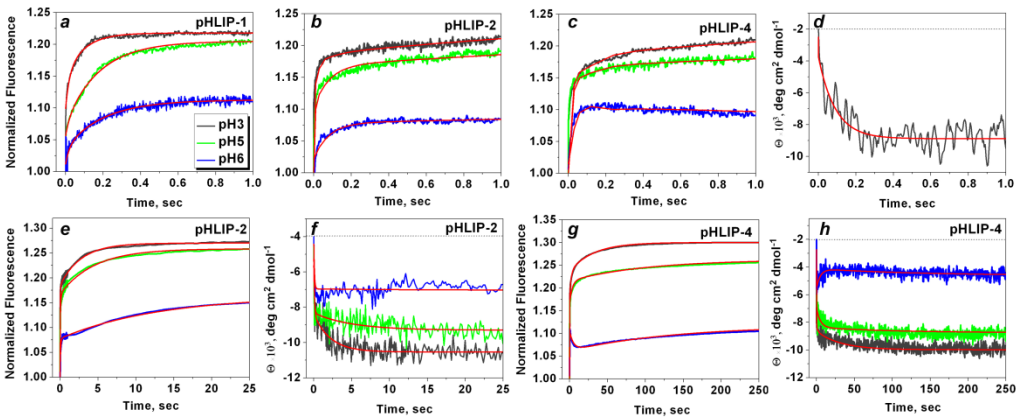

Fig. S6. Insertion and folding of pHLIP-4, -2 and -1 variants at different pHs. Kinetics of the fluorescence and CD changes recorded at different pH jump transitions (pH 8→6 - blue line; pH 8→5 green line; and pH 8→3.6 black line) for pHLIP-1 (***a***), pHLIP-2 short time scale (***b***) and long timescale (***e-f***), pHLIP-4 short time scale (***c***) and long timescale (***g-h***) are presented. Representative kinetics of the CD changes for the pH8→3.6 transition are shown (***d***) (similar signals were obtained for all pHLIP variants). All fitting curves are colored in red.

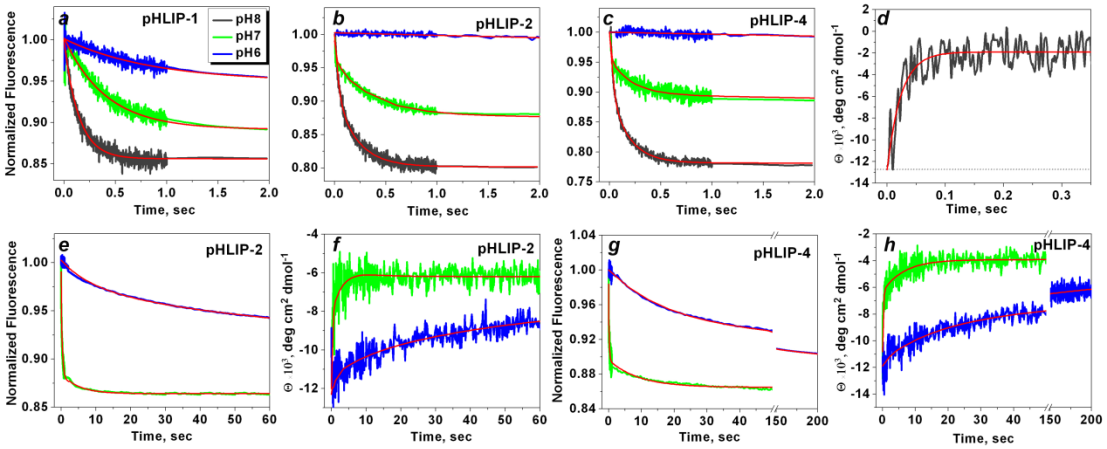

Fig. S7. Exit and unfolding of pHLIP-4, -2 and -1 variants at different pHs. Kinetics of the fluorescence and CD changes were recorded at different pH jump transitions (pH 3.6→6 - blue line; pH 3.6→7 - green line; and pH 3.6→8 - black line) for pHLIP-1 (***a***), pHLIP-2 short time scale (***b***) and long timescale (***e-f***), pHLIP-4 short time scale (***c***) and long timescale (***g-h***) are presented. Representative kinetics of the CD changes for the pH3.6→8 transition are shown (***d***) (similar signal was obtained for all pHLIP variants). All fitting curves are colored in red.

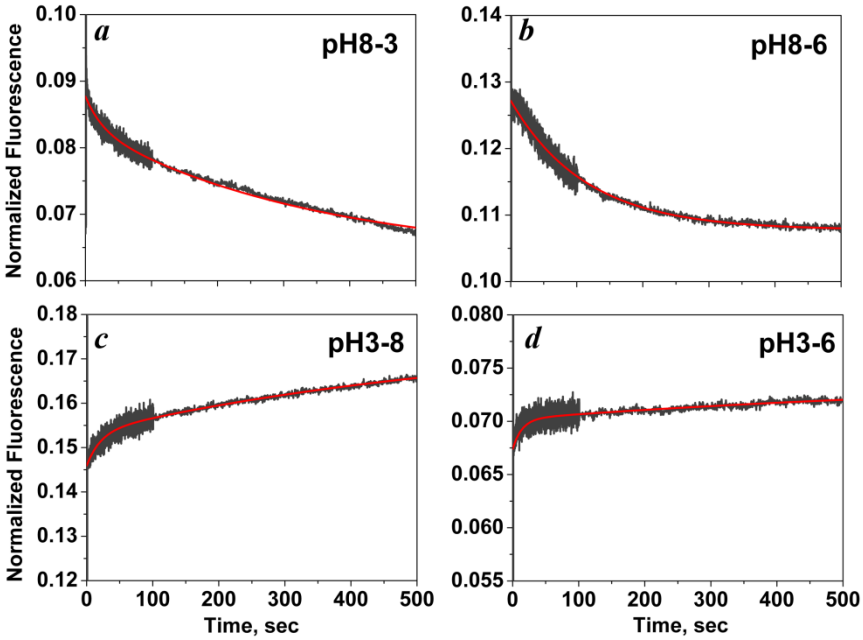

Fig. S8. Changes of FITC fluorescence on the inner leaflet of a bilayer in a result of pH drop or increase. POPC liposomes containing 1% of lipids with headgroups conjugated with pH-sensitive dye, FITC, were used to probe pH changes on inner leaflet of bilayer in a result of pH decrease (***a***, ***b***) and increase (***c***, ***d***). The kinetics of fluorescence changes were monitored at 519 nm with excitation at 496 nm. The fitting curves are colored in red.

Appendix 1

Two-State model

The two-state model is used to describe fast processes of folding of the pHLIP-2E variant, kinetic curves of which are fitted well by the single-exponential function. This model doesn't assume existence of intermediate states.

$$\mathbf{A} \underset{k_1^-}{\overset{k_1}{\rightleftharpoons}} \mathbf{B} \tag{1.1}$$

The transition from the state A to B is described by the differential equation:

$$\frac{d[A]}{dt} = -k_1[A] + k_1^-[B] \tag{1.2}$$

$$[A] + [B] = 1 \tag{1.3}$$

The variables A and B designate relative populations of the corresponding states. k_1 and k_1^- are the rates constant for the forward and backward reactions, respectively. We assume that initially all pHLIP molecules are in the state A and hence the initial conditions are:

$$A(0) = 1,\ B(0) = 0 \tag{1.4}$$

Exact solution of the differential equation 1.2 is the single-exponential function:

$$[A(t)] = \frac{k_1^-}{k_1+k_1^-} + \left(\frac{k_1}{k_1+k_1^-}\right) e^{-(k_1+k_1^-)t} \tag{1.5}$$

Some of the CD kinetic data were fitted by the single-exponential function:

$$S_{exp} = g_0 + g_1 \exp(-v_1 t) \tag{1.6}$$

where the characteristc rate v_1 expressed in a form of the rate constants is:

$$v_1 = k_1 + k_1^- \tag{1.7}$$

If we assume that equilibrium between the states A and B is strongly shifted to the right, meaning that $k_1 >> k^-_1$ and the difference between the rate constants at least an order of magnitude:

$$\frac{k_1}{k_1^-} \approx 10 \tag{1.8}$$

then we can estimate the rate of the forward reaction from the characteristic rate obtained in result of fitting of experimental data by single-exponential function:

$$k_1 \sim 0.91 v_1 \tag{1.9}$$

Appendix 2

Three-State model

In the majority of cases it was not possible to get an adequate fitting of the experimental data by the single-exponential function. Therefore we introduced a three-state model, which assumes the existence of a single intermediate:

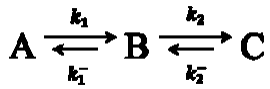

(2.1)

The transitions from one state to another are described by the differential equations:

$$\frac{d[A]}{dt} = -k_1[A] + k_1^-[B] \quad (2.2)$$

$$\frac{d[B]}{dt} = k_1[A] - (k_1^- + k_2)[B] + k_2^-[C] \quad (2.3)$$

$$[A] + [B] + [C] = 1 \quad (2.4)$$

The variables *A*, *B* and *C* designate relative populations of the corresponding states. We assume that initially all the pHLIP molecules are in the state A and hence the initial conditions are:

$A(0) = 1, B(0) = C(0) = 0$ (2.5)

Finally the equilibrium will be reached and the equilibrium populations can be easily found by the graph technique (Markin, V. S., and Y. A. Chizmadzhev. 1974. Induced Ion Transport. Nauka, Moscow), where the arrows represent corresponding transitions in the scheme (2.1) and can be substituted with their rate constants:

$$A_0 = \frac{\leftarrow\leftarrow}{\leftarrow\leftarrow+\rightarrow\leftarrow+\rightarrow\rightarrow} = \frac{k_1^- k_2^-}{k_1^- k_2^- + k_1 k_2^- + k_1 k_2}$$

$$B_0 = \frac{\rightarrow\leftarrow}{\leftarrow\leftarrow+\rightarrow\leftarrow+\rightarrow\rightarrow} = \frac{k_1 k_2^-}{k_1^- k_2^- + k_1 k_2^- + k_1 k_2} \quad (2.6)$$

$$C_0 = \frac{\rightarrow\rightarrow}{\leftarrow\leftarrow+\rightarrow\leftarrow+\rightarrow\rightarrow} = \frac{k_1 k_2}{k_1^- k_2^- + k_1 k_2^- + k_1 k_2}$$

To obtain the time evolution of all states one can exclude *B* and *C* from the system (2.2-2.4) and obtain the differential equation for *A*:

$$\frac{d^2[A]}{dt^2} + (k_1 + k_1^- + k_2 + k_2^-)\frac{d[A]}{dt} + (k_1^- k_2^- + k_1 k_2 + k_1 k_2^-)A - k_1^- k_2^- = 0 \qquad (2.7)$$

In general form the solution of the equation 2.7 is given by the two-exponential function:

$$A(t) = A_0 + A_1 \exp(-v_1 t) + A_2 \exp(-v_2 t) \qquad (2.8)$$

where the characteristic rates v_1 and v_2 are expressed in the form of rate constants:

$$v_1 = \frac{1}{2}(k_1 + k_1^- + k_2 + k_2^-) + \sqrt{\frac{1}{4}(k_1 + k_1^- + k_2 + k_2^-)^2 - (k_1^- k_2^- + k_1 k_2 + k_1 k_2^-)} \qquad (2.9)$$

$$v_2 = \frac{1}{2}(k_1 + k_1^- + k_2 + k_2^-) - \sqrt{\frac{1}{4}(k_1 + k_1^- + k_2 + k_2^-)^2 - (k_1^- k_2^- + k_1 k_2 + k_1 k_2^-)} \qquad (2.10)$$

The population of the state B is found from the equation 2.2:

$$B = \frac{1}{k_1^-}\frac{dA}{dt} + \frac{k_1}{k_1^-}A$$

$$= \frac{1}{k_1^-}[k_1 A_0 + A_1(k_1 - v_1)\exp(-v_1 t) + A_2(k_1 - v_2)\exp(-v_2 t)] \qquad (2.11)$$

and finally the population of the state C is given:

$$C = 1 - A - B$$

$$= 1 - \left(1 + \frac{k_1}{k_1^-}\right)A_0 - \left[1 + \frac{k_1 - v_1}{k_1^-}\right]\exp(-v_1 t)\,A_1 - \left[1 + \frac{k_1 - v_2}{k_1^-}\right]\exp(-v_2 t)\,A_2 \qquad (2.12)$$

Thus, the population of the states *B* and *C* can be expressed via A_0, A_1, and A_2. Taking into account that $A(0) = 1$ and $B(0) = 0$ we can obtain:

$$A_0 + A_1 + A_2 = 1 \qquad (2.13)$$

$$\frac{1}{k_1^-}[k_1A_0 + A_1(k_1 - v_1) + A_2(k_1 - v_2)] = 0 \quad (2.14)$$

Solving the equations (2.13) and (2.14) one can find:

$$A_0 = \frac{k_1^- k_2^-}{k_1^- k_2^- + k_1 k_2^- + k_1 k_2} \quad (2.15)$$

$$A_1 = \frac{k_1 - v_1(1 - A_0)}{v_1 - v_2} \quad (2.16)$$

$$A_2 = \frac{-k_1 + v_1(1 - A_0)}{v_1 - v_2} \quad (2.17)$$

If the transitions between the states *B* and *C* are much slower than between the states *A* and *B*, then the equations 2.15-2.17 could be significantly simplified and the amplitudes A_0, A_1, and A_2 can be expressed via the rate constants k_i in a closed form:

$$A_1 \approx \frac{k_1}{(k_1 + k_1^-)}\left[1 - \frac{2k_1^- k_2}{(k_1 + k_1^-)^2}\right] \quad (2.18)$$

$$A_2 \approx \frac{k_1}{(k_1 + k_1^-)} \frac{k_1 k_1^- k_2}{(k_1 k_2 + k_1 k_2^- + k_1^- k_2^-)}\left[1 - \frac{2k_1^- k_2}{(k_1 + k_1^-)^2}\right] \quad (2.19)$$

Let us designate the spectral (fluorescence or CD) signal of the different states *A*, *B* and *C* by S_A, S_B, S_C. Then the spectral signal of the whole system is:

$$S_{theor} = S_A A + S_B B + S_C C \quad (2.20)$$

Substituting here the expressions for the populations of the different states using equations 2.8; 2.11 and 2.12 one can obtain:

$$S_{theor} = S_C + A_0\left[S_A + \frac{S_B k_1}{k_1^-} - S_C\left(1 + \frac{k_1}{k_1^-}\right)\right] + A_1 \exp(-v_1 t)\left[S_A + \frac{S_B(k_1 - v_1)}{k_1^-} - S_C\left(1 + \frac{k_1 - v_1}{k_1^-}\right)\right] + A_2 \exp(-v_2 t)\left[S_A + \frac{S_B(k_1 - v_2)}{k_1^-} - S_C\left(1 + \frac{k_1 - v_2}{k_1^-}\right)\right] \quad (2.21)$$

Experimentally it was found that most of the pHLIP-1 and -2 kinetic curves could be adequately fitted by the two-exponential function:

$$S_{exp} = g_0 + g_1 \exp(-v_1 t) + g_2 \exp(-v_2 t) \quad (2.22)$$

Therefore the experimental measurements S_{exp} provide five parameters: two characteristic rate constants v_1 and v_2 and three characteristic fluorescence amplitudes g_0, g_1 and g_2. Comparing S_{theor} and S_{exp} we can find the relationships between the theoretical and experimental parameters:

$$g_0 = S_A A_0 + \frac{S_B k_1}{k_1^-} A_0 + S_c - S_c \left(1 + \frac{k_1}{k_1^-}\right) A_0 \quad (2.23)$$

$$g_1 = A_1 \left[S_A + S_B \frac{k_1 - v_1}{k_1^-} - S_c \left(1 + \frac{k_1 - v_1}{k_1^-}\right)\right] \quad (2.24)$$

$$g_2 = A_2 \left[S_A + S_B \frac{k_1 - v_2}{k_1^-} - S_c \left(1 + \frac{k_1 - v_2}{k_1^-}\right)\right] \quad (2.25)$$

And the rates are given by the equations 2.9 and 2.10. Unfortunately, the theoretical description involves seven parameters: four rate constants k_1, k^-_1, k_2, and k^-_2, and three fluorescence/CD amplitudes S_A, S_B, S_C against five experimental parameters, which make it impossible to find the parameters unless we would make assumptions. First, we concentrate our attention only on the rate constants. Second, we noticed that $v_1 >> v_2$, thus the equations 2.9 and 2.10 can be expanded into a series. The major terms in this expansion are:

$$v_1 \approx (k_1 + k_1^-) + \frac{k_1^- k_2}{(k_1 + k_1^-)} \quad (2.26)$$

$$v_2 \approx k_2^- + \frac{k_1 k_2}{(k_1 + k_1^-)} \quad (2.27)$$

If we assume that the equilibrium between the states A, B and C is strongly shifted to the right, meaning that $k_1 >> k^-_1$ and $k_2 >> k^-_2$, and the difference between the rate constants is at least an order of magnitude:

$$\frac{k_1}{k_1^-} \approx 10, \qquad \frac{k_2}{k_2^-} \approx 10 \quad (2.28)$$

then the rate of the forward reaction could be estimated from the characteristic rate obtained as the result of the fitting of the experimental data by the single-exponential function:

$$k_1 \sim \frac{v_1}{1.1} - \frac{v_2}{12.21} \quad (2.29)$$

$$k_2 \sim 1.0091 v_2 \quad (2.30)$$

Appendix 3

Four-state model

The adequate fitting of the pHLIP-2E-bt and -btPeg kinetic data was achieved only by the three-exponential function. Therefore we introduced four-state model, which assumes existence of two intermediates:

$$\mathbf{A} \underset{k_1^-}{\overset{k_1}{\rightleftharpoons}} \mathbf{B} \underset{k_2^-}{\overset{k_2}{\rightleftharpoons}} \mathbf{C} \underset{k_3^-}{\overset{k_3}{\rightleftharpoons}} \mathbf{D} \tag{3.1}$$

The transitions in this system are described by the set of equations:

$$\frac{d[A]}{dt} = -k_1[A] + k_1^-[B] \tag{3.2}$$

$$\frac{d[B]}{dt} = k_1[A] - (k_1^- + k_2)[B] + k_2^-[C] \tag{3.3}$$

$$\frac{d[C]}{dt} = k_2[B] - (k_2^- + k_3)[C] + k_3^-[D] \tag{3.4}$$

$$[A] + [B] + [C] + [D] = 1 \tag{3.5}$$

The variables *A*, *B*, *C* and *D* designate relative populations of the corresponding states. We assume that initially all pHLIP molecules are in the state A and hence the initial conditions are:

$$A(0) = 1,\ B(0) = C(0) = D(0) = 0 \tag{3.6}$$

Finally the equilibrium will be reached and the equilibrium populations can be easily found by the graph technique:

$$A_0 = \frac{\leftarrow\leftarrow\leftarrow}{\leftarrow\leftarrow\leftarrow + \rightarrow\leftarrow\leftarrow + \rightarrow\rightarrow\leftarrow + \rightarrow\rightarrow\rightarrow} = \frac{k_1^- k_2^- k_3^-}{k_1^- k_2^- k_3^- + k_1 k_2^- k_3^- + k_1 k_2 k_3^- + k_1 k_2 k_3}$$

$$B_0 = \frac{\rightarrow\leftarrow\leftarrow}{\leftarrow\leftarrow\leftarrow+\rightarrow\leftarrow\leftarrow+\rightarrow\rightarrow\leftarrow+\rightarrow\rightarrow\rightarrow} = \frac{k_1 k_2^- k_3^-}{k_1^- k_2^- k_3^- + k_1 k_2^- k_3^- + k_1 k_2 k_3^- + k_1 k_2 k_3} \tag{3.7}$$

$$C_0 = \frac{\rightarrow\rightarrow\leftarrow}{\leftarrow\leftarrow\leftarrow+\rightarrow\leftarrow\leftarrow+\rightarrow\rightarrow\leftarrow+\rightarrow\rightarrow\rightarrow} = \frac{k_1 k_2 k_3^-}{k_1^- k_2^- k_3^- + k_1 k_2^- k_3^- + k_1 k_2 k_3^- + k_1 k_2 k_3}$$

$$D_0 = \frac{\rightarrow\rightarrow\rightarrow}{\leftarrow\leftarrow\leftarrow+\rightarrow\leftarrow\leftarrow+\rightarrow\rightarrow\leftarrow+\rightarrow\rightarrow\rightarrow} = \frac{k_1 k_2 k_3}{k_1^- k_2^- k_3^- + k_1 k_2^- k_3^- + k_1 k_2 k_3^- + k_1 k_2 k_3}$$

Solution of these equations is given by the three-exponential functions with the characteristic rates v_1, v_2, v_3 and it is rather cumbersome. We can assume that the first transition is very fast and the equilibrium is strongly shifted toward the state B, which means $k_1^- \approx 0$. Then

$$v_1 \sim k_1, \tag{3.8}$$

and

$$[A](t) = A_1 \exp(-v_1 t) \approx \exp(-k_1 t) \tag{3.9}$$

Remaining equations are:

$$\frac{d[B]}{dt} = k_1[A] - (k_1^- + k_2)[B] + k_2^-[C] \tag{3.10}$$

$$\frac{d[C]}{dt} = k_2[B] - (k_2^- + k_3)[C] + k_3^-[D] \tag{3.11}$$

$$[A] + [B] + [C] + [D] = 1 \tag{3.12}$$

To solve this set one can exclude *D*:

$$\frac{d[C]}{dt} = k_2[B] - (k_2^- + k_3)[C] + k_3^-(1 - [A] - [B] - [C]) \tag{3.13}$$

and then exclude *C*:

$$\frac{d^2[B]}{dt^2} + (k_2 + k_2^- + k_3 + k_3^-)\frac{d[B]}{dt} + (k_2^- k_3^- + (k_3 + k_3^-)k_2)[B] + [-(k_1 + k_2^- + k_3 + k_3^-)k_1 + k_2^- k_3^-]\exp(-k_1 t) - k_2^- k_3^- = 0 \quad (3.14)$$

Solution of this differential equation is given by

$$B = B_0 + B_1 \exp(-v_1 t) + B_2 \exp(-v_2 t) + B_3 \exp(-v_3 t) \quad (3.15)$$

with similar expressions for C and D. The first characteristic rate v_1 is given by the equation 3.8, and v_2 and v_3 are determined by:

$$v_i = -0.5(k_2 + k_2^- + k_3 + k_3^-) \pm \sqrt{0.25(k_2 + k_2^- + k_3 + k_3^-)^2 - k_2^- k_3^- - (k_3 + k_3^-)k_2} =$$

$$-0.5(k_2 + k_2^- + k_3 + k_3^-) \pm 0.5\sqrt{(k_2 + k_2^- - k_3 - k_3^-)^2 - 4k_2^- k_3^-} \quad (3.16)$$

If we assume that the rates of consequent stages significantly decrease, i.e. $k_2, \bar{k}_2 >> k_3, \bar{k}_3$, then one can expand expression 3.16 into series and find solution in a simple form:

$$v_2 \approx (k_2 + k_2^-) + \frac{k_2^- k_3}{(k_2 + k_2^-)} \quad (3.17)$$

$$v_3 \approx \frac{k_2 k_3 + k_2 k_3^- + k_2^- k_3^-}{(k_2 + k_2^-)} \quad (3.18)$$

We can reasonably assume that the equilibrium (3.1) between the states B, C and D is strongly shifted to the right, meaning that $k_2, >> \bar{k}_2$ and $k_3 >> \bar{k}_3$. The difference should be at least an order of magnitude:

$$\frac{k_2}{k_2^-} \approx 10, \ \frac{k_3}{k_3^-} \approx 10 \quad (3.19)$$

and the rate constants are:

$$k_1 \sim v_1 \tag{3.20}$$

$$k_2 \sim \frac{v_2}{1.1} - \frac{v_3}{12.21} \tag{3.21}$$

$$k_3 \sim 0.991 v_3 \tag{3.22}$$

CHAPTER 4

Published in Proceedings of National Academy of Sciences (PNAS) on March 25th 2013

Biological Sciences - Applied Biological Sciences

A Family of pH (Low) Insertion Peptides for Tumor Targeting

Dhammika Weerakkody[1], Anna Moshnikova[1], Mak S. Thakur[1], Valentina Moshnikova[1], Jennifer Danniels[1],Donald M. Engelman[2], Oleg A. Andreev[1], Yana K. Reshetnyak[1]

[1]Physics Department, University of Rhode Island, 2 Lippitt Rd., Kingston, RI, 02881, USA

[2]Department of Molecular Biophysics and Biochemistry, Yale, P.O. Box 208114, New Haven, CT 06520-8114, USA

Running title: Targeting tumor acidity

Keywords: acidity, cancer marker, biophysical properties, imaging, fluorescence

Financial Support: The work was supported by the James Monroe fellowship to VM, NIH grants CA138468 to YKR, and CA133890 and GM073857 to OAA, DME, YKR. Masspec was done in RI-INBRE core facility funded by NCRR /NIH P20RR016457.

Corresponding author: Yana K. Reshetnyak, Physics Department, University of Rhode Island, 2 Lippitt Rd., Kingston, RI, 02881, USA, Phone: (401) 874-2060, Fax: (401) 874-2380, E-mail: reshetnyak@mail.uri.edu

Abstract

Cancer is a complex disease with a range of genetic and biochemical markers within and among tumors, but a general tumor characteristic is extracellular acidity, which is associated with tumor growth and development. Acidosis could be a universal marker for cancer imaging and the delivery of therapeutic molecules, but its promise as a cancer biomarker has not been fully realized in the clinic. We have discovered a unique approach for the targeting of acidic tissue using the pH-sensitive folding and transmembrane insertion of pH (low) insertion peptide (pHLIP). The essence of the molecular mechanism has been elucidated, but the principles of design need to be understood for optimal clinical applications. Here, we report on a library of 16 rationally designed pHLIP variants. We show how the tuning of the biophysical properties of peptide–lipid bilayer interactions alters tumor targeting, distribution in organs, and blood clearance. Lead compounds for PET/single photon emission computed tomography and fluorescence imaging/MRI were identified, and targeting specificity was shown by use of noninserting variants. Finally, we present our current understanding of the main principles of pHLIP design.

Introduction

The promise of exploiting tumor acidosis as a cancer biomarker has not been fully realized in clinical practice, even though the acidity has been a known property since the work of Otto Warburg nearly a century ago. The problem has been to find a practical way to target acidity. While studying membrane protein folding, we discovered a peptide (pH (Low) Insertion Peptide called pHLIP®) that reversibly folds and inserts across membranes in response to pH changes, and this discovery has led to a novel way to target acidic tissue. Our biophysical studies have revealed the molecular mechanism of pHLIP action, which is based on the increase of hydrophobicity of carboxyl groups when they become protonated under mildly acidic conditions, leading to peptide insertion into a membrane (1-4). We have shown that pHLIP can target acidic tissue and selectively translocate polar, cell-impermeable molecules across cell membranes in response to low extracellular pH (1, 5-10). As noted in the Molecular Imaging and Contrast Agent Database (MICAD) at NCBI, a pHLIP labeled with a fluorescent dye or a PET-agent (^{64}Cu-DOTA) is a marker for *in vivo* acidity (1, 5, 6), and it has recently been reported that a pHLIP peptide labeled with SPECT (^{99}Tc) probe targets acidic tumors (7), as well as PET (^{18}F) probe (Daumar et al., in press in Bioconjugate Chemistry). All prior studies *in vivo* were carried out with the WT-pHLIP sequence and showed that a good contrast and tumor to blood ratio can be achieved only more than 24 hours after pHLIP injection, when it has accumulated in the tumor and largely cleared from the blood (6, 7). However, for the use of pHLIP-based radioactive imaging agents in the clinic, a more rapid background signal reduction is absolutely essential. To address this important need, to

tune tumor targeting properties, and to broaden our understanding of the molecular mechanism of pHLIP action, we designed a set of 16 pHLIP variants based on chemical and physical principles. Comprehensive biophysical studies performed with non-labeled peptides were correlated with investigations of tumor targeting and organ distributions of fluorescent versions of the pHLIP variants. As a result, a set of design criteria has been established, and pHLIP candidates for imaging and therapeutic applications, including lead compounds for PET/SPECT and fluorescence/MR imaging, have been identified.

Materials and methods

Conjugation of pHLIP variants with fluorescent dyes

pHLIP variant wer prepared by solid-phase peptide synthesis using Fmoc (9-fluorenylmethyloxycarbonyl) chemistry and purified by reverse phase chromatography at the W.M. Keck Foundation Biotechnology Resource Laboratory at Yale. For cell and in vivo stides variatns were conjugated with AlexaFluor®750-C_5-maleimide, Tetramethylrhodamine-5-maleimide, single isomer or BODIPY®-TMR-C_5-maleimide (Invitrogen). The details of peptides conjugation could be found in Supplementary data.

Steady-state fluorescence and circular dichroism measurements

Peptide intrinsic fluorescence and circular dichroism (CD) measurements were carried out on a PC1 ISS spectrofluorometer (ISS, Inc.) and a MOS-450 spectrometer (Biologic, Inc.), respectively, under temperature control at 25^{o}C. Peptide fluorescence spectra were recorded with the spectral widths of excitation and emission slits set at 4 and 2 nm, respectively, using excitation wavelengths of 295 or 280 nm. The concentrations of the peptides and POPC liposomes were 7 μM and 1.5 mM, respectively. The method of liposome preparation and oriented circular dichroism measurments could be found in Supplementary data.

Titration experiments

Samples containing 5 μM of peptides and varying concentrations of lipids were prepared using an electronic repeater pipette (Eppindorf). Different pHs were used for

peptides with different pKas of insertion; the pH of the solution was one pH unit below the apparent pK value for each peptide. The samples at high and low pHs were allowed to equilibrate at 4°C overnight or 2 hours, respectively, before the measurements. The peptide intrinsic fluorescence spectra were measured using 280 nm excitation at 25°C with the emission polarizer set at 90° to reduce the contribution of scattered light. A series of POPC blanks with the same concentrations of lipids at pH8 were measured with the same instrument settings and were subtracted from the corresponding fluorescence spectra of peptides in the presence of POPC. The areas under the emission spectra were calculated and the values were normalized to the first point (the emission of the peptide in the absence of POPC). The titration data were fitted by the peptide-membrane partition model to calculate the mole-fraction partition coefficient, *K*

$$F = F_0 + \Delta F \frac{K \cdot C_{lip}}{W + K \cdot C_{lip}}$$

where F_0 and ΔF are the fluorescence intensity at the beginning and fluorescence increase as a result of the titration (in our case F_0 is 1), C_{lipids} is the concentration of lipids; *W* is the molar concentration of water (55.3 M). Nonlinear least squares curve fitting procedures using Levenberg-Marquardt algorithm were implemented in Origin 8.5.0 SR1. The Gibbs free energy (ΔG) was calculated according to the equation:

$$\Delta G = -RT \cdot ln(K)$$

Where *R* is the gas constant and *T* is the temperature in Kelvin.

pH-dependence

The pH-dependent partitioning of the peptides into lipid bilayers was investigated by the shift of the position of the peptide intrinsic fluorescence spectral maximum for the pHLIP variants induced by a drop of pH from 8 to 3 by addition of HCl in the presence of POPC liposomes. 3 μM of the peptide was incubated overnight with 2 mM of 100-nm POPC liposomes, and the pH was decreased by the addition of aliquots of 4, 2, 1 and 0.1 M HCl. The resulting pHs were measured using a micro-electrode probe (Thermo Electron Corporation, Orion Ross Micro pH electrode). Fluorescence spectra were recorded at each pH value. The spectra were analyzed by decomposition algorithms using an on-line PFAST toolkit (Protein Fluorescence And Structural Toolkit: http://pfast.phys.uri.edu/) to obtain spectral maxima (λ_{max}). Finally, the positions of the fluorescence spectral maxima (λ_{max}) of the single component solutions were plotted versus pH and the Henderson–Hasselbalch equation was used to fit the data:

$$\lambda_{max} = \lambda^2_{max} + \frac{(\lambda^1_{max} - \lambda^2_{max})}{1 + 10^{n\cdot(pH-pKa)}}$$

where λ^1_{max} and λ^2_{max} are the beginning and end of the transition, *n* is the cooperativity parameter, and the *pK*a is the midpoint of the transition. The details of assumptions made for the analysis of pH-dependence data could be found in Supplementary.

Stopped–flow fluorescence measurements

Stopped–flow fluorescence measurements were carried out on a SFM-300 mixing apparatus connected to a MOS-450 spectrometer (Biologic, Inc.) under temperature control. All solutions were degassed for several minutes under vacuum before loading

into the syringes to minimize air bubbles. pHLIP variants (7 μM) were pre-incubated with POPC (1.5 mM) at pH 8.0 to reach binding equilibrium, and insertion was induced by fast mixing (5 ms dead time) of equal volumes of pHLIP-POPC variants at pH 8.0 and appropriately diluted HCl, to obtain a drop of pH from 8 to the desired value. Each kinetic curve was recorded several times (~10) and then averaged, excluding the first 2-3 shots.

Cell lines

Human cervix adenocarcinoma (HeLa) and human lung carcinoma (A549) cells were acquired from the American Type Culture Collection. Human lung carcinoma and human cervix adenocarcinoma with stable expression of green fluorescent protein (GFP), A549-GFP and HeLa-GFP, respectively, were acquired from Cell Biolabs Inc. Cells were authenticated, stored according to supplier's instructions, and used within 3 months after frozen aliquot resuscitations. Cells were cultured in Dulbecco's Modified Eagle's Medium (DMEM) supplemented with 10% fetal bovine serum (FBS), 10 μg/mL of ciprofloxacin in a humidified atmosphere of 5% CO_2 and 95% air at 37°C. The pH5.9 medium was prepared by mixing 13.3 g of dry DMEM in 1 L of deionized water. Human cervical epithelial cells (HCvEpC), human mammary epithelial cells (HMEpC) and human bronchial epithelial cells (HBEpC) were acquired from Cell Applications Inc. Cells were authenticated, stored according to supplier's instructions, and used within 2 months. HCvEpC, HMEpC and HBEpC cells were cultured in cervical, mammary and bronchial epithelial cell growth medium, respectively, provided by Cell Applications Inc.

Fluorescence Microscopy

HeLa-GFP and A549-GFP ells were grown in 35-mm dishes with 14-mm glass-bottom windows coated with poly-d-lysine or collagen. Cells were washed with DMEM not containing FBS, pH 5.9 or 7.4 and then incubated with 2 μM of Rho- or BODIPY-labeled Var-3, K-Var3, Var7 or K-Var7 peptides at pH 5.9 or pH 7.4. After 30 minutes of incubation, cells were washed 4-5 times. Fluorescent images were acquired with a Retiga CCD camera (Qimaging, Burnaby, BC, Canada) mounted to an inverted Olympus IX71 microscope (Olympus America, Inc., Center Valley, PA).
The details of cellular uptake quantification could be found in Supplementary data.

Cytotoxicity Assay

HeLa, A549, HCvEpC, HMEpC or HMEpC cells were loaded in the wells of 96-well plates (~5,000 cells per well) and incubated overnight. The increasing amounts of pHLIP variants (1, 2, 4 and 8 μM) were added to HCvEpC, HMEpC or HMEpC cells, or growth medium was replaced with the medium without FBS containing increasing amounts of pHLIP in case and after 3 hours of incubation an equal volume of the medium containing 20% of FBS was added in case of Hela and A549 cells. After 24, 48 and 72 hours of incubation, a colorimetric reagent (CellTiter 96 AQ_{ueous} One Solution Assay, Promega) was added for 1 hour followed by measuring absorbance at 490 nm to assess cell viability. All samples were prepared in triplicate. None of the tested pHLIP variants showed any cytotoxic effect.

Animal studies

Athymic female nude mice ranging in age from 4 to 6 weeks and weighing from 15 to 18 g were obtained from Harlan Laboratories (Indianapolis, IN). In total, 266 mice were used in the experiments, and the number of mice used to study each pHLIP variant can be found in Tables S2-S5 of the Supplementary Data. Mouse tumors were established by subcutaneous injection of HeLa-GFP or A549-GFP cells (10^6 cells/0.1 ml/flank) in the right flank of each mouse. When tumors reached 5-6 mm in diameter, tail vein injections of 40 μM of 100 μl of Alexa750-pHLIPs were performed. Animals were imaged at 4 and 24 hours post-injection on a **FX** Kodak ***in-vivo*** image station under gas anesthesia with supplemental heat provided to maintain core body temperature. Animals were euthanized at 4 or 24 hours, and necropsy was performed immediately after euthanization. Tumors and major organs were collected for further imaging. The tumor/organ ratio was calculated according to the equation:

$$\frac{Tumor}{Organ} = \frac{F_{tumor} - F_{backg}}{F_{organ} - F_{backg}}$$

where F_{tumor} , F_{organ} and F_{backg} are the mean fluorescence intensities of tumor, organ and background signal, respectively. The contrast-to-noise ratio (CNR) was calculated according to the equation:

$$CNR = \frac{F_{tumor} - F_{backg}}{SD_{backg}}$$

where SD_{backg} is the standard deviation of the background signal. Fluorescence intensity was obtained from image analysis using Kodak software. Statistical analysis of the data was performed using the "Statistica 5.0" package. The p-level was computed based on the two-tailed test. All animal studies were conducted according to

an approved University of Rhode Island animal protocol (AN07-01-015), in compliance with the principles and procedures outlined in the NIH Guide for the Care and Use of Animals.

Results

Design of pHLIP variants

We have reported the basic molecular mechanism of the interaction of WT-pHLIP with lipid bilayers (1, 3, 11). In these studies we found three states of the peptide: State I, in solution as an unstructured monomer at neutral pH when no lipid membrane is present; State II, bound at the surface of a lipid bilayer as a largely unstructured monomer at neutral pH, and State III, inserted across the bilayer as a monomeric helix at acidic pH. To broaden our understanding of the main principles of pHLIP peptide interactions with membranes and to select the best sequences for clinical use, we employed our knowledge and designed 16 variants of the WT-pHLIP (Var0) sequence:

Var0-WT ACEQNPIY WARYADWLFTTPLLLLDLALLV DADEGT

Var1-2D1D ACEDQNPY WARYADWLFTTPLLLLDLALLV DG

Var2-2D1D ACEDQNPY WRAYADLFTPLTLLDLLALW DG

Var3-3D ACDDQNP WRAYLDLLFPTDTLLLDLLW

Var4-3E ACEEQNP WRAYLELLFPTETLLLELLW

Var5-3Da ACDDQNP WARYLDWLFPTDTLLLDL

Var6-3Db CDNNNP WRAYLDLLFPTDTLLLDW

Var7-3Ea ACEEQNP WARYLEWLFPTETLLLEL

Var8-3Eb CEEQQP WAQYLELLFPTETLLLEW

Var9-3Ec CEEQQP WRAYLELLFPTETLLLEW

Var10-2D ACEDQNP WARYADWLFPTTLLLLD

Var11-2E ACEEQNP WARYAEWLFPTTLLLLE

Var12-1D ACEDQNP WARYADLLFPTTLAW

Var13-1E ACEEQNP WARYAELLFPTTLAW

Var14-Rev Ac-TEDAD VLLALDLLLLPTTFLWDAYRAW YPNQECA-Am

Var15-2N CDDDDDNPNY WARYANWLFTTPLLLLNGALLV EAEET

Var16-2P CDDDDDNPNY WARYAPWLFTTPLLLLPGALLV EAEET

Biophysical studies

First, we studied the interaction of the pHLIP variants with lipid bilayers, employing the fluorescence and CD spectroscopic techniques previously used (3). The intrinsic tryptophan fluorescence and CD spectra of non-labeled variants measured in solution at pH8 in the absence and presence of POPC liposomes and in the presence of liposomes at low pH (pH 4-5) indicate that each peptide interacts with a lipid bilayer in a pH-dependent manner and that the peptides form transmembrane helices in state III (Supplementary Table S1 and Figure S1).

The partitioning of pHLIP variants into bilayers at pHs 8 and 4-5 was assessed in titration experiments by measuring changes of intrinsic peptide fluorescence (Figure 1). On average, the partitioning of the variants into the membrane at low pH is about 50 fold higher than at high pH. As expected, the truncated variants Var5-13 have lower affinities for the membrane at neutral pH compared to WT and other variants, since a number of hydrophobic residues were removed from the sequences. In general, variants with Glu residues have slightly higher affinities compared to the same variants with Asp (since Glu is more hydrophobic due to the additional methylene

group). The highest affinity was observed for Var15, which forms helical structure at neutral pH. At low pH, the lowest affinity for the lipid bilayer was observed for the most truncated versions Var10-13 and variants (Var15 and 16) with no protonatable residues in the TM, which reflects the reduced stability of the TM helix. The numbers below are the differences between the Gibbs free energies of the interactions of variants with the membrane at low and high pHs (in kcal/mol): $\Delta\Delta G = \Delta G_{pH4} - \Delta G_{pH8}$

Var1 Var2 Var3 Var4 Var5 Var6 Var7 Var8 Var9 Var10 Var11 Var12 Var13 Var14 Var15 Var16

2.17 0.28 2.23 1.72 2.31 1.93 2.39 2.19 2.07 1.79 1.94 1.95 1.15 1.78 0.82 1.47

The above numbers reflect both the differences in binding affinities, and to some degree, the strength of helical structure formation in the membrane. The largest differences are observed for Var3, Var5 and Var7. The smallest differences are found for Var2 and Var15 due to the strong interactions of these peptides with the bilayer in state II at pH8.

The pKa of peptide insertion is determined by the pKa of protonation of Asp/Glu residues in the TM and at the inserting end of the peptide. As charged carboxyl groups located at the transition zone between the aqueous and hydrophobic environments sink more deeply into the bilayer, the pKa is progressively raised by the reduced dielectric constant, and the pKa of Asp/Glu residues increases. Thus, all truncated variants (Var5-13), which demonstrated weaker interactions with lipid bilayer surfaces at neutral and high pHs, would have lower pKa's of insertion. The pKa of pHLIP variant insertion was measured by following the shift of the position of the intrinsic peptide emission maximum as the pH is changed from 8 to 2 (Figure 2). As expected, the shift

of pKa to lower pHs correlates with the truncation of the pHLIP sequence. Thus, the pKa of Var10, with a single Asp residue in its TM, is the lowest (pKa=4.5). All variants containing Glu residues (Var7-9, 11, 13) have higher pKa values compared to the related sequences with Asp residues (Var5-6, 10, 12), again as expected if the increased hydrophobicity of the Glu causes a deeper association with the bilayer, lowering the dielectric and raising the pK.

To this point, we have considered the equilibrium energies of progressive binding and insertion events, but it is also important to note that sequence variation will alter the kinetics of insertion. The barrier for insertion includes the resistance to the passage of the inserting terminal end of the peptide from the aqueous compartment outside to the aqueous compartment inside a cell or liposome. We have found in recent work that the kinetics of insertion correlates with the number of protonatable groups at the inserting end or the presence of polar cargo (12). The characteristic membrane insertion time for WT-pHLIP is about 30 sec, and slightly faster kinetics were observed for Var14, which is the reverse sequence of WT. Var14 has the same number of protonatable residues at its N-terminus as WT has at its C terminus, except for the free C-terminus itself. The data are consistent with the view that the acetylated N-terminus of Var14 inserts across the bilayer and the amidated C-terminus stays outside, reversing the direction of insertion. The characteristic time of Var1-2 insertion, which has fewer protonatable residues at its C-terminus than WT, was about 1-2 sec, which correlates well with our recent findings (12). Further truncation of the peptide inserting end, which reduces the number of protonatable residues, resulted in faster peptide insertion, completed within first 30-100 msec for Var3-13. Var15-16 have no protonatable

residues in the TM, while they have the same number of Asp/Glu as WT at the inserting end, and as a result the time of insertion was reduced to 10-11 sec relative to WT. The kinetics data are shown in Figure 3.

Tumor targeting and distribution of Alexa750-pHLIPs in organs

We used a mouse xenograft model to assess the tumor targeting and organ distribution of the pHLIP variants. Tumors were created by subcutaneous injection of HeLa-GFP cancer cells in the right flanks of each mouse, and were grown to about 5 mm in diameter. To perform biodistribution studies, pHLIP variants were conjugated with Alexa750. We demonstrated that the kinetics of insertion of Alexa750-WT-pHLIP into lipid bilayers is similar to the kinetics of insertion of non-labeled peptide (Supplementary Figure S2). Fluorescently labeled pHLIPs were given as single intravenous injections, and the major organs and tumors were collected at 4 and 24 hours after fluorescent pHLIP administration. The GFP and NIR signals were monitored in tumors and organs after sacrificing the mice. The mean intensities of NIR fluorescence normalized to the signal in kidneys at 4 hours are shown on Supplementary Figure S3. The mean intensities of NIR fluorescence of all organs and the number of mice used in the study for each variant are given in Supplementary Table S2 and Table S3.

The pHLIP variants that show higher affinities for membranes at high pH have higher short-term liver uptake (Var 1, 2, 4, 14-16), however the liver is cleared at 24 h except for Var1. Var3 has high tumor targeting compared to kidney and compared to other pHLIPs as well. Whole-body (data not shown) and organ imaging confirmed that the truncated variants Var5-13 have much faster blood clearance than WT, and at 4 hours

the signal has accumulated in the tumor, while being washed out of the organs. Tumor targeting was minimal for the shortest pHLIP variants Var12-13. The tumor/muscle, tumor/kidney and tumor/liver ratios are given in Figure 4 for all pHLIP variants calculated at 4 and 24 h after injection. Variants 0, 3-4, 14-16 have the highest tumor/muscle ratio at 24 hours. The same pHLIP variants have the highest tumor/kidney ratios, while only Var3 shows significantly less accumulation in the liver. Among the truncated pHLIP variants, Var7 demonstrates the highest tumor targeting.

This body of work allows us to propose different pHLIP variants for different applications. We have selected Var3 and Var7 as the best candidates for future studies for fluorescence/MRI and SPECT/PET imaging, respectively, guided by the fact that the imaging time window for the stable fluorescence and MRI agents can be much wider than for the short half-life SPECT and PET agents. Var3 had the highest tumor/organ ratios, especially at 24 hours after construct administration. Var7 had a lower tumor/organ ratio, but showed much faster blood clearance. The cytotoxicity of the selected pHLIP variants was evaluated on human cervix adenocarcinoma cells (HeLa), human lung carcinoma (A549) cells as well as human cervical (HCvEpC), mammary (HMEpC) and bronchial (HBEpC) epithelial cells. Peptides at concentrations of up to 8 μM were evaluated up to 72 hours incubation with cells, and no toxicity was observed.

pH-insensitive K-pHLIPs

As a control, we have previously used K-pHLIP-WT, where the two key Asp residues in the TM part of the peptide were replaced by Lys residues (1). K-pHLIP cannot

interact with a membrane in a pH-dependent manner over the range of neutral and low pHs we are studying, and therefore should not target acidic tumors. Because of the potential clinical applications of Var3 and Var7 we synthesized and tested K-versions of each:

K-Var3 ACDDQNP WRAYLKLLFPTKTLLLKLLW

K-Var7 ACEEQNP WARYLKWLFPTKTLLLKL

Each of these peptides failed to interact with lipid bilayers in a pH-dependent fashion (Figure 5a-b). No shift in the position of the peptide fluorescence maximum was seen for either of the K-pHLIPs in the presence of lipid as a result of pH decrease, and the CD spectra do not change and do not exhibit the minimuma at 208 and 225 nm that are characteristic signals reporting alpha-helical conformations. The CD spectra reveal a negative band at 234 nm and a positive band at 221 nm, suggestive of an exciton split doublet (3, 13) possibly arising from peptide aggregation.

Var3 and Var7, as well as K-Var3 and K-Var7 were conjugated with two different fluorescent dyes: zwitterionic, tetramethylrhodamine (Rho), and non-charged, BODIPY to ensure that distribution and localization of fluorescent peptides is independent of the choice of dye. The fluorescence images demonstrating cellular uptake of Rho- and BODIPY-labeled Var3, Var7, K-Var3 and K-Var7 are shown in Figure 5c-d and Supplementary Figure S4, respectively. The fluorescence signal of cells treated with fluorescent Var3 and Var7 at pH7.4 was weaker compare to cells treated with peptides at pH5.9. The cellular uptake of Var3 was 1.12 times higher at low pH compare to neutral pH, and uptake of Var7 was 1.34 times higher at low pH. Our biophysical data show that the affinity of Var3 for a membrane at pH8 is higher than the affinity of Var7 at the same pH, therefore we see slightly higher cellular

uptake of Var3 at pH7.4 compare to Var7 and a less pronounced difference in cellular uptake between neutral and low pHs for Var3. For the cases of K-Var3 and K-Var7, the fluorescence signal was very similar when cells were treated at either high or low pHs, moreover the fluorescence signal at pH7.4 was slightly higher than at pH5.9. Also, the distributions of fluorescent signals for D- and E-variants and K-variants were different. K-Var3 and K-Var7 were distributed as cytoplasmic dots. In contrast to pHLIP variants, K-pHLIPs are positively charged and partially aggregated, and, most probably, might be taken up by endocytosis and trapped in endosomes in a pH-independent manner, while cellular uptake of Var3 and Var7 is pH-dependent.

Biodistribution and tumor targeting of Alexa750-K-pHLIPs were also investigated using xenograft models in mice. In contrast to Var3 and Var7, K-pHLIPs did not show significant tumor targeting (Figure 5e-f and Supplementary Table S4). To demonstrate that tumor targeting by Var3 and Var7 and the lack of tumor targeting by K-Var3 and K-Var7 is independent of choice of tumor model and imaging fluorescent probe, we used BODYPI labeled Var3, Var7, K-var3 and K-Var7, which were tested on tumors created by subcutaneous injection of A549-GFP human lung carcinoma cells. The organs were collected at 4 hours and analyzed (Supplementary Table S5). The tumor to muscle ratio at 4 hours for Var3 and Var7 labeled with BODIPY and Alexa750 was 6.0±0.9, while for K-Var3 and K-Var7 it was 2.6±0.3 (Figure 5g). Thus, the replacement of the Asp/Glu residues by Lys in the TMs of Var3 and Var7 leads to the loss of both pH-dependent interactions with membranes and targeting of acidic tumors, supporting a central role for the carboxyl groups in targeting.

Discussion

Rapid cell growth and an inadequate blood supply produce hypoxic conditions that cause a partial use of glycolysis in tumor cells, resulting in acidification of the cytosol, to which the cell adjusts by pumping protons into the external environment. But, hypoxia and low blood supply are not the only mechanisms responsible for the development of an acidic environment within solid tumors (14). Malignant cancers have an elevated glucose uptake even under normal oxygen conditions, overwhelming the mitochondrial capacity and using glycolysis for the overflow. This condition is known as "aerobic glycolysis" or the Warburg effect (15). Cells exhibiting a Warburg effect catabolize glucose at a high rate (16, 17), and the use of glycolysis results in a much higher level of production of H^+ and lactic acid, which are pumped across cell plasma membranes into the extracellular space, where they accumulate in poorly perfused regions (18-20). In addition to the lactic acid-output, intracellular titration of acid with bicarbonate and the engagement of the pentose phosphate shunt releases CO_2 from tumor cells. Expression of carbonic anhydrase 9 and 12 on the tumor cell surface catalyzes the extracellular trapping of acid by hydrating cell-generated CO_2 into HCO_3^- and H^+ (21, 22). These mechanisms combine to create an acidic extracellular milieu favoring tumor growth, invasion and development.

The pHLIP peptides can exploit tumor acidity as a useful biomarker. Based on the results of our previous and current investigations, design principles can be formulated to set directions for different clinical uses:

i) all pHLIP peptides have a membrane-binding sequence, which contains a number of hydrophobic residues essential for membrane targeting;

ii) a pHLIP is stable across a lipid bilayer at low pH;

iii) to achieve pH-dependent targeting, at least one protonatable group (Asp or Glu, or any other) needs to be in the sequence;

iv) in addition to the membrane-binding sequence, a pHLIP peptide may contain a membrane inserting sequence (the C-terminus for most investigated pHLIPs or the acetylated N-terminus of the reverse pHLIP sequence), which crosses the lipid bilayer and emerges in the cytoplasm. The protonatable residues could be only in the inserting sequence or in both the TM and inserting parts of the peptide;

v) the number of protonatable residues increases the cooperatively of the transition, narrowing the pH range over which insertion occurs;

vi) the non-inserting flanking sequence may be used for modulation of peptide solubility, for example by adding polar and negatively charged residues at the non-inserting end (all pHLIP peptides are soluble in aqueous solution at neutral and high pHs).

The list of the major biophysical properties that affect tumor targeting by pHLIP peptides could be found in Supplement data.

Based on the studies reported here, and motivated by potential clinical applications, we selected two pHLIP variants for further development (in addition to WT-pHLIP): Var3 and Var7. For each of these variants we tested versions with the TM carboxyl groups replaced by amino groups (D to K and E to K), and showed that the K-peptides lose their abilities to interact with membranes in a pH-dependent manner and to target

tumors *in vivo*. Var3 demonstrates high tumor to organ ratios at 24 hours (similar to WT) and could be well suited for optical imaging or MRI one day after construct administration. Var3 might also be suitable for fluorescence-guided surgery, marking a tumor with fluorescently-labeled pHLIP and performing surgery on the next day, when the contrast index is the highest. Var7 is one of the truncated versions of pHLIP, which could be appropriate for SPETC/PET imaging, since it demonstrates fast tumor targeting and blood clearance.

In this report, we show that the biophysical principles that guide pHLIP peptide interactions with lipid bilayers can be used to determine peptide performance *in vivo*, and we identify two pHLIP variants as appropriate candidates for uses in clinical imaging of acidic tissues, such as solid tumors.

Acknowledgements

We are grateful to Prof. Jason Lewis, MSKCC for reading the manuscript and helpful discussion.

GRANT SUPPORT

The work was supported by the NIH grants CA138468 to YKR, and CA133890 and GM073857 to OAA, DME, YKR. Masspec was done in RI-INBRE core facility funded by NCRR /NIH P20RR016457.

FIGURE LEGENDS

Figure 1. Titration of pHLIP variant binding to liposomes at high and low pHs. The titration of the pHLIP variants with increasing concentration of POPC liposomes at pH8 (***a***) and pH4-5 (***b***) are followed using intrinsic peptide fluorescence changes. For comparison the mole-fraction partition coefficients for Var0 (WT-pHLIP) at pH8 and 5 are $4.87x10^4$ and $1.54x10^6$, respectively, and the corresponding Gibbs free energies are 6.04 and 7.98 kcal/mol.

Figure 2. pH-dependent bilayer insertion of variants. Peptide intrinsic fluorescence changes are used to follow the insertion as a function of pH (transition from the state II to state III as the pH is lowered).

Figure 3. Kinetics of insertion. Representative kinetic curves for the insertion of variant peptides into the lipid bilayer are shown, the characteristic time of insertion of Var0 (WT-pHLIP) is about 40 sec.

Figure 4. **Tumor to organ fluorescence ratios.** Tumor to muscle, tumor to kidney and tumor to liver ratios calculated at 4 and 24 hour time points are shown for all pHLIP variants.

Figure 5. Comparisons with control K-pHLIPs. The CD (***a***) and tryptophan fluorescence (***b***) spectra of K-Var3 and K-Var7 show that these variants lose the ability to interact with a lipid bilayer in a pH-dependent manner. (***c-d***) Cellular uptake at pH7.4 and 5.9 of Var3, K-Var3, Var7 and K-Var7 labeled with Rhodamine are shown. The cellular uptake of four peptides labeled with BODIPY are shown at both pHs in Supplementary Figure S4. (***e-f***) Whole-body NIR fluorescence images of mice obtained at 4 and 24 hours after *i.v.* administration of Var3, K-Var3 (***e***) and Var7, K-

Var7 (***f***) conjugated with Alexa750. The tumor is indicated by arrows on the NIR images as reported by the GFP signal shown in adjacent images. Images obtained at different time points are presented with maximum contrast, the contrast-to-noise ratios are: Var3, 4h – 103; Var3, 24h – 186; Var7, 4h – 85; Var7, 24h – 360; K-Var3, 4h – 87; K-Var3, 24h – 54; K-Var7, 4h – 22; K-Var7, 24h – 16. (***g***) The A549-GFP tumor to muscle ratios calculated for 4 hours for BODIPY-pHLIPs and –K-pHLIPs and HeLa-GFP tumor to muscle ratios calculated for 4 and 24 hours time points for Alexa750-pHLIPs and –K-pHLIPs are shown. The mean fluorescence of HeLa-GFP and A549-GFP tumors and organs at 4 and 24 hours after Alexa750-K-pHLIPs and at 4 hours after BODIPY-pHLIPs and –K-pHLIPs administration are given in the Supplementary Table S4 and S5, respectively.

References

1. Andreev OA, Dupuy AD, Segala M, Sandugu S, Serra DA, Chichester CO, et al. Mechanism and uses of a membrane peptide that targets tumors and other acidic tissues in vivo. Proc Natl Acad Sci U S A. 2007;104:7893-8.
2. Musial-Siwek M, Karabadzhak A, Andreev OA, Reshetnyak YK, Engelman DM. Tuning the insertion properties of pHLIP. Biochim Biophys Acta. 2010;1798:1041-6.
3. Reshetnyak YK, Segala M, Andreev OA, Engelman DM. A monomeric membrane peptide that lives in three worlds: in solution, attached to, and inserted across lipid bilayers. Biophys J. 2007;93:2363-72.
4. Barrera FN, Weerakkody D, Anderson M, Andreev OA, Reshetnyak YK, Engelman DM. Roles of carboxyl groups in the transmembrane insertion of peptides. J Mol Biol. 2011;413:359-71.
5. Reshetnyak YK, Yao L, Zheng S, Kuznetsov S, Engelman DM, Andreev OA. Measuring tumor aggressiveness and targeting metastatic lesions with fluorescent pHLIP. Mol Imaging Biol. 2011;13:1146-56.
6. Vavere AL, Biddlecombe GB, Spees WM, Garbow JR, Wijesinghe D, Andreev OA, et al. A novel technology for the imaging of acidic prostate tumors by positron emission tomography. Cancer Res. 2009;69:4510-6.
7. Macholl S, Morrison MS, Iveson P, Arbo BE, Andreev OA, Reshetnyak YK, et al. In Vivo pH Imaging with (99m)Tc-pHLIP. Mol Imaging Biol. 2012.

8. Reshetnyak YK, Andreev OA, Lehnert U, Engelman DM. Translocation of molecules into cells by pH-dependent insertion of a transmembrane helix. Proc Natl Acad Sci U S A. 2006;103:6460-5.

9. An M, Wijesinghe D, Andreev OA, Reshetnyak YK, Engelman DM. pH-(low)-insertion-peptide (pHLIP) translocation of membrane impermeable phalloidin toxin inhibits cancer cell proliferation. Proc Natl Acad Sci U S A. 2010;107:20246-50.

10. Wijesinghe D, Engelman DM, Andreev OA, Reshetnyak YK. Tuning a polar molecule for selective cytoplasmic delivery by a pH (Low) insertion peptide. Biochemistry. 2011;50:10215-22.

11. Andreev OA, Karabadzhak AG, Weerakkody D, Andreev GO, Engelman DM, Reshetnyak YK. pH (low) insertion peptide (pHLIP) inserts across a lipid bilayer as a helix and exits by a different path. Proc Natl Acad Sci U S A. 2010;107:4081-6.

12. Karabadzhak Alexander G, Weerakkody D, Wijesinghe D, Thakur Mak S, Engelman Donald M, Andreev Oleg A, et al. Modulation of the pHLIP Transmembrane Helix Insertion Pathway. Biophysical journal. 2012;102:1846-55.

13. Roy RS, Gopi HN, Raghothama S, Gilardi RD, Karle IL, Balaram P. Peptide hairpins with strand segments containing alpha- and beta-amino acid residues: cross-strand aromatic interactions of facing Phe residues. Biopolymers. 2005;80:787-99.

14. Chiche J, Brahimi-Horn MC, Pouyssegur J. Tumour hypoxia induces a metabolic shift causing acidosis: a common feature in cancer. J Cell Mol Med. 2010;14:771-94.

15. Warburg O, Wind F, Negelein E. The metabolism of tumors in the body. J Gen Physiol. 1927;8:519-30.

16. Gillies RJ, Robey I, Gatenby RA. Causes and consequences of increased glucose metabolism of cancers. J Nucl Med. 2008;49 Suppl 2:24S-42S.

17. Newell K, Franchi A, Pouyssegur J, Tannock I. Studies with glycolysis-deficient cells suggest that production of lactic acid is not the only cause of tumor acidity. Proc Natl Acad Sci U S A. 1993;90:1127-31.

18. Grillon E, Farion R, Fablet K, De Waard M, Tse CM, Donowitz M, et al. The spatial organization of proton and lactate transport in a rat brain tumor. PLoS One. 2011;6:e17416.

19. Rehncrona S. Brain acidosis. Ann Emerg Med. 1985;14:770-6.

20. Xiong ZG, Pignataro G, Li M, Chang SY, Simon RP. Acid-sensing ion channels (ASICs) as pharmacological targets for neurodegenerative diseases. Curr Opin Pharmacol. 2008;8:25-32.

21. Swietach P, Vaughan-Jones RD, Harris AL. Regulation of tumor pH and the role of carbonic anhydrase 9. Cancer Metastasis Rev. 2007;26:299-310.

22. Ihnatko R, Kubes M, Takacova M, Sedlakova O, Sedlak J, Pastorek J, et al. Extracellular acidosis elevates carbonic anhydrase IX in human glioblastoma cells via transcriptional modulation that does not depend on hypoxia. Int J Oncol. 2006;29:1025-33.

Figures

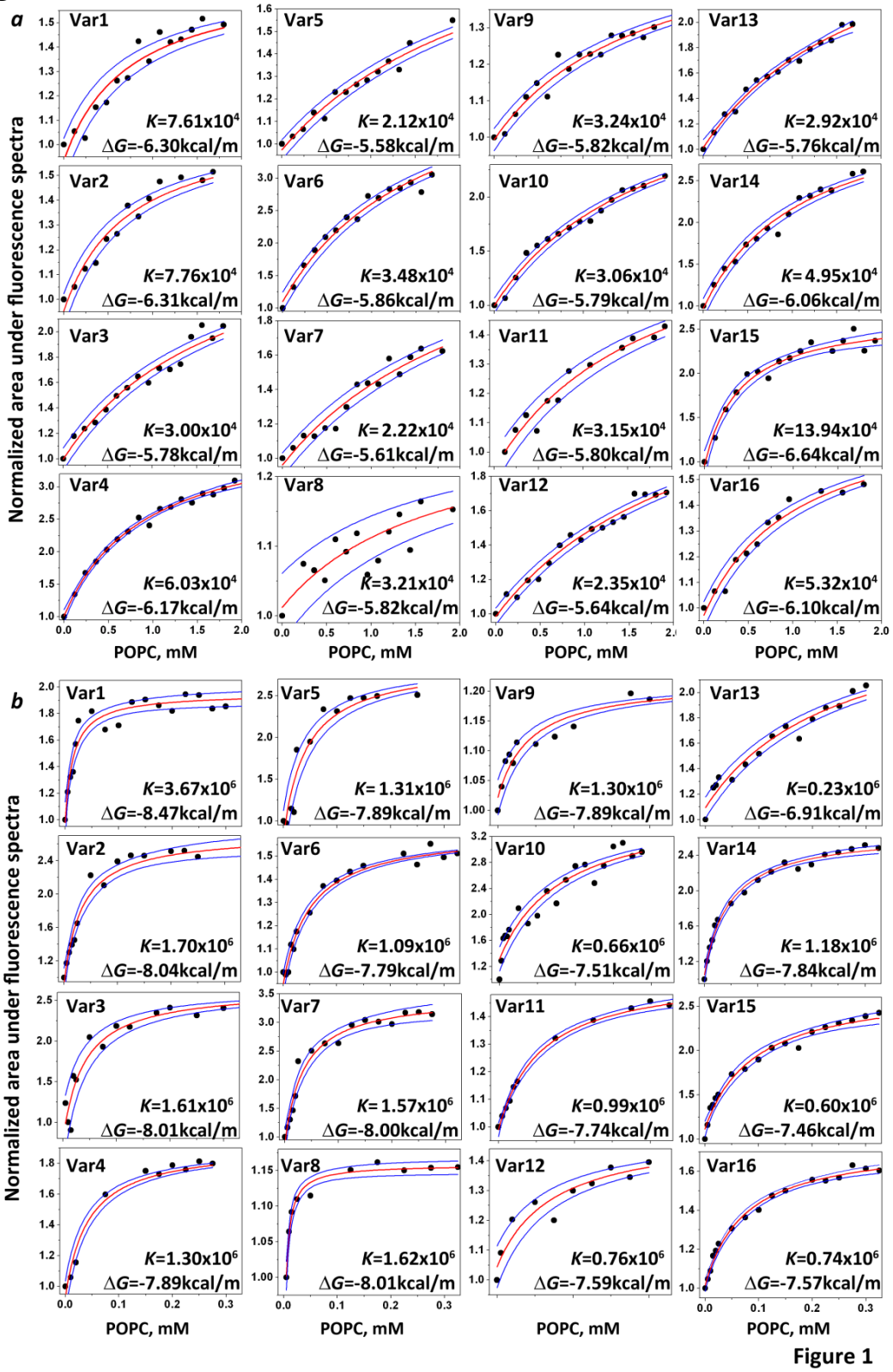

Figure 1

Figure 1. Titration of pHLIP variant binding to liposomes at high and low pHs. The titration of the pHLIP variants with increasing concentration of POPC liposomes at pH8 (***a***) and pH4-5 (***b***) are followed using intrinsic peptide fluorescence changes. For comparison the mole-fraction partition coefficients for Var0 (WT-pHLIP) at pH8 and 5 are 4.87×10^4 and 1.54×10^6, respectively, and the corresponding Gibbs free energies are 6.04 and 7.98 kcal/mol.

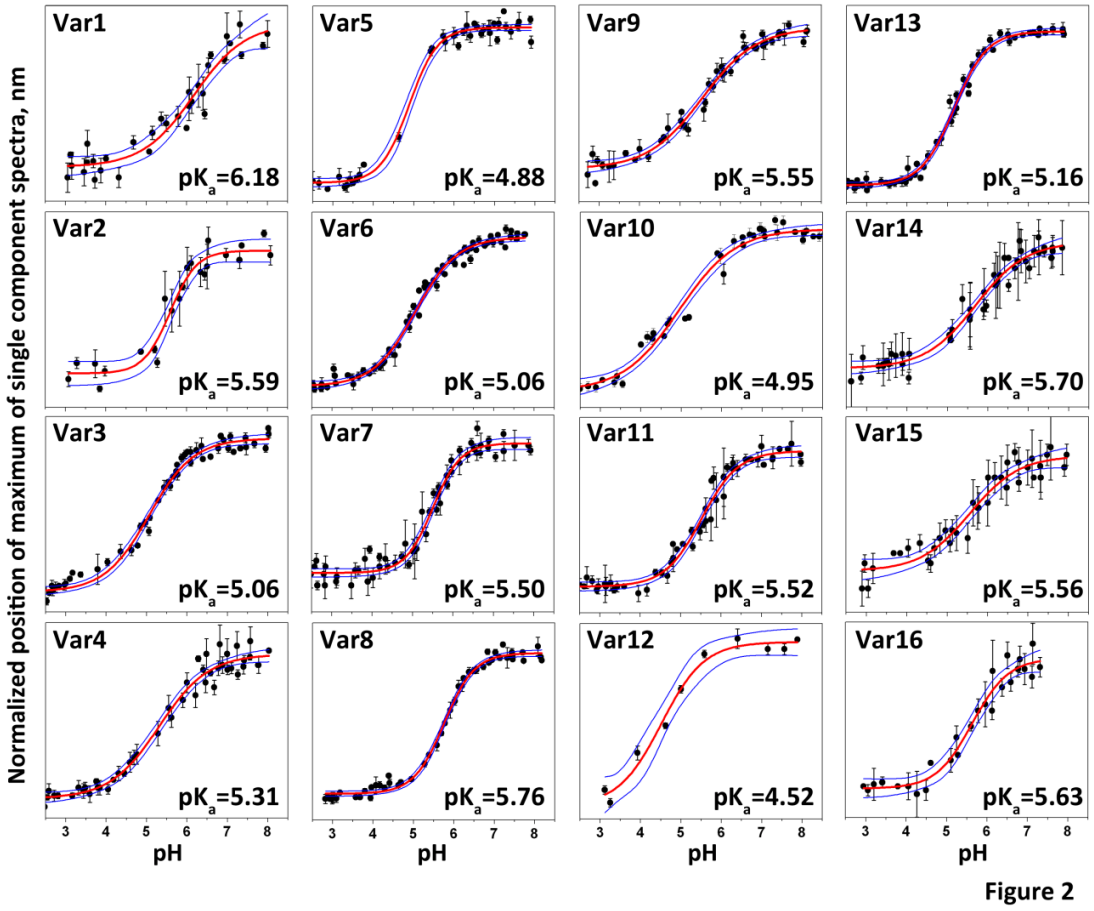

Figure 2. pH-dependent bilayer insertion of variants. Peptide intrinsic fluorescence changes are used to follow the insertion as a function of pH (transition from the state II to state III as the pH is lowered).

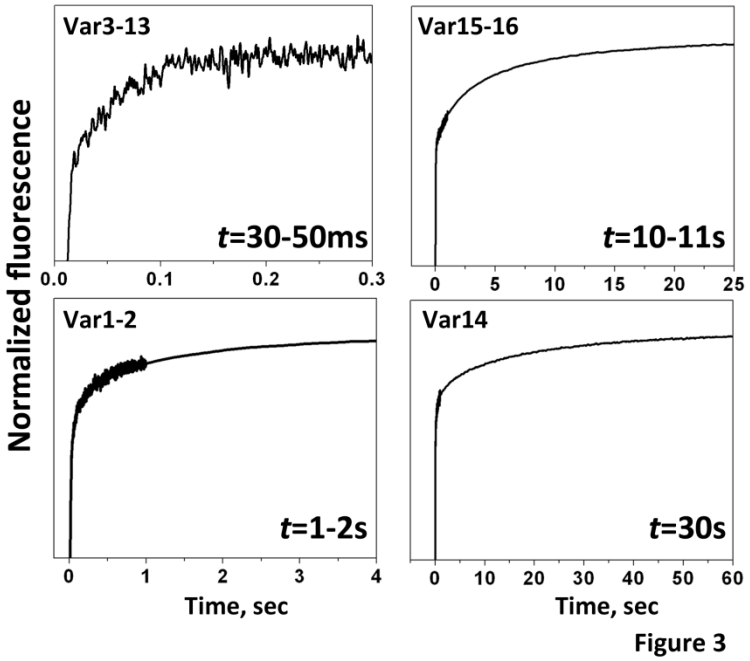

Figure 3. Kinetics of insertion. Representative kinetic curves for the insertion of variant peptides into the lipid bilayer are shown, the characteristic time of insertion of Var0 (WT-pHLIP) is about 40 sec.

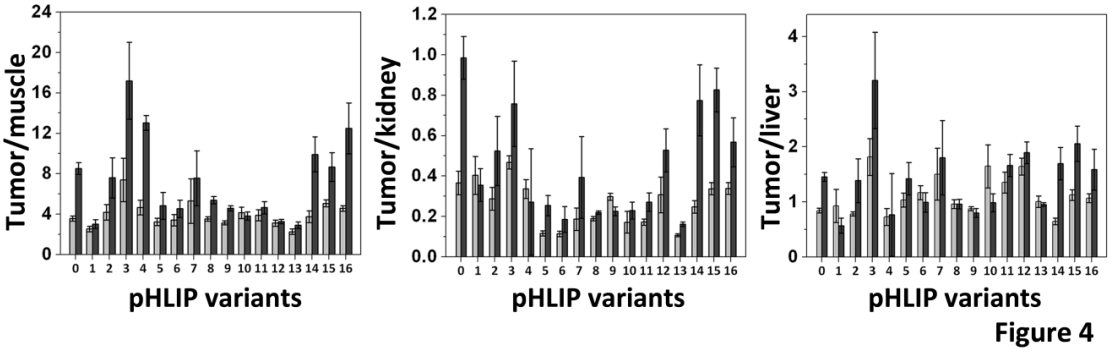

Figure 4. **Tumor to organ fluorescence ratios.** Tumor to muscle, tumor to kidney and tumor to liver ratios calculated at 4 and 24 hour time points are shown for all pHLIP variants.

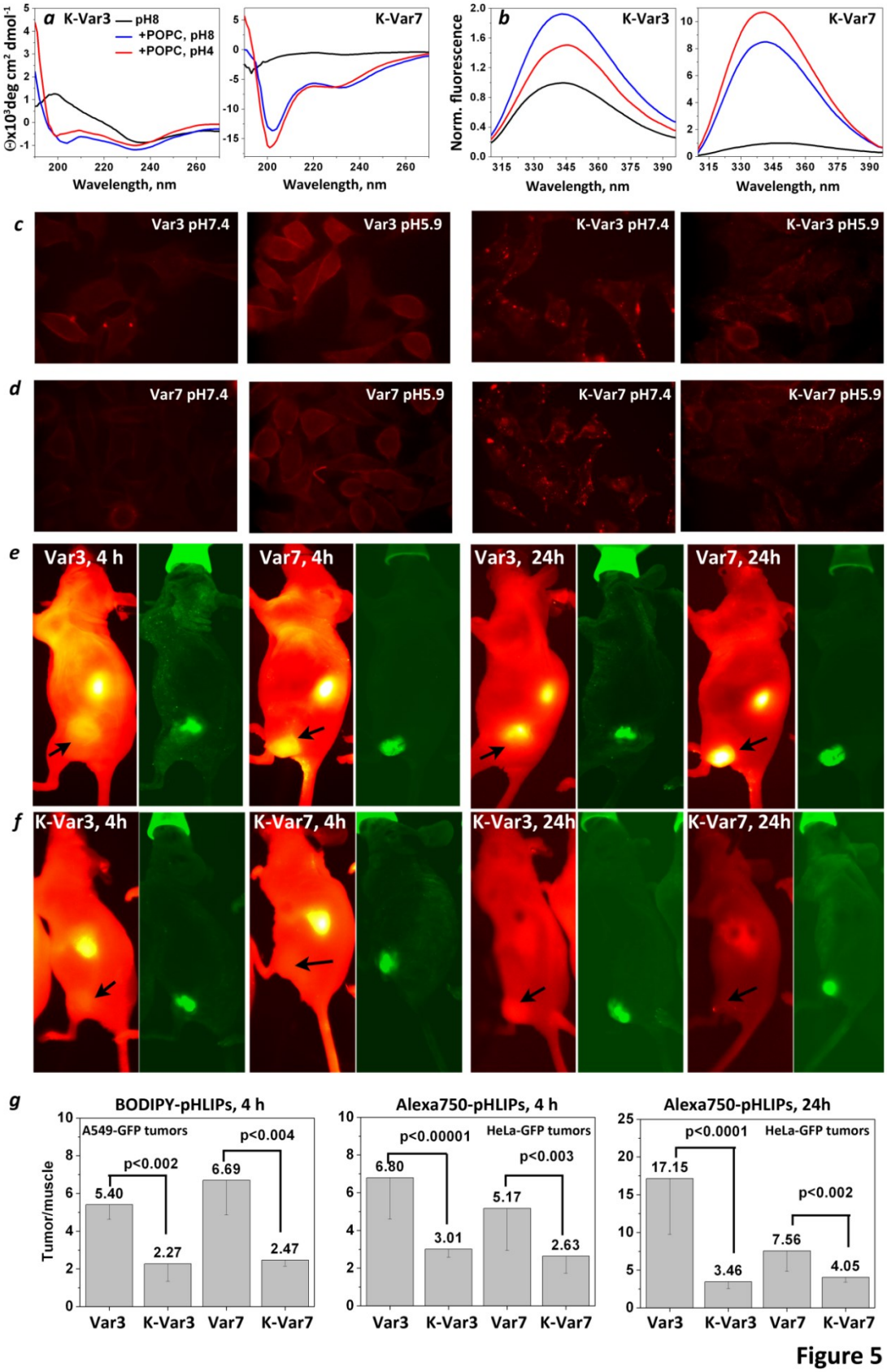
a
K-Var3
pH8
+POPC, pH8
+POPC, pH4
K-Var7
Θx10³deg cm² dmol⁻¹
Wavelength, nm
b
K-Var3
K-Var7
Norm. fluorescence
Wavelength, nm
c
Var3 pH7.4
Var3 pH5.9
K-Var3 pH7.4
K-Var3 pH5.9
d
Var7 pH7.4
Var7 pH5.9
K-Var7 pH7.4
K-Var7 pH5.9
e
Var3, 4 h
Var7, 4h
Var3, 24h
Var7, 24h
f
K-Var3, 4h
K-Var7, 4h
K-Var3, 24h
K-Var7, 24h
g
BODIPY-pHLIPs, 4 h
A549-GFP tumors
p<0.002
p<0.004
5.40
2.27
6.69
2.47
Tumor/muscle
Alexa750-pHLIPs, 4 h
p<0.00001
HeLa-GFP tumors
p<0.003
6.80
3.01
5.17
2.63
Alexa750-pHLIPs, 24h
p<0.0001
HeLa-GFP tumors
p<0.002
17.15
3.46
7.56
4.05
Var3
K-Var3
Var7
K-Var7

Figure 5

Figure 5. Comparisons with control K-pHLIPs. The CD (***a***) and tryptophan fluorescence (***b***) spectra of K-Var3 and K-Var7 show that these variants lose the ability to interact with a lipid bilayer in a pH-dependent manner. (***c-d***) Cellular uptake at pH7.4 and 5.9 of Var3, K-Var3, Var7 and K-Var7 labeled with Rhodamine are shown. The cellular uptake of four peptides labeled with BODIPY are shown at both pHs in Supplementary Figure S4. (***e-f***) Whole-body NIR fluorescence images of mice obtained at 4 and 24 hours after *i.v.* administration of Var3, K-Var3 (***e***) and Var7, K-Var7 (***f***) conjugated with Alexa750. The tumor is indicated by arrows on the NIR images as reported by the GFP signal shown in adjacent images. Images obtained at different time points are presented with maximum contrast, the contrast-to-noise ratios are: Var3, 4h – 103; Var3, 24h – 186; Var7, 4h – 85; Var7, 24h – 360; K-Var3, 4h – 87; K-Var3, 24h – 54; K-Var7, 4h – 22; K-Var7, 24h – 16. (***g***) The A549-GFP tumor to muscle ratios calculated for 4 hours for BODIPY-pHLIPs and –K-pHLIPs and HeLa-GFP tumor to muscle ratios calculated for 4 and 24 hours time points for Alexa750-pHLIPs and –K-pHLIPs are shown. The mean fluorescence of HeLa-GFP and A549-GFP tumors and organs at 4 and 24 hours after Alexa750-K-pHLIPs and at 4 hours after BODIPY-pHLIPs and –K-pHLIPs administration are given in the Supplementary Table S4 and S5, respectively.

SUPPLEMENTARY DATA

A Family of pH (Low) Insertion Peptides for Tumor Targeting

Dhammika Weerakkody, Anna Moshnikova, Mak S. Thakur, Valentina Moshnikova, Jennifer Danniels, Donald M. Engelman, Oleg A. Andreev, Yana K. Reshetnyak

Conjugation of pHLIP variants with fluorescent dyes

The lyophilized powder of a peptide was dissolved in a solution containing 3M urea, and the peptide solution was transferred to buffer using a G-10 size-exclusion spin column, or was dissolved directly in phosphate buffer at pH8 for biophysical studies. The concentrations of the peptides were determined by absorbance (for Var0-2 and Var14-16: $\varepsilon_{280} = 13{,}940\ M^{-1}\ cm^{-1}$; and for Var3-13 and K-Var3, K-Var7: $\varepsilon_{280} = 12{,}660\ M^{-1}\ cm^{-1}$).

For studies on cultured cells and animals each pHLIP variant was conjugated with AlexaFluor®750 C_5-maleimide (Invitrogen, catalog #A30459), and Var3, Var7, K-Var3 and K-Var7 were conjugated with Tetramethylrhodamine-5-maleimide, single isomer (Invitrogen, catalog #T6027) or BODIPY®-TMR C_5-maleimide (Invitrogen, catalog #B30466) in DMF or DMSO at a ratio of 1:1.1 of dye:peptide and incubated at room temperature for about 6 hours and then at 4ºC until the conjugation reaction was completed. The reaction progress was monitored by reverse phase HPLC. The purity of products was assessed by analytical HPLC and peak identity was confirmed by SELDI-TOF mass spectrometry.

Liposome preparation

Large unilamellar vesicles (LUVs) were prepared by extrusion. POPC (1-palmitoyl-2-oleoyl-sn-glycero-3-phosphocholine, Avanti Polar Lipids, Inc.) dissolved in chloroform at a concentration of 1 mg/ml were desolvated on a rotary evaporator and dried under high vacuum for several hours. The phospholipid film was then rehydrated in 100 mM phosphate buffer, pH 8.0, vortexed for 2 hours, and repeatedly extruded through membranes with 100 or 50 nm pore sizes to obtain LUVs.

Oriented circular dichroism measurements

Oriented circular dichroism was measured from supported bilayers deposited on a stack of quartz slides with special polish for far UV measurements, with spacers of 0.2 mm thickness on one side of each slide (Starna). Quartz slides were cleaned by sonication for 10 min in cuvette cleaner solution (Decon Contrad 5% in water), 2-propanol, acetone, 2-propanol and rinsed with deionized water. Then the slides were immersed in a mixture of concentrated sulfuric acid and hydrogen peroxide (ratio 3:1) for 5-10 min to completely remove any remaining organic material form the slides. Slides were then thoroughly rinsed with and stored in deionized water (Milli-Q purified water kept at 25 °C). A POPC lipid monolayer was deposited on the clean quartz substrate by the Langmuir-Blodgett (LB) method using a KSV minitrough. For the LB deposition, a POPC lipid solution in chloroform was spread on the subphase and allowed to evaporate chloroform for about 30 min, followed by monolayer compression to 32 mN/m. An initial layer was deposited by retrieving the slide from the subphase at a rate of 15 mm/min. The second layer of the bilayer was created by

fusion. For this step, the monolayer on the slide was incubated with a solution of POPC vesicles (50 nm in diameter obtained by extrusion) mixed with the peptide solution at pH 4 (0.5 mM POPC and 10 μM peptide). The fusion occurred during 6 hour incubation at 100% humidity. Then, excess vesicles were carefully removed and the slides were stacked to make a pile filled with the peptide solution (5 μM) at pH 4. Bilayers with the peptide solution were allowed an additional 6 hour equilibration. Measurements were taken at 3 steps during the process: when the monolayers were incubated with the excess of liposomes, soon after spaces between slides were filled with the peptide solution and 6 hours after the second measurement. 14 slides (28 bilayers) were assembled and OCD spectra were recorded on a MOS-450 spectrometer with 2 s sampling time. Control measurements were carried out of the peptide between slides with and without supported bilayers and in the presence of an excess of POPC liposomes.

Assumptions made for the analysis of pH-dependence data

Peptide intrinsic fluorescence changes are used to follow the insertion as a function of pH (transition from the state II to state III as the pH is lowered). Decomposition of the fluorescence spectra measured at various pHs gives the positions of the maxima, and the single component solutions are shown. The Henderson–Hasselbalch equation with cooperativity was used to fit the experimental points, and the fitting curves and 95% confidence intervals are shown by the red and blue lines, respectively. Each graph notes the apparent pK of the peptide's insertion into the membrane obtained from the fitting of the experimental data. The pKa of Var0 (WT-pHLIP) is 6.0. The pKa values

obtained by fitting of the experimental data by the Henderson–Hasselbalch equation with a fixed cooperativity parameter (n=1) are very similar to the data shown in the figure: Var1=6.14; Var2=5.59; Var3=5.09; Var4=5.32; Var5=4.84; Var6=5.06; Var7=5.51; Var8=5.75; Var9=5.59; Var10=4.92; Var11=5.52; Var12=4.52; Var13=5.16; Var14=5.69; Var15=5.59; Var16=5.63. It is assumed that there is a linear relation between the position of the maximum and the contribution of state II (or state III) (state I is the peptide in solution at pH8; state II is the peptide in the presence of POPC liposomes at pH8; state III is the result of folding and insertion of the peptide with POPC when the pH is dropped from 8 to 3.6 by the addition of an aliquot of HCl). However, due to the fact that the quantum yields in states II and III are slightly different, there was a slight non-linearity, so we completed the analysis by estimating the contributions of the states for WT-pHLIP and found that the apparent pK shifts no more than on 0.05 pH units toward lower pHs. Since this shift is less than the experimental error, we present the pKa values for transitions from the state II to III based on the analysis of the positions of spectral maxima.

Quantification of cellular uptake

For quantification of cellular uptake of BODIPY-labeled Var3 and Var7 at pH7.4 and 5.9 we used A549-GFP cells in suspension. 2 μM of fluorescently labeled peptides were incubated with cells in DMEM media at pH7.4 and 5.9 for 30 min at 37°C and 5% CO_2. Then, cells were pelleted by centrifugation (2000 rpm, 4 min) at room temperature, the supernatant was removed and the pellet was washed three times with the same media and resuspended in 50 μL, and the cell suspension solution was placed

into cell counting chambers. The phase-contrast, GFP and BODIPY fluorescent signals were measured and analyzed using ImagePro Plus program.

Biophysical properties, which affect tumor targeting

- The apparent pK of peptide insertion into membrane determines the proportion of available peptide molecules inserted into plasma membrane of cancer cells at various pHs. Currently we have pHLIP peptides with pKas varying over the range from 4.5 to 6.5 for insertion into POPC lipid bilayers. Various pHLIP variants might be used to probe the pHs of more or less acidic tumors. The insertion of pHLIP responds to the pH at the surfaces of cancer cells, not that of the surrounding fluid. Due to the transmembrane potential gradient, protons accumulate at the surfaces of cells in close vicinity of membrane, and the pH is lower than in the bulk extracellular environment or in blood. Current methods of measuring pH *in vivo* report the average value of extracellular pH in tumors, which can vary from 6.0 to 7.2, but the pH at the surfaces of cancer cells are likely to be lower.

- pHLIP is a relatively hydrophobic peptide, therefore significant initial association with a lipid bilayer or plasma membrane occurs at neutral pH. The strength of this interaction (state II) is determined by the balance of hydrophobic and polar/charged residues in the pHLIP sequence. Stronger partitioning of the peptides onto bilayers at neutral pH increases the time of circulation in the blood. Long circulation time is a disadvantage for SPECT/PET imaging, since the short half-life-time probes are used and tumor targeting and blood clearance need to be very fast (at least within 4 hours). However, long circulation times of pHLIP variants in the blood could be very well

suited for fluorescence or MR imaging, as well as for the delivery of therapeutic agents. We find that all pHLIP variants that have higher affinities for membranes at neutral pH show high tumor/organ ratios at 24 hours post-injection.

- An important parameter is the difference between the Gibbs free energy of peptide binding to membranes at low pH vs. high pH. This parameter reflects the difference in the affinity of the peptide to membrane at low and neutral pH and the strength of formation of transmembrane helix at low pH. A larger $\Delta\Delta G$ will ensure a greater differentiation between the inserted and non-inserted peptides as a function of pH.

- For applications *in vivo*, the kinetics of peptide insertion across the lipid bilayer are important for rapid equilibration with tissues and clearance from the blood. Based on insertion kinetics we can group all pHLIP peptides into: i) the peptides with protonatable residues both in the TM and in the inserting end show the slowest kinetics of insertion (minutes); ii) peptides that are truncated at the inserting end and have few or no protonatable residues at the inserting end, partition in bilayer much faster (seconds), iii) peptides that have protonatable residues at the inserting end but not in the TM show intermediate times of insertion (~20 s), and finally, peptides with only one protonatable residue in the TM have the fastest kinetics of insertion, which coincides with time of formation of helical structure (~100 msec).

- Exit kinetics should be different in cells and liposomes, since peptides that have protonatable residues that are translocated across a cell membrane move them to the neutral pH of the cytoplasm. To exit the cell membrane, these groups must be protonated, which is much less likely in the cytoplasm, so these peptides become anchored in a cell. Such an “anchor” can significantly (by orders of magnitude)

reduce the rate of peptide exit, and the peptide could stay in the plasma membrane for weeks. Such an effect would explain our observation that mouse tumors are stably labeled with fluorescent WT-pHLIP.

Tables

Parameters	Name	State I	State II	State III	Name	State I	State II	State III
λ_{max} S θ_{225} x10^3	**Var1**	349 1 -2.42	345 1.47 -3.85	339 1.81 -9.46	**Var9**	353 1 -2.39	350 1.28 -3.20	339 2.10 -7.90
	Var2	350 1 -2.74	345 2.08 -3.76	342 2.76 -8.64	**Var10**	350 1 -2.40	347 1.47 -2.46	340 2.86 -8.40
	Var3	353 1 -2.07	347 1.66 -3.94	338 2.08 -13.49	**Var11**	351 1 -2.14	345 2.60 -3.08	340 3.20 -9.02
	Var4	353 1 -2.32	340 2.66 -10.14	345 3.32 -15.28	**Var12**	353 1 -0.82	352 1.36 -0.96	341 2.90 -4.80
	Var5	351 1 -2.20	355 2.05 -3.38	340 3.52 -6.25	**Var13**	355 1 -1.76	349 1.72 -2.28	340 3.61 -6.14
	Var6	353 1 -2.12	350 0.96 -2.89	339 1.64 -6.95	**Var14**	351 1 -2.00	346 1.54 -3.79	344 2.94 -9.91
	Var7	352 1 -2.64	345 1.74 -4.12	340 3.08 -8.82	**Var15**	351 1 -4.30	339 2.14 -8.94	339 2.52 -10.08
	Var8	353 1 -0.89	353 1.19 -1.22	337 2.48 -9.43	**Var16**	346 1 -5.41	345 1.89 -7.03	339 2.14 -8.57

Table S1. The three states of each pHLIP variant. The spectral parameters of the pHLIP variants in states I, II and III are presented. The parameters were obtained from analysis of the fluorescence and CD spectra shown in Figure 1: the maximum position of the fluorescence spectrum λ_{max}, in nm; S – the normalized area under the spectra (normalization was done on the area under the spectrum in State I); θ_{225} **x** 10^3, deg cm^2 $dmol^{-1}$ – the molar ellipticity at 225 nm.

	Var0-WT ***n*** **= 9**	**Var1-2D1D** ***n*** **= 6**	**Var2-2D1D** ***n*** **= 5**	**Var3-3D** ***n*** **= 7**	**Var4-3E** ***n*** **= 4**	**Var5-3Da** ***n*** **= 5**
Kidney	3630.6±485.6	4324.0±444.6	3456.3±585.4	6125.6±1004.1	6755.6±698.7	3097.0±528.3
Tumor	1373.8±334.5	1812.4±819.0	1145.3±737.5	3054.9±726.2	2439.3±443.2	559.4±95.6
Heart	621.4±152.3	752.9±398.4	554.6±421.2	855.0±331.6	980.5±187.3	334.0±43.4
Lungs	1003.6±297.5	1016.6±567.7	761.1±506.8	803.1±256.2	1077.3±84.2	405.4±34.5
Liver	1651.4±470.2	2309.7±1457.0	1432.4±950.8	1829.6±741.6	3615.3±1099.4	561.2±103.0
Spleen	546.4±131.4	757.5±445.0	539.3±372.3	675.6±244.6	987.3±320.8	432.2±63.0
Bladder	825.4±495.8	1030.5±646.3	665.3±486.4	1104.6±628.7	1198.8±719.3	452.4±47.6
Stomach	909.2±277.1	1249.6±783.1	1092.0±793.5	1029.6±355.0	1239.8±438.8	470.8±71.7
Intestine	884.2±260.5	1116.4±646.0	590.9±347.0	574.3±221.9	888.5±442.9	257.6±23.0
Muscle	476.8±110.1	766.5±285.3	413.7±248.9	541.9±180.3	629.8±97.9	250.6±17.9
Brain	270.1±46.3	303.1±113.3	233.5±72.9	350.6±95.6	372.3±13.9	193.2±13.5

	Var6-3Db ***n*** **= 5**	**Var7-3Ea** ***n*** **= 16**	**Var8-3Eb** ***n*** **= 5**	**Var9-3Ec** ***n*** **= 5**	**Var10-2D** ***n*** **= 6**	**Var11-2E** ***n*** **= 6**
Kidney	2536.1±297.2	3583.3±427.9	3729.2±749.0	3367.9±667.6	3575.0±540.4	4164.3±833.5
Tumor	461.6±71.6	970.1±449.1	910.6±180.1	1169.4±297.9	819.9±306.7	981.0±357.9
Heart	262.2±29.5	351.1±81.0	515.0±284.4	613.4±250.6	341.5±87.7	532.3±104.5
Lungs	266.4±23.7	413.3±135.6	526.0±62.2	958.0±367.2	412.8±42.4	560.2±42.2
Liver	414.8±31.8	695.1±244.2	938.2±79.2	1309.2±255.3	539.0±114.3	744.2±57.1
Spleen	316.0±50.6	479.3±310.6	443.8±86.8	629.2±96.1	423.4±29.3	495.7±46.5
Bladder	298.6±38.3	554.4±243.4	608.8±113.3	942.0±204.0	420.0±77.3	623.0±145.3
Stomach	268.6±31.2	605.6±205.6	563.4±93.3	934.2±251.3	513.1±70.2	763.0±107.8
Intestine	246.4±35.0	437.8±109.2	380.6±87.7	471.8±98.9	321.6±109.2	353.3±14.7
Muscle	220.8±30.0	277.8±67.2	339.0±50.7	450.8±97.8	281.5±70.0	330.2±22.2
Brain	180.2±18.7	206.3±36.0	230.2±18.4	222.0±16.7	217.4±26.4	241.5±24.7

	Var12-1D ***n*** **= 7**	**Var13-1E** ***n*** **= 6**	**Var14-Rev** ***n*** **= 5**	**Var15-2N** ***n*** **= 5**	**Var16-2P** ***n*** **= 6**
Kidney	2004.5±527.7	2653.7±357.1	4162.9±210.7	5657.0±843.8	3733.0±582.9
Tumor	614.5±186.7	459.0±99.3	1245.0±308.7	2075.8±252.2	1407.0±142.1
Heart	368.7±100.4	351.7±61.5	691.0±104.7	837.6±188.0	342.7±28.9
Lungs	423.8±122.0	349.7±78.9	808.2±116.3	1190.8±419.3	451.0±85.2
Liver	435.9±139.0	457.2±46.8	1863.0±312.6	1888.8±303.1	1344.0±153.2
Spleen	295.7±75.5	365.2±20.4	527.8±64.6	717.4±61.9	370.7±24.0
Bladder	287.2±51.5	414.7±102.9	648.6±235.5	743.6±59.8	525.7±121.2
Stomach	341.2±84.6	483.3±96.1	685.6±101.3	556.6±94.6	361.2±61.5
Intestine	227.5±59.0	277.8±31.1	839.8±196.9	720.4±52.9	403.3±67.3
Muscle	270.8±30.7	261.8±24.4	421.4±35.8	500.6±37.1	396.0±37.8
Brain	207.0±33.0	211.0±13.5	290.6±27.2	405.0±65.5	216.7±14.9

Table S2. Mean NIR fluorescence with standard deviation calculated for each organ collected at 4 hours after Alexa750-pHLIP variant administration, ***n*** is the number of animals. The mean fluorescence values of organs were normalized to the signal in kidney for each mouse, then averaged for each variant and presented in Figure S3.

	Var0-WT ***n*** **= 9**	**Var1-2D1D** ***n*** **= 4**	**Var2-2D1D** ***n*** **= 9**	**Var3-3D** ***n*** **= 7**	**Var4-3E** ***n*** **= 3**	**Var5-3Da** ***n*** **= 5**
Kidney	854.4±186.9	3349.5±2262.1	1525.2±472.4	1141.8±416.7	1151.4±262.4	431.0±121.5
Tumor	818.8±157.4	1366.1±776.7	881.4±560.6	950.9±434.1	1106.3±651.1	252.2±67.6
Heart	248.5±33.3	580.9±280.2	240.3±94.3	186.0±31.3	255.0±75.1	166.0±16.0
Lungs	355.7±38.8	758.3±422.8	351.9±190.9	190.4±31.8	287.7±93.6	198.6±15.3
Liver	602.2±104.4	2211.1±973.9	660.8±427.5	366.3±72.0	737.3±90.4	209.0±18.2
Spleen	226.1±13.0	626.3±368.0	285.3±170.8	199.0±25.5	249.3±30.7	184.0±14.5
Bladder	250.2±27.5	861.6±743.0	301.3±183.5	221.6±33.2	282.3±72.8	188.0±10.8
Stomach	248.9±33.1	884.0±619.8	353.2±178.4	198.4±18.2	257.0±28.0	201.8±16.3
Intestine	270.2±40.5	808.7±473.3	237.2±75.3	184.3±19.5	261.3±34.8	141.6±2.1
Muscle	197.6±31.0	555.4±320.9	213.5±88.9	158.7±21.6	185.3±45.1	141.4±5.1
Brain	166.3±10.8	253.5±73.8	164.8±30.8	147.7±8.1	163.0±24.3	136.8±3.2
	Var6-3Db ***n*** **= 5**	**Var7-3Ea** ***n*** **= 17**	**Var8-3Eb** ***n*** **= 5**	**Var9-3Ec** ***n*** **= 5**	**Var10-2D** ***n*** **= 5**	**Var11-2E** ***n*** **= 4**
Kidney	380.5±46.0	785.3±200.9	1287.1±307.6	1242.2±280.6	1013.5±104.4	828.6±129.1
Tumor	218.6±40.8	453.1±173.2	441.6±102.0	441.2±53.9	345.1±140.2	400.3±61.0
Heart	142.8±4.9	173.3±20.3	201.8±19.8	247.0±92.6	196.8±79.3	186.3±10.6
Lungs	148.8±8.4	181.6±24.2	330.2±76.0	270.6±58.6	198.4±17.3	207. ±3±8.7
Liver	220.2±5.7	299.8±51.7	455.6±76.9	536.0±101.4	338.3±47.5	285.5±12.4
Spleen	164. ±69.0	200.1±22.6	244.8±39.1	273.6±7.3	217.0±71.8	204.3±15.1
Bladder	156.0±10.8	187.2±23.5	236.8±37.7	264.2±30.6	207.4±60.2	214.3±18.2
Stomach	152.0±4.3	185.8±26.2	249.4±59.1	258.2±38.2	227.9±89.2	198.5±9.3
Intestine	141.4±3.8	207.8±28.9	192.6±14.2	233.0±19.8	194.4±73.3	173.0±9.5
Muscle	134.2±1.8	154.5±15.0	171.6±15.7	182.2±8.1	180.6±64.6	173.0±6.1
Brain	137.6±2.9	147.8±7.5	154.6±6.7	159.0±7.4	165.5±30.7	157.8±2.6
	Var12-1D ***n*** **= 6**	**Var13-1E** ***n*** **= 3**	**Var14-Rev** ***n*** **= 5**	**Var15-2N** ***n*** **= 5**	**Var16-2P** ***n*** **= 6**	
Kidney	469.8±72.1	444.9±88.9	1157.4±147.5	1618.9±283.3	819.3±124.1	
Tumor	323.7±93.8	218.3±15.1	867.4±286.1	1416.0±468.6	575.5±231.1	
Heart	202.7±23.7	157.7±6.7	230.8±23.7	370.8±52.3	164.2±20.1	
Lungs	221.1±30.7	184.7±8.3	285.4±67.0	473.2±68.9	171.3±29.5	
Liver	252.3±32.9	224.0±21.9	567.2±130.6	742.8±50.2	421.5±52.7	
Spleen	165.8±98.0	158.3±10.4	221.6±40.7	295.8±34.5	183.3±13.9	
Bladder	242.7±26.6	188.0±16.6	274.6±36.8	417.6±26.6	166.7±11.2	
Stomach	197.4±23.9	170.3±11.7	189.8±22.2	288.6±55.5	166.5±20.7	
Intestine	166.7±20.0	152.7±±12.1	289.4±72.0	296.0±36.8	168.3±7.1	
Muscle	184.6±28.2	147.7±7.4	188.8±25.9	260.8±14.3	147.0±7.4	
Brain	159.5±17.9	146.7±2.5	168.6±14.0	214.2±9.3	145.0±6.9	

Table S3. Mean NIR fluorescence with standard deviation calculated for each organ collected at 24 hours after administration of Alexa750-pHLIP variants, ***n*** is the number of animals. The mean fluorescence values of each organ was normalized to the signal in kidney at 4 hours (Table S2) for each mouse, then averaged for each variant and presented in Figure S3.

	K-Var3, 4h ***n*** **= 11**	**K-Var3, 24h** ***n*** **= 8**	**K-Var7, 4h** ***n*** **= 10**	**K-Var7, 24h** ***n*** **= 10**
Kidney	921.6±306.2	254.5±91.9	852.5±345.0	235.2±15.5
Tumor	395.9±107.6	220.0±70.0	306.0±107.6	185.7±9.8
Heart	319.6±140.2	165.4±51.1	228.2±56.2	156.4±27.7
Lungs	296.1±66.9	154.1±16.0	225.0±80.0	136.2±10.7
Liver	2637. ±6446.4	684.2±138.5	1920.4±752.3	538.2±65.2
Spleen	1057.5±416.6	284.3±32.0	552.3±140.8	255.2±80.1
Bladder	331.1±100.1	176.5±26.7	265.4±70.9	155.3±11.0
Stomach	286.2±70.0	168.4±20.2	260.6±84.0	156.7±15.5
Intestine	298.7±46.0	173.9±±14.5	289.7±84.9	166.9±9.7
Muscle	201.3±29.9	141.115.6	178.8±31.4	127.7±4.2
Brain	192.5±25.9	139.7±5.9	158.8±28.5	134.3±2.9

Table S4. Mean NIR fluorescence with standard deviation calculated for each organ collected at 4 and 24 hours after Alexa750-K-pHLIP variant administration, ***n*** is the number of animals.

	Var3, 4h ***n*** **= 4**	**K-Var3, 4h** ***n*** **= 4**	**Var7, 4h** ***n*** **= 4**	**K-Var7, 4h** ***n*** **= 4**
Kidney	154.3±14.4	128.8±10.6	189.5±51.0	121.3±4.6
Tumor	325.0±11.4	151.5±16.7	308.0±115.8	136.3±9.3
Heart	128.3±8.1	114.5±6.0	124.0±13.1	111.5±3.5
Lungs	127.5±11.4	116.0±7.0	124.0±11.6	111.0±1.4
Liver	391.5±78.9	152.8±19.8	210.5±67.6	142.3±30.5
Spleen	122.0±3.9	118.3±4.5	125.0±10.4	113.0±4.2
Bladder	241.7±23.8	150.8±19.3	233.0±64.6	143.8±18.8
Stomach	257.0±66.2	233.0±75.2	269.8±76.6	212.5±26.6
Intestine	197.8±26.7	159.0±42.3	222.5±118.3	133.0±19.3
Muscle	150.5±6.8	126.8±3.0	141.0±20.5	119.3±4.8
Brain	142.0±13.0	135.3±11.8	131.5±23.5	130.5±7.9

Table S5. Mean NIR fluorescence with standard deviation calculated for each organ collected at 4 hours after BODIPY-labeled Var3, K-Var3, Var7 and K-Var7 administration, ***n*** is the number of animals.

Figures

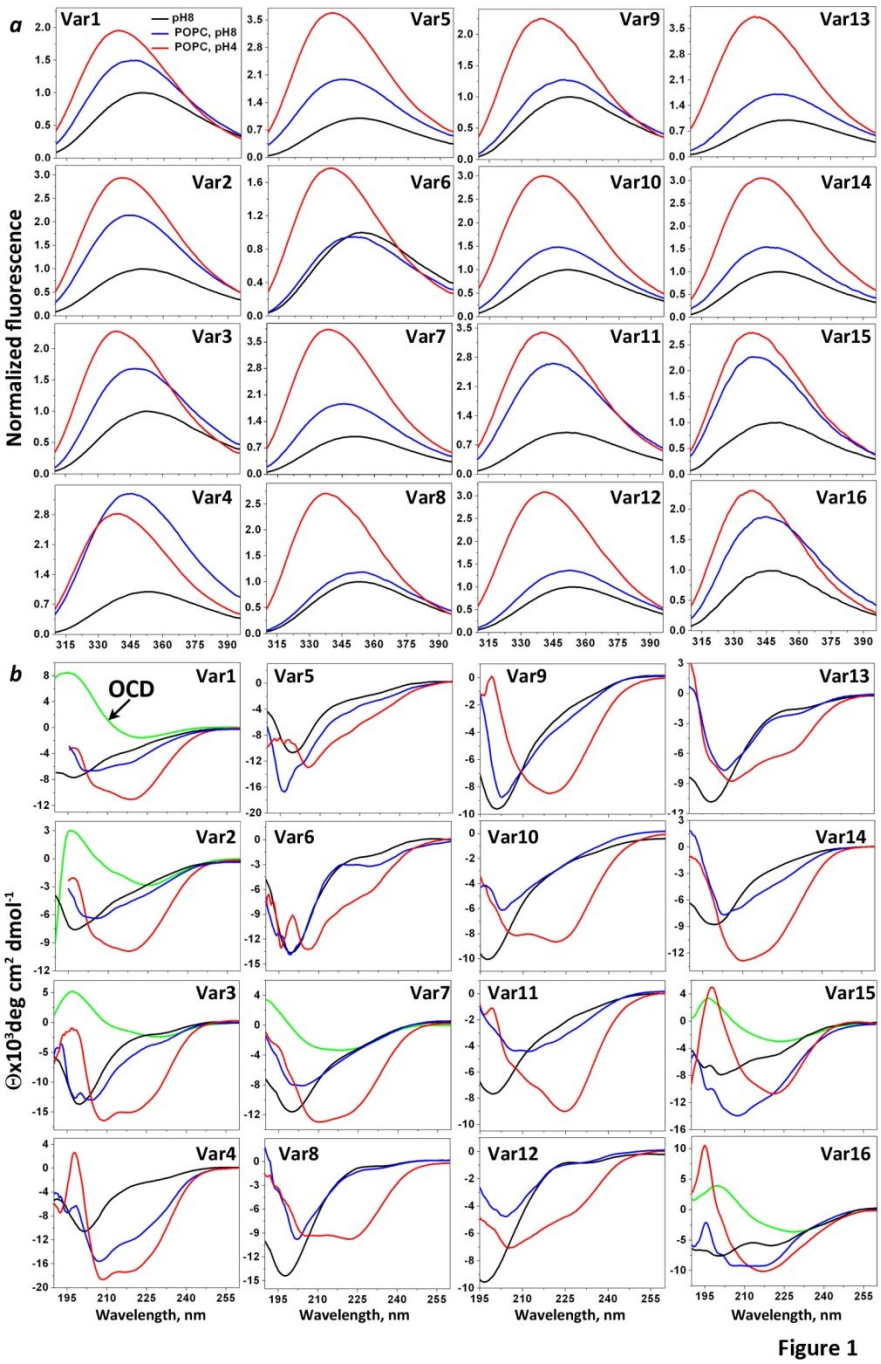

Figure S1. Three states of pHLIP variants. The pHLIP variants were studied for the presence of the three basic states of pHLIP: state I is the peptide in solution at pH8; state II is the peptide in the presence of POPC liposomes at pH8; state III is the folding and insertion of the peptide

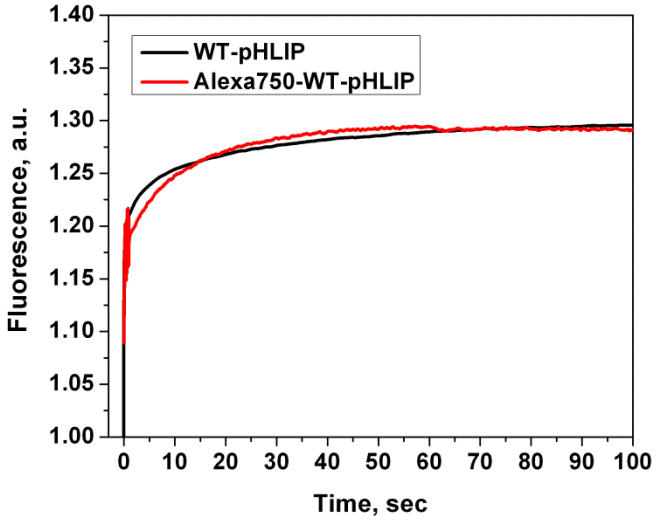

Figure S2. Comparison of the kinetics of WT-pHLIP and Alexa750-WT-pHLIP insertion into membrane. The changes of tryptophan fluorescence signal of Alexa750-WT-pHLIP in presence of POPC liposome in a result of pH drop from 8 to 4-5 was recorded in a stopped-flow apparatus, multiplied by (-1), normalized and compared with the kinetics of insertion of non-labeled WT.

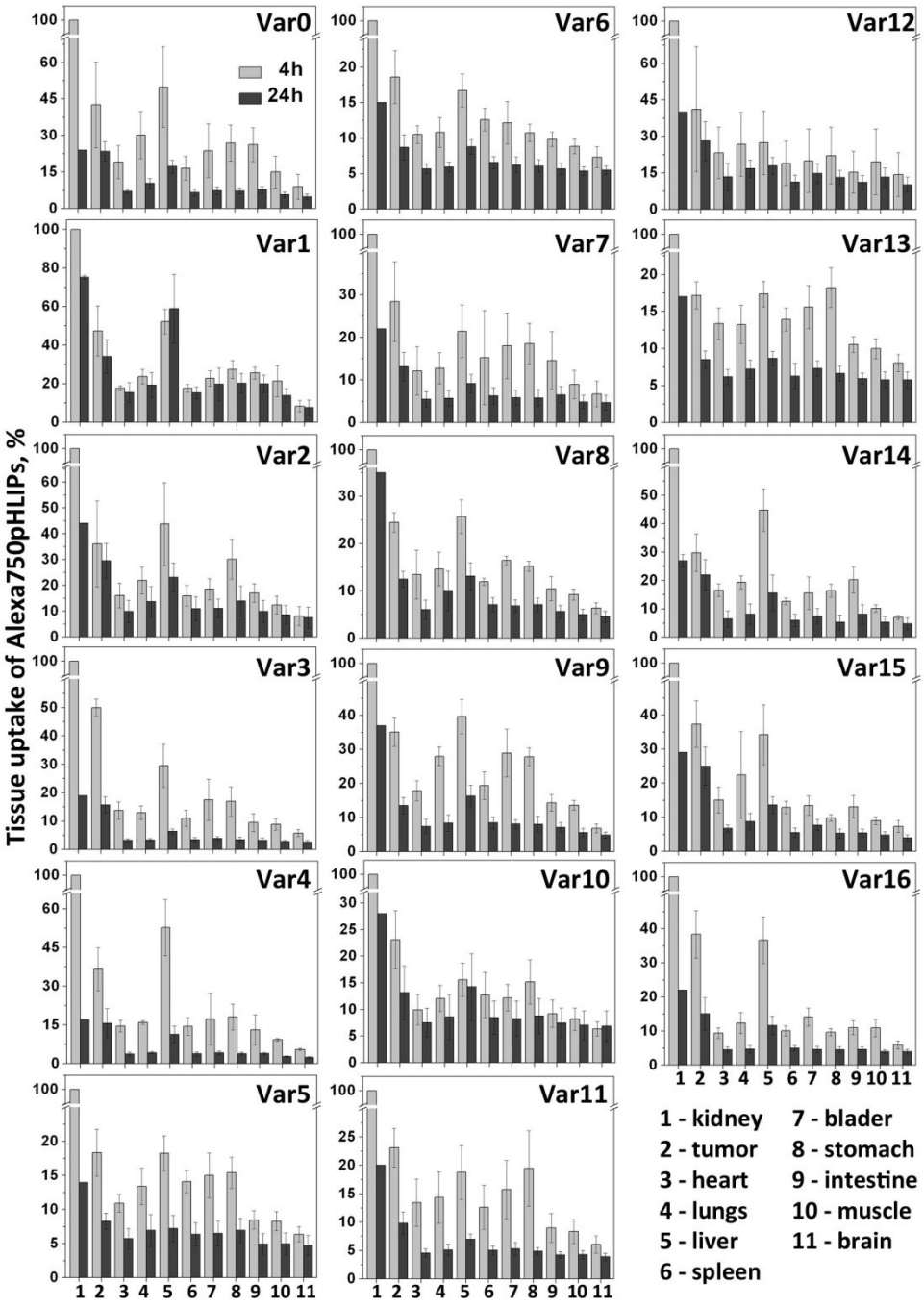

Figure S3. **Distribution of Alexa750-pHLIP in organs and tumors.** Normalized mean NIR fluorescence of tumor and organs at 4 and 24 hours after construct administration are shown (the signals in kidney at 4 hours are taken as 100%). The non-normalized values of fluorescence are given in Supplementary Tables S2 and S3.

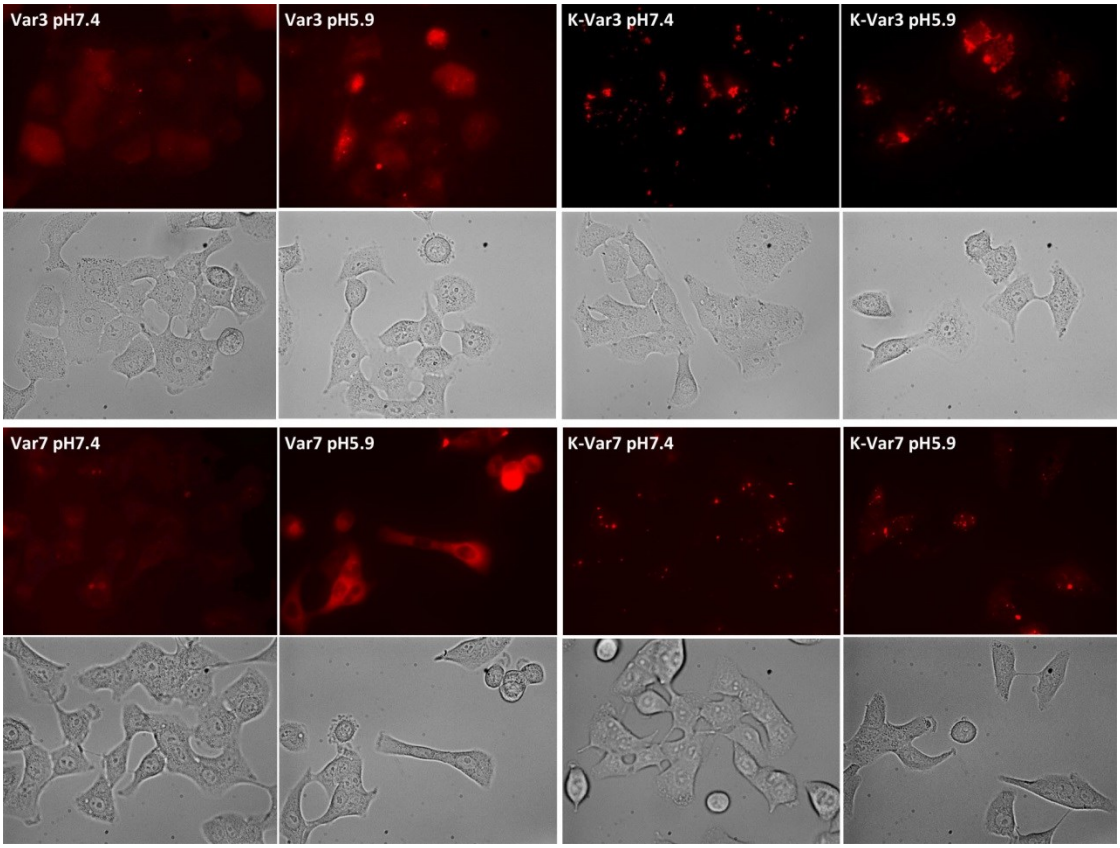

Figure S4. Cellular uptake of BODIPY labeled Var3, Var7, K-Var3 and K-Var7. Fluorescence and phase-contrast images of cells treated with fluorescence peptides at pH7.4 and 5.9 for 30 min and washed 4-5 times of the same media are shown. Also cell experiments were carried out with Alexa750-labeled Var3, Var7, K-Var3 and K-Var7. Despite the fact that the signal was low (due to the low NIR sensitivity of the Retiga CCD camera) the distribution of the signal in cells was the same as in the case of Rho and BODIPY-labeled peptides.